# Proteomic Analysis of Three Dimensional Organotypic Liver Models

Lucas Trung Vu

Dissertation submitted to the faculty of Virginia Polytechnic Institute and State University in partial fulfillment of the requirements for the degree of:

Doctor of Philosophy
in
Chemical Engineering

Chair: Padmavathy Rajagopalan
Co-chair: Richard F. Helm
T.M. Murali
Chang Lu
Richey M. Davis

September 15th 2015

Blacksburg, VA

Keywords: Shotgun Proteomics, Liver, *In vitro*

# Proteomic Analysis of Three Dimensional Organotypic Liver Models

Lucas Trung Vu

## Abstract

*In vitro* liver models that closely mimic the *in vivo* microenvironment are central for understanding hepatic functions and intercellular communication processes. Bottom-up shotgun proteomic analysis of the hepatic cells can lend insight into such processes. This technique employs liquid chromatography-tandem mass spectrometry (LC-MS/MS) for relative quantification of protein abundances by measuring intensities of their corresponding peptides. Organotypic 3D liver models have been developed in our laboratory that consist of hepatocytes and liver sinusoidal endothelial cells (LSECs) separated by a polyelectrolyte multilayer (PEM), which serves as a mimic for the Space of Disse. Each component within these models is easily separable allowing for systematic evaluation of the cells and PEMs. In this study, proteomes of hepatocytes from PEM containing models, cultured with and without LSECs, were compared to those from monolayers. Changes in core metabolism were evaluated among all culture conditions. Overall, all cultures were ketogenic and performed gluconeogenesis. The presence of the PEM led to increases in proteins associated with mitochondrial-based β-oxidation and peroxisomal proteins. The PEMs also limited production of structural proteins, which are linked to dedifferentiation of hepatocytes, suggesting that cell-ECM interactions are essential for maintenance of their liver-like state. The presence of LSECs increased levels

of carboxylesterases and other phase I and phase II detoxification enzymes suggesting that intercellular signaling mediates enzyme abundance. Taken together, these results suggest that the cell-cell (from the LSECs) and cell-ECM (from the PEMs) interactions exert different, yet crucial effects, and both are required for the preservation of metabolic liver functions and differentiated phenotypes. Changes in the PEMs as a result of cell culture were also evaluated but exhibited minimal differences at this time point. Proteomes of LSECs monolayers were also characterized. Enzymes related to the metabolism of amino acids, lipids, oxidative phosphorylation and phase I and phase II detoxification processes were all identified in LSECs monolayers highlighting their role in these processes. Characterization of 3DHL LSECs was not possible due to ion suppression resulting from the presence of excess contaminant proteins. Nonetheless, this study provides a foundation in which LSECs from 3D liver models can be compared against in future studies.

## Acknowledgments

First and foremost, I would like to thank my family. Mom and Dad, thanks for always being there to listen to me and giving me the best advice that you could in any situation. This degree is not only my achievement but also yours as well. To my brothers, Ivan and Jeffrey, thank you for always being there, I love you both very much and without you guys there to calm me down while I was doing this, I might not have been able to do it.

I also offer my deepest thanks to my primary advisor, Professor Padma Rajagopalan, for all of your guidance, support and advice throughout my graduate studies here at Virginia Tech. I sincerely thank you for everything that you have taught me but most importantly, I am very grateful to you for pushing me to always be better and giving me the opportunity to grow as a scientist in your group.

To my co-advisor, Professor Rich Helm, thank you for giving me the opportunity to learn in your lab and for taking the time to teach and advise me over the past couple of years. I have gained several skills that I know will serve me well in the future. I would also like to thank you for supporting me throughout my graduate studies here at Virginia Tech.

Collectively, I thank both of my advisors for their patience throughout these past few years, I realize now that it was not an easy task but I am forever grateful that you both took a chance on me.

To all of my lab mates in the Rajagopalan research group, past and present, including Dr. Adam Larkin, Dr. Era Jain, Dr. Gaurav Jain, Cigdem Arca, Brandon Veres, Sophia Orbach, Margaret Cassin, Andrew Ford, Rebekah Less and Kristen Sheerer, thank you for being there and listening to me with both personal and research related issues. All of

those late nights, afternoon coffees, and scientific debates are memories that I will cherish for the rest of my life. I wish you all nothing but the best.

To my lab mates in the Helm research group, Dr. Keith Ray, Dr. Sherry Hildreth, Evan Foley and Jody Jervis. Keith and Sherry, thank you for all of the help with proteomics and helping me learn mass spectrometry. Jody, thanks for your help with reagents and sample prep. Finally, thank you to all of you for all around good conversations.

## Table of contents

## List of figures

## List of tables

# Chapter 1: Introduction

## 1.1 Background and significance

The liver is a highly vascularized organ and performs many physiological functions including synthesis of blood plasma proteins, carbohydrate, lipid, and amino acid metabolism, biotransformation of drugs and environmental toxins and bile acid production [1-3]. The liver is divided into two major sections, the right and left lobes where each lobe is made of units known as lobules as shown schematically in **Figure 1**.

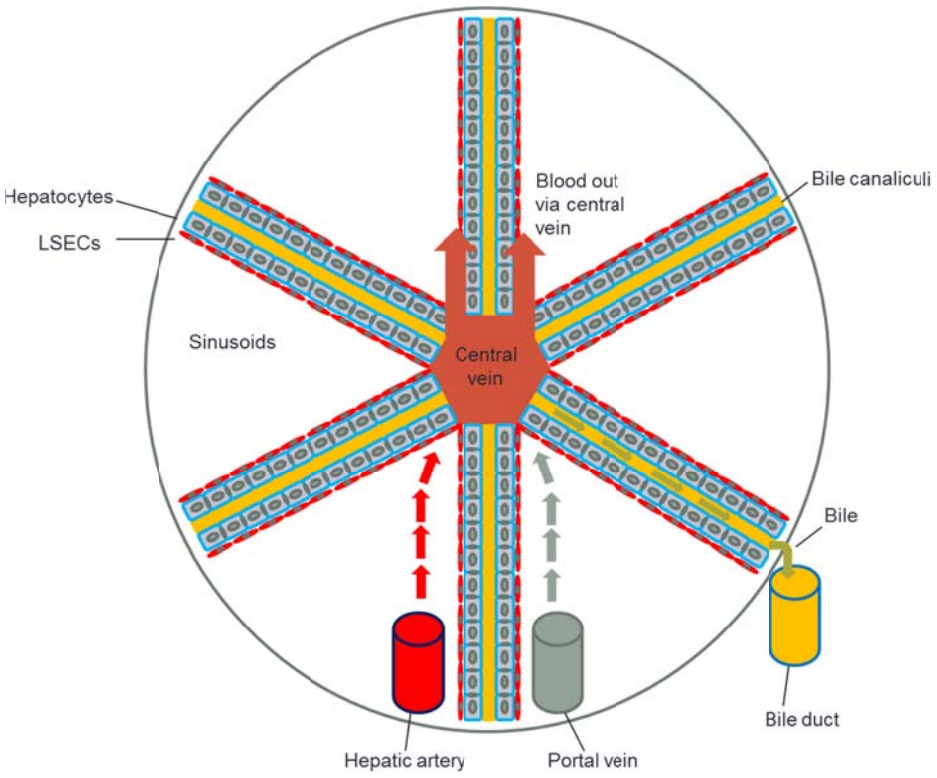


**Figure 1: Schematic of the liver lobule which consists of sinusoids where the exchange of macromolecules to and from the blood as well as bile transport occurs.**

Each lobule contains sinusoids, which are blood vessels that contain fenestrated endothelium. The sinusoid is where the transfer of nutrients and oxygen occurs between the blood and the hepatocytes, the parenchymal cells of the liver. These sinusoids are made of hepatic cords that radiate from the central vein with hepatocytes on both sides. Blood enters the

liver through both the portal vein from the gut and the hepatic artery from the heart and exits through the central vein [1]. The majority of the blood supply (~75%) comes from the portal vein, which stems from the spleen and gastrointestinal (GI) tract, with the remaining coming from the hepatic artery [4]. Bile canaliculi are present between plates of hepatocytes, allowing for the transport of bile to the bile duct. Bile from the bile duct is subsequently stored in the gallbladder.

The liver can be broken up into three distinct regions known as the periportal, midzonal and pericentral regions [3]. Oxygen concentrations vary across these regions [3, 5]. For example, oxygen concentrations at the periportal region range between 84-90 μM while at the pericentral region are 42-49 μM [6, 7]. In addition to varying oxygen concentrations, different metabolic functions, such as glucose and lipid metabolism, are performed in each of these regions [3, 8, 9]. While glycolysis is performed by all hepatocytes, it has been shown that this process is mainly performed in the pericentral region [3, 10-12]. Conversely, gluconeogenesis occurs mainly in the periportal region [10-12]. Studies have also shown that fatty acid β-oxidation occurs in the periportal region while lipogenesis occurs in the pericentral region [13-15].

Hepatocytes (appromiately 70% by volume) are the parenchymal cell of the liver and are responsible for most of the major functions performed by the organ. *In vivo*, the hepatocytes exhibit a polygonal morphology and have distinct apical and basal surfaces that aid in the maintenance of polarity of the cells [16]. The apical and basal surfaces also allow for the transport of molecules between the parenchyma, biliary system and the blood. For example, bile acids are transported through the bile canaliculi across the apical surface to the bile duct and albumin is transported along the basal surface where it is released into systemic circulation. The basal surfaces of hepatocytes are also in contact with the Space of Disse (SoD), allowing

exchange of waste, nutrients, as well as oxygen between the parenchyma and the blood. Thus, both of the apical and basal surfaces are essential and allow for maintenance of the highly differentiated state of hepatocytes and proper liver function [16]. The non-parenchymal cells (NPCs) of the liver include the liver sinusoidal endothelial cells (LSECs, approximately 10% by volume), Kupffer cells (KCs, approximately 5% by volume), hepatic stellate cells (HSCs, approximately 5% by volume), and other cell types, such as natural killer (NK) cells (approximately 10% by volume). Hepatocytes are separated from the NPCs by a protein rich interface known as the SoD, which contains ECM proteins, proteoglycans, glycosaminoglycans, and other molecules that help to maintain the highly differentiated state of hepatic cells [1, 17, 18]. *In vivo*, the thickness of the SoD ranges from 0.5 – 1 μm [18, 19]. Studies have shown a gradient of ECM components within the SoD exists, however, the predominant components are type I and type III collagens and fibronectin [20, 21].

LSECs line the sinusoidal wall and function as the scavengers [1, 22]. Studies have demonstrated that LSECs possess scavenger receptors (SRs) [22] such as SR-A [23], SR-B[24] SR-H [25] and also FC-λRIIb2 (Commonly referred to as SE-1) [26]. LSECs also exhibit high endocytotic activity enabling effective uptake of plasma proteins [27, 28], acetylated low density lipoproteins (AcLdL) [29], chylomicrons [30], lysosomal enzymes [31] and ECM components, such as collagen and hyaluronic acid [32-34]. LSECs play a role in the immune response via the uptake of viral particles and endotoxins such as lipopolysaccharides (LPS) [34-37]. LSECs have been described as a molecular sieve because they exhibit features called fenestrae, which are nanoscale pores that enable the passage of endogenous factors, such as oxygen, and waste between the blood and the parenchyma [1, 22]. The size of these fenestrae is species dependent and ranges between 100 nm – 200 nm in diameter [38].

KCs are the resident liver macrophages and are derived from circulating monocytes [39]. KCs are responsible for the removal of waste and cellular debris such as damaged red blood cells and their vesicles [1, 40, 41]. These cells predominantly reside in the hepatic lumen but can migrate between the endothelium and the parenchyma, and also possess high endocytotic activity [42]. Due to their location within the sinusoid, KCs are the first macrophages that come into contact with the bacteria and endotoxins derived from the GI tract highlighting their role as part of the immune response in the liver [43]. Studies have shown that KCs become activated in response to the endotoxin, LPS [44, 45] and activate the inflammatory pathways in hepatocytes via toll like receptor (TLR) signaling [44, 46-48]. KCs are also the main mediators of the acute phase response via secretion of pro-inflammatory cytokines such as interleukin-6 (IL-6) tumor necrosis factor α (TNF-α) and nitric oxide (NO) [49-51] and anti-inflammatory cytokines such as IL-10 and transforming growth factor-β (TGF-β) [49, 52]. KCs also secrete these same cytokines during liver regeneration [53-55].

HSCs typically reside in the SoD and are quiescent under healthy conditions [1]. Under healthy conditions, HSCs are responsible for the storage of retinoic acid and vitamin A (retinol) in their lipid droplets [1, 56, 57]. HSCs are also highly involved in ECM remodeling by synthesizing matrix metalloproteinases (MMPs) [58-60], which degrade ECM proteins. HSCs also synthesize tissue inhibitors of metalloproteinases (TIMPs), to regulate ECM degradation by binding to MMPs thus causing their inactivation [61-63]. However, during diseased states, such as liver fibrosis, an imbalance of this regulatory process occurs where increased TIMP expression leads to the inactivation of MMPs [64]. HSCs become activated as evident by the lack of lipid droplets and myofibroblastic morphology. They also exhibit proliferative and fibrogenic phenotypes resulting in the secretion of large amounts of ECM proteins such as type I and type

III collagens, in the Space of Disse, causing the progression of fibrosis [1, 56, 65, 66]. During fibrogenesis, ~ 4-8 fold increase in type I and type III collagen, ~8-fold increase in hyaluronan and ~2-fold increases in heparin sulfate concentrations over normal healthy conditions have been observed [67, 68].

### 1.2 *In vitro* hepatic cultures

Efforts to study the liver *in vitro* have mainly used hepatocytes cultured in monolayer or sandwiched between layers of collagen (**Figure 2**).

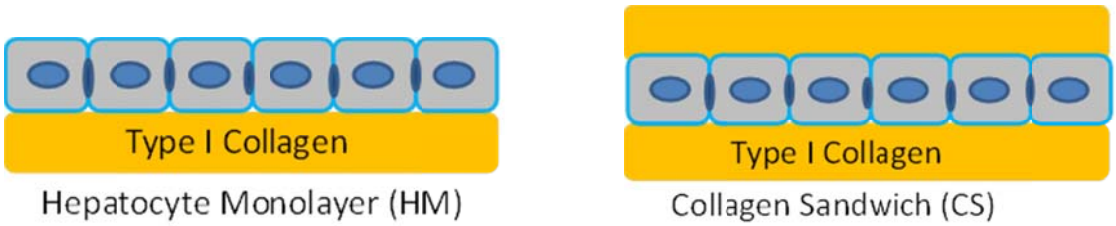


**Figure 2: Schematic representation of hepatocyte monolayers and collagen sandwich hepatocyte cultures.**

However, due to dedifferentiation, monolayers lose their hepatic phenotypes and functions beginning as early as 4 hours in culture, thus limiting their use for long term studies [69]. Collagen sandwich (CS) cultures maintain hepatocyte polarity and have been shown to promote stable hepatic functions, such as albumin and urea secretions, for up to six weeks in culture [70, 71]. Other studies have also used hepatocyte spheroids, which have been shown to maintain stable hepatic functions due to the presence of homotypic interactions [72-78]. However, due to the absence of a blood vessel structure, transport of oxygen and nutrients relies solely on diffusion [73]. Earlier studies have shown that oxygen diffusion is limited within spheroids, and is only exhibited up to 100 μm - 200 μm in depth, resulting in necrosis of the cells in the core [73, 79]. While HM, CS, and mono-cellular spheroids have all been widely studied, the lack heterotypic interactions with the NPC types limit their physiological relevance to *in vivo*

situations. To address this issue, co-cultures of hepatocytes and other cell types including LSECs [80], fibroblasts [81, 82], and other cell types [83, 84] have been developed and has been shown to maintain hepatic phenotypes for several weeks, highlighting the importance of heterotypic cellular interactions. Encapsulation of more than one cell type in spheroids has also been shown to enhance hepatic function and has been established as models for toxicological studies. Hepatocytes have been encapsulated in spheroids with fibroblasts [85, 86], HSCs [87], and with LSECs and fibroblasts together [88]. Chen *et al.* designed human ectopic artificial livers (HEALs) by encapsulating hepatocytes, fibroblasts and LSECs in a RGD (arginine-glycine-aspartic acid) modified poly(ethylene glycol) diacrylate gel [88]. They reported up to ~3-fold higher mRNA expression of the detoxification enzymes, Cytochrome p450 (CYP) 3A4, 1A2, 2D6, 2E1, and 2C in the 3D HEALs in comparison to 2D cultures. HEALs also exhibited sustained albumin and urea production over 8 days indicating that these cultures maintained hepatic functions. While these cultures facilitate heterotypic cellular interactions, they do not recapitulate the stratified architecture of the liver.

Thus, recent studies have focused upon development of relevant *in vitro* cultures that mimic both the stratified architecture and facilitate heterotypic interactions [19, 89-93]. Mimicking the SoD is the main focus of these studies where researchers have begun using synthetic materials [92, 94, 95], native ECM [93, 96, 97] and biomaterials [19, 89-91] to recreate the interface. Kasuya *et al.* utilized a microporous polyethylene terephthalate (PET) membrane to separate hepatocytes, bovine pulmonary microcapillary endothelial cells (BPMECs), and HSCs [92, 94, 95]. In this culture, hepatocyte and HSCs were seeded below the membrane, while BPMECs were seeded directly above. Varying pore sizes on the membrane ranging from 0.4 μm – 8 μm were used to determine which promoted the greatest extent of morphogenesis. It was determined

that direct contact between BPMECs and HSCs as facilitated by larger pore sizes cause increased migration of HSCs resulting in ~80% coverage of the top surface of the membrane after 14 days in culture [98]. This also resulted in ~60 % decreased coverage of BPMECs and a loss of their phenotype as measured by AcLdL staining, thus less morphogenesis was observed. However, the optimal pore size of 1 μm promoted HSCs contacts with the ECs which allowed for maintained phenotype for up to 40 days and thus, promoted morphogenesis. In a separate study, it was also shown that the extent of morphogenesis was also temporally regulated [99]. Induction of morphogenesis was performed by activating BPMECs via a Matrigel™ overlay method which has been shown to promote capillary tube formation using primary human umbilical vein endothelial cells (HUVECs) [100]. Upon 8 days of culture, HSCs were given enough time to make contact with the BPMECs before induction of morphogenesis. When Matrigel™ was added on day 8, morphogenesis decreased by ~ 40% as compared to when induction was performed on day 2. These results suggest highlight the importance of recapitulating the spatial characteristics of the liver. Jindal *et al*. developed a 3D model where hepatocytes were embedded within a type I collagen gel with rat heart microvessel endothelial cells (RHMECs) seeded directly above [96, 97]. Their results demonstrated that the excretion of proline by RHMECs resulted in ~2-fold increased albumin secretion during the first week of culture [96]. Upon addition of a competitive inhibitor of proline, albumin secretion decreased by up to ~60%. This indicates the presence of intercellular signaling via the diffusion of small molecules, plays a role in maintaining hepatic functions. This study was recently extended to include LSECs sandwiched above, below and in the same plane as the embedded hepatocytes and hepatic phenotypes and functions were compared among the three different configurations [101]. LSEC phenotype was measured by hepatic sinusoidal endothelial cell marker, cluster of differentiation

32b (CD32b), and was shown to be preserved for up to four weeks in culture when LSECs were present either below or in the same plane as the hepatocytes. Both of these configurations also exhibited up to ~2-fold higher albumin secretion over the 28 days as compared to cultures in which LSECs were seeded above the hepatocytes. However, urea productions did not differ among the culture conditions. The reasons for the differences in the observed trends were not addressed in this study. Nonetheless, this study supports the claim that both multicellular interactions and spatial orientation can enhance hepatic function. However, these studies were not able to capture all of the features of the SoD in terms of its mechanical and chemical properties, thus limiting its physiological relevance.

Another method that has been used to mimic the SoD employs polyelectrolyte multilayers (PEMs) [19, 89, 90]. PEMs are thin films that assembled using a layer-by-layer (LbL) deposition method [102, 103]. These films are assembled by sequentially depositing oppositely charged polyelectrolytes (PEs) on a surface to the desired amount of layers [104]. Deposition of each sequential PE is driven by electrostatic interactions between each layer [103, 105]. LbL provides the advantages of controlling the film thickness and tuning the physical properties of the resulting film by changes in pH, concentration, and deposition time of the PE solutions [105-108]. *In vitro* liver models using PEMs, which were assembled using biocompatible cationic and anionic PEs, were either directly deposited on cells [89-91] or assembled on an inert substrate prior to culture [19, 106]. Kim *et al.* deposited a PEM comprising alternating layers of the PEs, chitosan (cationic layer) and hyaluronic acid (anionic layer), directly above a monolayer of primary rat hepatocytes [89, 90]. Human LSECs were seeded above the PEM, resulting in all hepatic cells exhibiting differentiated characteristics [89]. Phenotypes of each of the individual cells were preserved in these cultures as indicated by di-peptidyl peptidase IV immunostaining

for the presence of bile canaliculi in the hepatocytes and AcLdL uptake, a functional marker of LSECs [89]. Hepatic functions were also maintained in the liver models which exhibited up to ~2-fold increased albumin secretion in liver models over a 7 day culture period. These values were similar to what was observed for CS cultures, whereas HM cultures exhibited ~50% decrease [89]. Additionally, ~40% - 45% decrease in urea production was also observed in these cultures over a seven day culture period, similar to what was observed in CS cultures. HMs exhibited ~70% decrease in urea over the same time period. Additionally, CYP1A1/2 enzyme activities were also measured in the liver models and were shown to exhibit ~4-16 fold increase as compared to HM, CS, hepatocyte-PEM cultures, and co-cultures. The low viscosity (~1.6 mPa s - 2 mPa s) of the PEMs was similar to that of water indicating a high degree of hydration promoting the potential diffusion of signaling molecules, which would enable heterotypic cellular communication. This work was also performed using rat LSECs and was cultured over 12 days [90]. LSECs in the 3D liver models exhibited maintenance of the phenotypic marker, sinusoidal endothelial 1 (SE-1). These liver models also exhibited ~3-6 fold increased albumin secretions on day 12 over their 2D counterparts and HMs as compared to values on day 4 of culture [90]. Up to ~ 20% increased urea production was also observed over the culture period in the liver models whereas HMs exhibited ~60% decrease. Detzel *et al.* also showed that these liver models were able to maintain physiologically relevant ratios of cholic acid:cheonodioxycholic acid (CA:CDCA) between ~3.1 - 6.3 indicating maintenance of bile homeostasis, an important function in liver metabolism [91]. This work highlights that cell polarity, heterotypic cellular interactions, as well as mimicking the spatial characteristics are all essential for maintenance of hepatic functions and phenotypes.

Larkin *et al.* extended this work using a detachable, optically transparent PEM that exhibited a Young's modulus (YM) value of approximately 41 kPa under hydrated conditions [19, 106]. This YM value is similar to what has been reported for bulk liver tissues [19, 106]. 3D organotypic liver models incorporating hepatocytes, LSECs, and KCs were assembled using these PEMs as shown schematically in **Figure 3.**

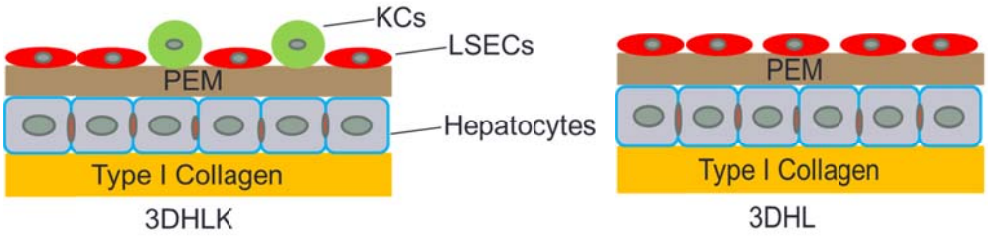


**Figure 3: Schematic of the 3D liver models consisting of hepatocytes, LSECs and KCs (3DHLK) and hepatocytes and LSECs (3DHL).**

In this figure, "H", "L", and "K" are hepatocytes, LSECs, and KCs respectively. These 3D models maintained expression of SE-1 and CD163, phenotypic markers for rat LSECs and rat KCs, respectively [19]. Hepatic functions such as albumin, urea, and CYP1A1 isozyme activity were also assessed. Albumin secretions were significantly higher in 3DHLK and 3DHL as compared to HM, CS, and their 2D co-culture counterparts throughout a 12 day culture period while urea production remained stable [19]. CYP1A1 activity exhibited ~15 fold increase in 3DHL cultures over a 12 day culture while ~50% less activity was shown in 3DHLK models. Additionally, in contrast to their monocellular and 2D counterparts, only 3D cultures exhibited proliferation of all cell types to cellular ratios similar to what has been observed *in vivo.* After 16 days of culture, the ratio of hepatocyte:LSECs was ~ 6.6- 6.7:1 in both the 3DHL and 3DHLK models while the ratio of hepatocytes:KCs was ~12.3:1 in the 3DHLK models [19]. Proliferation of the cell types were corroborated by the analysis of transcriptional signatures where gene sets implicated in liver development and regeneration, such as Proteinaceous Extracellular Matrix

and NCAM1 interactions, was among the top 30 that were up-regulated in 3DHLK as compared to 3DHL hepatocytes. Additional gene expression analyses performed on the 3DHLK hepatocytes also showed the up-regulation of the gene set, netpath IL-4 up, suggesting that this pathway was active. This result suggests that cytokine signaling could be a potential mediator in allowing the maintenance of hepatic phenotypes and functions, along with the observed proliferation trends as compared to 3DHL, HM and CS hepatocytes. The *in vivo*-like characteristics exhibited by these liver models makes them ideal to study a wide variety of processes including intercellular signaling and key factors associated with the maintenance of liver functions. A key aspect of these models is the ease of separation of each individual component. The ability to isolate individual model components allows for studies of the biochemistry of each cell type via investigations of their proteomes. Studies such as these would aid in a deeper understanding of how liver functions are affected by each cell type and can be performed using mass spectrometry.

### 1.3 Mass spectrometry

In general, mass spectrometry (MS) is an analytical technique that relies on the measurement of gas phase ions to characterize the structure and abundance of a variety of molecules via the mass to charge (*m/z*) ratio. This process is usually preceded by a liquid chromatography step for separation of these molecules by mass (size exclusion), electrostatic interactions (cationic or anionic), or phase (hydrophilic or hydrophobic interactions) before entry into the mass spectrometer [109]. A liquid sample containing the analyte(s) of interest is first ionized using either electrical or chemical ionization. One of the most commonly used methods for the analysis of peptides from digested proteins is electrospray ionization (ESI) where an acidic solution containing peptides is sprayed through a nozzle with an applied positively-

charged voltage. The application of dry heated nitrogen gas to the spray induces evaporation of the carrier solvent leaving the positively-charged peptides in the gas phase. These peptide ions (so-called "precursor" ions) travel through the mass analyzer where another voltage is applied that generates an electric field causing their acceleration. These ions enter a field free region to a detector that records the *m/z* along with the ion intensity. Since the chromatographic separation prior to the ionization step separates the peptides based upon a physiochemical feature, there will be a retention time for each ion along with a *m/z* value and ion intensity for each scan during the MS analysis. The *m/z* value combined with the retention time provides an exact mass retention time (EMRT) pair. When combined with ion intensity values for each scan, the combined EMRT and ion intensity is essentially a recording of a peptide peak in a normal chromatographic separation. The maximum ion intensity for an EMRT can be used to quantify the relative abundance of peptides between experimental conditions, but gives no information on the amino acid sequence for the particular EMRT.

Sequence information in MS-based proteomics is obtained through the use of a duty cycle where the mass spectrometer is programmed to switch between collecting the precursor ion EMRT data and subsequently fragmenting these ions. Fragmentation is induced through the application of high energy, which causes collision-induced fragmentation, resulting in product ions. This type of experiment is often referred to as tandem mass spectrometry or MS/MS. This fragmentation leads to the formation of b- and y- ions, resulting from ions that contain the N and C-terminus of the peptides respectively. The amino acid sequence can be deduced by calculating the residue masses from adjacent members of the ion series relative to the known masses of amino acids. The combined EMRT and associated fragmentation pattern (MS and MS/MS) are compared to predicted fragments from an *in silico* database to identify the peptide along with the

protein or proteins it was originally a part of. The relative peptide abundances can be calculated based on the intensity of the ions from the MS experiments across experimental conditions, which can then be used as a measure for relative changes in protein levels across similar sample types. This is commonly referred to as shotgun proteomics. While this process can provide relative abundances, such measures do not provide absolute concentrations, as each ion will have characteristic ionization and fragmentation efficiencies.

### 1.4 Data dependent and data independent analysis

Recent advances in liquid chromatography and tandem mass spectrometry (LC-MS/MS) have revolutionized the fields of proteomics [110, 111] to the point where it is now relatively routine to obtain protein profiles by quantifying peptides from any biological specimen with a sequenced genome. There are two types of analyses that can be characterized as shotgun proteomic techniques, data dependent analysis (DDA) and data independent analysis (DIA). Both techniques share a common goal that seeks to quantify relative protein abundances, study protein-protein interactions and characterize post-translational modifications (PTMs) in complex biological samples using peptides that are analyzed via LC-MS/MS (**Figure 4)** [112].

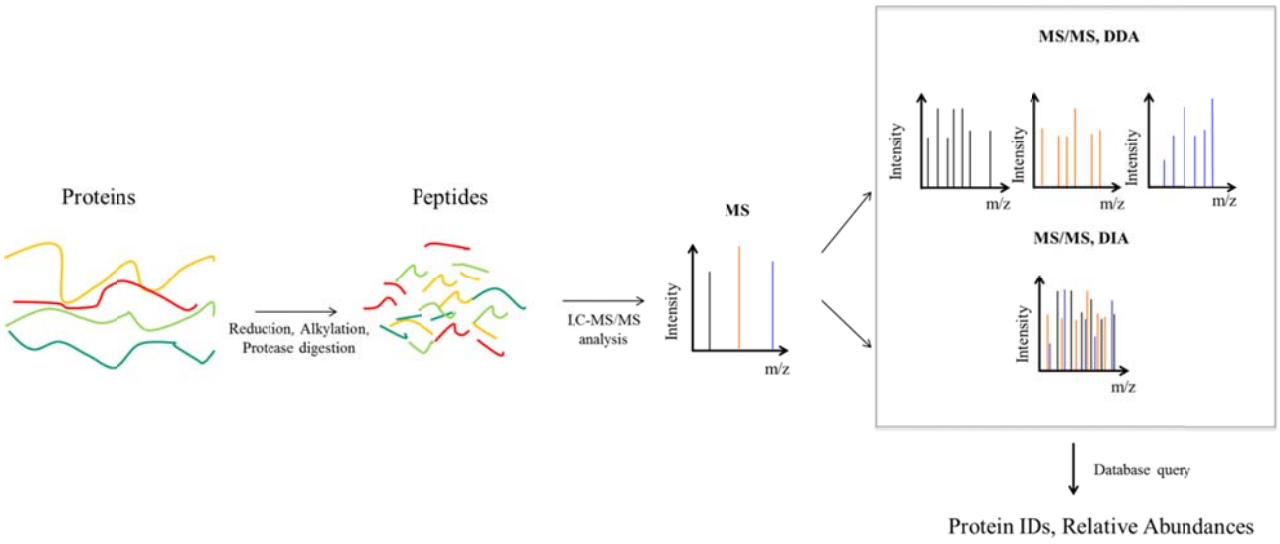


**Figure 4: Overview of the shotgun proteomics approach using both DDA and DIA approaches. The initial steps for both approaches are the same (see text for details). The main difference between DDA and DIA analyses reside the way in which peptides are fragmented. DDA uses an *a priori* set of criteria to fragment isolated peptides directly matching precursor and fragment ions. DIA methods fragment all peptides at once, relying upon time matching precursors and fragments through the use of gas phase ion mobility and vendor specific software. The resulting data sets are essentially the same (precursor and fragment ions), and this information is used in database queries to determine protein identifications (IDs) and subsequently relative abundances between experimental conditions.**

The processing of samples for DDA and DIA are the same as shown in **Figure 4**. Proteins are isolated from each experimental specimen and subjected to reduction, alkylation and protease digestion, producing peptides amenable to chromatographic separation, ionization, fragmentation and analysis. This "bottom up" approach is preferred for complex protein lysates as peptides are easier to separate, detect and analyze via LC-MS/MS, essentially due to their lower molecular weights relative to their intact counterparts [110]. Precursor ions and their respective fragments are obtained from the analysis and used to sequence a peptide that is queried against a protein database, such as UniProt, for identification. Relative protein levels can be obtained by comparing ion intensities (MS) across experimental conditions. Functional enrichment and targeted assays can be used to focus on particular processes, pathways or metabolites. The difference between DDA and DIA resides in the method by which fragmentation is accomplished (**Figure 4**).

In DDA experiments, select precursor ions are analyzed via LC-MS/MS based on criteria such as intensity, which is set *a priori*. This technique isolates particular precursor ions and fragments them one at a time, providing a direct link between the precursor and fragment ions. In a typical DDA experiment the instrument will acquire one precursor ion scan followed by 10 fragment ion scan, for the 10 most abundant precursor ions. As a consequence, DDA experiments spend a considerable amount of time collecting fragmentation data while the separation is still occurring. In contrast, a DIA experiment fragments all precursor ions at once switching between one precursor ion scan and one fragmentation scan. Thus DIA experiments can provide more information relative to DDA [113]. While the DIA experiment increases the amount of information that can be obtained from a sample, the downstream data analysis requires specialized software for extracting the sequence and protein identifications. Instrumental design is such that a DDA mass spectrometer cannot perform DIA experiments and *vice versa* as a DIA-based instrument require additional functional units that aid in matching precursor and fragment ions. The mass spectrometer used in the work described in this thesis (Waters™ Synapt G2-S), makes use of a drift tube where precursor ions of different charge states and sizes are separated in time followed by fragmentation. The timing of elution from the drift tube and the downstream fragment ions are then matched using proprietary software to permit assignment of precursor ions to their corresponding fragment ions. These matched sets are then queried against a database for peptide identification.

## 1.5 Protease digestion

One of the key features of a shotgun, bottom up approach is the analysis of proteins based on their peptide components [114]. Peptide generation is invariably accomplished by protease digestions with either trypsin [115, 116], lysyl endopeptidase [117-119] or a sequential

combination of the two [120-123]. Trypsin selectively cleaves proteins on the C-terminal side of arginine and lysine residues. Lysyl endopeptidase cleaves at the C-terminal side of lysine. One main difference between these two proteases is that their activities vary with the environment. Most digestions are aided by the use of strong denaturing agents, such as urea, allowing more access to the cleavage sites [124, 125]. However, trypsin activity has been shown to be limited under these harsh conditions where urea concentrations are typically 6-8 M [121]. Conversely, lysyl endopeptidase is still active under these conditions and is able to provide cleavage when protein denaturation is maximized [122, 126-128]. Recent studies have shown that the sequential combination of lysyl endopeptidase followed by trypsin permits more complete digestion [127, 129, 130]. Digestion with lysyl endopeptidase is typically done first because of its preserved activity in the presence of high concentrations of urea. Trypsin is subsequently added after dilution of the denaturing agent and the digestion is allowed to continue. This two-step process increases the amount of peptides that do not have "missed cleavages" or peptides that have sites that were not cleaved by either of the two proteases. Missed cleavages are problematic for database searching as allowing for high levels increases the search time dramatically due to the possibility of more potential peptides. Additionally, larger peptides typically do not ionize as well, reducing their overall ion intensities. Wiśniewski *et al.* performed a comparison between the sequential combination of the lysyl endopeptidase/trypsin as compared to trypsin alone using HeLa cells [120]. They observed ~2-fold increase in the amount of unique peptides resulting in ~30% more protein identifications when using sequential digestion. In another study used to compare digestion efficiencies, Glatter *et al.* measured the amount of fully cleaved (FCP) and missed cleaved peptides (MCP) in *saccharomyces cerevisiae* cultures [121]. Their results showed ~ 9% increase in FCPs and ~ 21% decrease in MCPs using the sequential combination of

lysyl endopeptidase followed by trypsin as compared to trypsin alone. However, this only resulted in ~ 2% increase in protein identification. Saveliev *et al.* used a different approach in which both trypsin and lysyl endopeptidase were added simultaneously under non-denaturing conditions to HeLa cells and yeast protein extract [131]. They demonstrated ~ 9.3 % and ~20% increase in protein identifications in HeLa and yeast cells respectively using sequential digestion. Taken together, these results demonstrate the advantages to the use of multiple proteases for protein digestion.

## 1.6 Quantification methods

Quantification has become a requirement in the field of proteomics especially with regards to biological studies where it is crucial to interpret the response of cells to their environment [132, 133]. This can be done through label or label free quantification which can provide absolute or relative quantification of proteins. Some labeling strategies that are typically employed are stable isotope labeling of amino acids (SILAC) and isobaric tags for relative and absolute quantitation (iTRAQ). SILAC relies on the incorporation of stable isotopes such as $^{15}N$ or $^{13}C$ into metabolically active cells. Cells are typically grown in media that lacks an essential amino acid but is supplemented by a non-radioactive isotopic form of that same constituent. As cell division occurs, each natural amino acid will be subsequently be replaced by its labeled form [134]. Studies have shown no adverse effects to NIH-3T3 cells in terms of morphology, doubling time and differentiation using this method [135]. This method has also been used in for determination of metabolic differences between a murine hepatocarcinoma cell line (Hepa1-6) and primary hepatocytes [136]. Relative abundances of proteins can be determined by measuring the intensity of the labeled peptides, which would have the same sequence but altered mass, as compared to those that are unlabeled. Alternatively, iTRAQ relies on the use of tags that bind to

amine groups of peptides [134]. These iTRAQ tags are all isobaric and consist of an amine reactive group, a reporter group, and a balance group making them indistinguishable during the LC step. During MS/MS fragmentation, the reporter ion is released and has a distinct mass [137]. These reporter ions can be used to measure the relative abundance of peptides which corresponds to the proteins of interest. Although these techniques are generally considered more accurate, they can become very expensive and laborious [138]. Label free quantification (LFQ) provides an alternative to these methods. LFQ relies on comparing intensities of peptide ions which has been shown to be directly related to the abundance of the protein [139]. LC-MS/MS data from a DIA experiment first has to be processed through specialized software, such as Protein Lynx Global Server (PLGS), for protein identification [140]. This program matches fragment ions with their associated precursors based on elution time and ion mobility profiles as described earlier. These peptides are then matched to proteins in a database such as provided by UniProt. To quantify the abundance of these proteins, techniques such as the TOP3 method are typically employed where the sum of the three most intense ions for a given protein are compared across experimental conditions [141, 142]. The commercial software Scaffold, and the open-source ISOQuant are available for these types of quantitative analyses. For biological interpretation of these results methods such as functional enrichment are typically utilized for statistical overrepresentation and identification of associated pathways as compared to a reference genome [143].

## 1.7 Liver proteomics

Proteomic investigations of liver cultures in the literature are somewhat limited. Most studies have focused upon characterizing the proteome using whole liver tissue [144-146], hepatocytes cultured in either sandwich or monolayer configurations [147-149] or specific

cellular compartments such as the plasma membranes or mitochondria [150-152]. Similar to many previous studies, these are also limited to relatively short culture periods, usually not exceeding 24 hours. Using freshly isolated whole liver tissue, elucidation of murine liver proteome identified approximately 2200 proteins [144]. Upon functional enrichment using gene ontology (GO), ~1500 proteins were annotated to the term metabolism ($p$-value = $7.2x10^{-37}$). Other studies have also been conducted using whole liver tissue in order to elucidate the mechanisms of liver regeneration after a partial hepatectomy (PHx) [153-156]. Kumar *et al.* observed up-regulation of processes corresponding to fatty acid and glucose metabolism through the first 3 hours of liver regeneration in mice subjected to either 70% or 90% PHx [153]. Additionally, increases in the cytokine IL-6 was also observed [157]. Similar trends were also observed 168 hours after 70% PHx where fatty acid, amino acid and bile acid metabolic processes were up-regulated as compared to sham operated rats [154]. Collectively, the results suggest a shift towards lipid metabolism during the liver regeneration. While these studies have broadened our understanding of liver biology, the effects of individual cell types was not addressed. Therefore, studies have also been performed on characterizing the differences between primary hepatocytes and cell lines. Hepa 1-6 cells, a murine hepatoma cell line, exhibited ~2-fold lower levels in ~2000 proteins as compared to primary murine hepatocytes cultured for 14 hours [136]. Proteins found in reduced levels included CYPs, mitochondrial proteins, and proteins related to fatty acid metabolism. The proteomes of the hepatoma cell lines, Hep3B and HepG2 cells, have also been compared to primary human hepatocytes [149]. Increased levels of vimentin and caldesmon were observed in both cell lines suggesting that they exhibited more similar proteomes to mesenchymal cells than primary hepatocytes. Additionally, proteins related to proliferation and cell motility were present in higher levels in the cell lines.

Detoxification enzyme levels were preserved in primary hepatocytes. These results demonstrate an inherent difference between hepatic cell lines and primary hepatocytes.

Dedifferentiation of cultured primary hepatocytes has also recently been evaluated. Cultured rat HMs exhibited increases in proteins related to cytoskeletal remodeling and cell migration over a 72 hour culture period as compared to Matrigel™ sandwiched cultures [148]. Additionally, reduced levels of proteins related to lipid, cholesterol and fatty acid metabolism were also observed. Matrigel™ sandwiched cultures consisting of primary human hepatocytes also exhibited loss of key liver metabolic functions such as glycolysis, xenobiotic metabolism and alcohol metabolic processes when cultured for 15 days as compared to freshly isolated cells [147]. However, these investigations do not take into account the interactions with the non-parenchymal cells. To begin addressing this, a proteomic analysis on all of the individual liver cell types (hepatocytes, LSECs, KCs, HSCs and cholangiocytes) was performed resulting in the identification of over 11,000 proteins, constructing the largest published murine liver proteome to date [158]. This allowed for the characterization of physiological roles for each liver cell type. For example, the top three most abundant proteins in hepatocytes were fatty acid binding protein 1 (Fabp1), carbamoyl phosphate synthase (Cps1) and glutathione-s-transferase (Gstp1) suggesting that these cells are involved in lipid metabolism, the urea cycle and biotransformation. KCs and cholangiocytes were enriched in S100 proteins and prothymosin proteins respectively, indicating their involvement in the immune response. HSCs were highly enriched in intracellular trafficking proteins such as annexins and Rab GTPases. LSECs were enriched in cytoskeletal proteins such as actins, myosins and tropomyosins and asialoglycoprotein receptors, highlighting their roles in transducing mechanical forces and membrane trafficking. Within this same study, proteomic changes induced by dedifferentiation

of primary hepatocytes were also evaluated over a 7 day culture where increases in cytoskeletal proteins were observed, matching previous observations [147, 148]. While this study has begun to elucidate the proteome of each of the liver cell types individually, the global changes induced on one cell type in the presence and absence of another has only been characterized for some proteins, including but not limited to, albumin, urea and some CYPs. Only two studies thus far have begun to elucidate these changes, although not at the proteomic level [96, 159]. Hepatocytes embedded within collagen (CS) and adipocyte-derived (Adipogel) were used to evaluate the effect of ECM on metabolites [159]. Changes in glucose, amino acid, and metabolic fluxes in the media led to the conclusion that the Adipogel matrix increased TCA cycle metabolism, urea cycle fluxes and amino acid uptake and transamination reactions throughout the culture period. This resulted in enhanced hepatic functions indicating that soluble factors from adipocytes contributed to these trends. While these studies have provided insight into overall liver function, additional studies with multicellular *in vitro* systems are needed to more fully understand ECM development and cellular signaling processes. Studies such as these would allow for a deeper understanding of liver biology and pathology. Considering the current body of information on organotypic liver models, there is a need for a proteomic evaluation of these systems to provide a more unbiased view of performance. The objectives of the work performed and described in this thesis are as follows:

1. Study the changes in the hepatocyte proteome in the presence and absence of LSECs in 3DHL organotypic liver models.
2. Study the changes in the PEM as a result of cell culture in the presence and absence of LSECs.
3. Characterize the proteome of LSEC monolayers.

# Chapter 2: Studying the changes in the hepatocyte proteome and PEMs in the presence and absence of LSECs in 3DHL organotypic liver models

In this chapter, contributions were made by Sophia M. Orbach and Margaret E. Cassin from the Rajagopalan research group. Sophia M. Orbach assembled the liver models and Margaret E. Cassin assembled the PEMs. All sample preparation and proteomic analyses were performed by Lucas T. Vu.

## 2.1 Introduction

The liver is a highly vascularized organ that performs many essential metabolic functions, including lipid, cholesterol, and carbohydrate metabolism [1]. Other liver functions include the biotransformation of toxins and xenobiotics to substances that can be excreted [1, 3]. The majority of these functions are carried out by the hepatocytes, the parenchymal cells that constitute about 80% of a mammalian liver's cell mass [1, 3]. The non-parenchymal cells (NPCs) include the liver sinusoidal endothelial cells (LSECs), Kupffer cells (KCs), hepatic stellate cells (HSCs), and other cell types such as those involved in the immune response (*i.e.*, natural killer cells) [1, 49]. Hepatocytes are separated from NPCs *in vivo* by a protein-rich interface that contains extracellular matrix (ECM) proteins, proteoglycans, glycosaminoglycans and other molecules that help maintain the highly differentiated state of hepatic cells [1]. This interfacial region, termed as the Space of Disse (SoD), is where the mass transfer between blood plasma and liver cells takes place [160].

Efforts to study the liver *in vitro* have mainly used hepatocytes cultured in monolayers (hepatocyte monolayers, HMs) or sandwiched between layers of type I collagen (collagen sandwich, CS) [70, 71, 147, 148, 161]. While monolayers begin to lose hepatic phenotypes within 4 hours [69], CS cultures have been shown to promote stable hepatic functions for up to six weeks [70, 71]. HM and CS have been widely studied, but lack of heterotypic interactions

with NPCs limiting their physiological relevance to *in vivo* situations. To address this issue, co-cultures of hepatocytes and NPCs have been developed and were shown to maintain hepatic phenotypes for several weeks [74, 75, 80-84]. Encapsulation of one or more cell types in spheroids has also been shown to enhance hepatic functions such as albumin, urea, and cytochrome p450 enzyme activities and have been established as models for toxicological studies [85, 87, 88, 162-164]. While these cultures facilitate cell-cell interactions, they do not recapitulate the stratified architecture of the liver [165].

An *in vitro* liver model that incorporated a polyelectrolyte multilayer (PEM) as a SoD mimic has recently been described [19, 89, 90]. These PEMs are thin films, composed of the biocompatible polyelectrolytes, which exhibit physical and chemical properties similar to the bulk liver and the Space of Disse. The low viscosity of these PEMs allows for the diffusion of soluble molecules enabling for heterotypic cellular communications. Models incorporating hepatocytes, LSECs, and KCs were assembled used the PEM to separate the cell types and were arranged to mimic the three dimensional *in vivo* architecture. These models exhibited maintenance of hepatic phenotypes and functions throughout a 16-day culture period and exhibited cellular ratios similar to those observed *in vivo* [19]. One main advantage to the use of these liver models is the ease of separation of the individual components. Therefore, various combinations of hepatocytes, PEMs and NPCs can be constructed and evaluated, allowing insights to both cell-cell communication and metabolic processes [19, 89, 90].

Previous work on liver models directed towards understanding signaling events typically evaluate processes at the transcriptional level [19, 81, 88, 166, 167]. Comparison of CS cultures to HMs suggested up-regulation of genes related to alcohol, cholesterol, fatty acid, xenobiotic, and carbohydrate metabolism [166]. To expand this further, the genomic signatures of 3D PEM-

based liver models consisting of hepatocytes, KCs and LSECs were compared against those without KCs [166]. It was determined that gene sets related to liver development, proliferation, and the interleukin-4 (IL-4) pathway were up-regulated in the presence of KCs, suggesting modulation of these processes through intercellular signaling.

Transcriptional profiling does not account for control at post-transcriptional or post-translational levels [110]. As a result, there is a poor correlation between transcript and protein abundances with time-matched samples [146, 158, 168-170]. Untargeted proteomic analysis can provide insight into protein abundances, which may not directly reflect enzymatic activities. Nonetheless, the determination of protein abundances can contribute to understanding liver physiological processes, including the effects of the local environment. Abundance changes can then be evaluated in subsequent studies using targeted approaches and/or enzyme activity measurements. These proteomic datasets can add to the body of information required to model and eventually predict performance through application of the tools of systems biology.

Most liver proteome studies have been performed on single cell types and/or cell lines, generally with an emphasis on defining primary versus. cell line differences [136, 149] or evaluating the dedifferentiation of primary hepatocytes [147, 148]. Primary rat hepatocyte dedifferentiation was evaluated by comparing protein profiles of HMs to those sandwiched with collagen and the commercial matrix Matrigel™ where it was shown that the sandwich constructs limited dedifferentiation [148]. Another recent comprehensive study of freshly isolated mouse primary liver cells (hepatocytes, LSECs, KCs, HSCs, and cholangiocytes) resulted in identification of over 11,000 proteins. In this same study, hepatocyte dedifferentiation was also evaluated, where enrichment of structural proteins such as the annexins were shown to be indicative of this process [158]. While these studies provide an initial view of liver proteome

landscape, evaluation of the effects of NPCs and the ECM on hepatocyte proteomes has not been explored over extended culture periods. We report here on the effects of a PEM and LSECs on hepatocyte proteomes in 3D organotypic liver models. To the best of our knowledge, this is the first study to investigate these effects on hepatocyte proteomes allowing for insights into intercellular signaling and hepatic biochemistry.

## 2.2 Materials and methods

### 2.2.1 Chemicals and reagents

Cell culture supplies including Dulbecco's Modified Eagle Medium (DMEM), phosphate-buffered saline (PBS), penicillin, streptomycin and human plasma fibronectin and trypsin (0.25% EDTA) were purchased from Life Technologies (Grand Island, NY). 4-[2-hydroxyethyl] piperazine-1-ethanesulfonic acid (HEPES), glucagon, glutaraldehyde, ethylenediaminetetraacetic acid (EDTA), hyaluronic acid (HA), hydrocortisone, Percoll, Type IV collagenase, chloroform, ammonium bicarbonate (AmBic), urea, trifluoroacetic acid (TFA), sodium 3-hydroxybutyrate, lithium acetoacetate and mass spectrometry grade trypsin and endothelial cell growth supplement were purchased from Sigma Aldrich (St. Louis, MO). Mass spectrometry grade lysyl endopeptidase (Lys-C) was purchased from Wako (Richmond, VA). LC-MS grade solvents were purchased from Spectrum Chemicals (New Brunswick, NJ). All other chemicals, unless noted otherwise, were purchased from Fisher Scientific (Pittsburgh, PA).

### 2.2.2 Isolation and culture of hepatocytes and non-parenchymal cells

The primary hepatocytes and LSECs were harvested from two adult female Lewis rats (Harlan, Dublin, VA) that weighed between 170 and 200 grams. Animal care and surgical procedures were conducted as per procedures approved by Virginia Polytechnic Institute and State University's Institutional Animal Care and Use Committee. Hepatocytes were isolated

using a two-step collagenase perfusion as previously described [19, 89, 90, 171]. Viability of isolated hepatocytes were ≥ 97% and was determined via trypan blue exclusion. Hepatocytes were cultured on a type I collagen coated 12-well plates at a density of 500,000 cells per well. Hepatocyte cultures were maintained in high glucose (25mM) DMEM supplemented with 10% (v/v) heat inactivated fetal bovine serum (FBS), 200 U/mL penicillin and 200 μg/mL streptomycin, 0.5 U/mL insulin, 4 nM glucagon, and 16 μM hydrocortisone. Media exchange was performed daily. LSECs were purified using a differential adhesion method [19, 90] and were cultured on a fibronectin coated flask. LSECs were maintained in endothelial cell medium consisting of Media 199 supplemented with 10% (v/v) heat inactivated FBS, 100 U/mL penicillin and 100 μg/mL streptomycin, and 30 μg/mL endothelial cell growth supplement.

### 2.2.3 Type I collagen isolation

Type I collagen was isolated from rat tail tendons as previously reported [71, 172]. Briefly, tendons were dissected from tails and dissolved in a 3% acetic acid solution overnight at 4°C. The solution was subsequently passed through cheesecloth filters and centrifuged at 13,000 *x g* for 2 hours at 4°C. The supernatant was precipitated using 30% (w/v) sodium chloride and the resultant precipitate was dissolved in 0.6% (v/v) acetic acid for 48 hours at 4°C. The solution was dialyzed against 1 mM hydrochloric acid and sterilized by chloroform. The concentration of collagen was determined by measuring the optical density at 280 nm.

### 2.2.4 Polyelectrolyte multilayer (PEM) assembly

Type I Collagen (cationic) and HA (anionic) were used for the assembly of PEMs using methods as previously described [19, 106]. Collagen was diluted in 1% (v/v) acetic acid and HA was dissolved in 18 MΩ cm water. Both solutions were maintained at a concentration of 1.5 mg/mL and a pH of 4.0. PEMs were assembled on a hydrophobic polytetrafluoroethylene

(PTFE) substrate (McMaster-Carr, Atlanta, GA) using a robotic deposition system (NanoStrata Tallahassee, FL). The PTFE substrates were sonicated in toluene for one hour, rinsed in 18 MΩ cm water, and dried overnight. Water contact angle measurements were used to verify the hydrophobicity of the substrate and ranged between 110°-115° (Averaged over 10 measurements per substrate). Deposition times of 30 min were used for each polyelectrolyte with a 10 minute rinse in 18 MΩ cm water maintained at a pH of 4.0 between each deposition. The PEMs used in these studies consisted of 15 bilayers (BL). A BL is defined as the deposition of one cationic and one anionic layer. PEMs were cross-linked with 8% (w/v) glutaraldehyde for 30 seconds, rinsed in deionized (DI) water for 48 hours, dried and stored at room temperature. Prior to cell culture, PEMs were sterilized under germicidal UV for 1 hour.

**2.2.5 Liver model assembly**

Hepatocytes were cultured on a type I collagen gel for 72 hours. The PEMs were overlaid above the hepatocytes and were hydrated with hepatocyte media for 1 hour at 37°C. LSECs were then seeded above the PEMs at a density of 25,000 cells per well to form the three-dimensional liver model, which will be referred to as 3DHL throughout. “H” and “L” refer to the hepatocytes and LSECs respectively. 3DH liver models were formed by overlaying the PEMs, but without the addition of LSECs. The 3DHL, 3DH and HM cultures were maintained for three days with the media exchanged every 24 hours. Spent culture medium was snap frozen in liquid nitrogen and stored at -80°C. All experiments were performed in triplicate.

**2.2.6 Hepatocyte isolation and processing of lysates**

Hepatocytes were separated from both the 3DHL and 3DH liver models by lifting the PEM from the culture. The hepatocytes on the underlying gel were washed with PBS and released from the collagen gel using a 0.1% collagenase solution in Krebs-Ringer buffer. HM cultures were

subjected to the same digestion with collagenase. Hepatocytes were collected by centrifugation at 800 *x g* for 2 minutes and were subsequently lysed and treated with a protease inhibitor cocktail (Sigma-Aldrich). The lysis buffer contained the following components: 4.3 mM Tris-HCl, 660 μM Tris, 500 μM EDTA, 15 mM NaCl, 350 μM SDS, 0.1% (v/v) Triton X-100, 310 μM sodium azide and 150 μM sodium vanadate and was supplemented with a protease inhibitor (PI) cocktail. The PI cocktail contained 104mM 4-(2-Aminoethyl) benzenesulfonyl fluoride hydrochloride (AEBSF), 80 μM Aprotinin, 4 mM Bestatin, 1.4 mM epoxide 64 (E-64), 2 mM Leupeptin and 1.5 mM Pepstatin A (Sigma-Aldrich). Protein concentrations were determined using a commercial BCA protein assay kit (ThermoFisher). LC-MS grade methanol was added to hepatocyte lysates (70 μg) and incubated at -80°C overnight. Samples were centrifuged (13,000 *x g*, 20 min) and the protein pellets were dried in a vacuum concentrator and re-suspended in freshly prepared 8 M urea in 100 mM ammonium bicarbonate (AmBic) to a concentration of approximately 1 mg/mL. The proteins were reduced using dithiothreitol (DTT, 45 mM in 100 mM AmBic) for 1 hour at 37°C and subsequently alkylated at room temperature in the dark for 30 minutes with iodoacetamide (100 mM in 100 mM AmBic). Excess iodoacetamide was quenched with DTT/100 mM AmBic, which also diluted the urea to approximately 2M.

Protein digestion utilized a two-step procedure [120]. Lys-C was added at a ratio of 1:50 (Lys-C:protein) and incubated overnight at 37°C with shaking. After dilution with 100 mM AmBic, trypsin was added at the same ratio as was used with Lys-C. Incubation was performed for 4 hours at 37°C with shaking. Digestion was quenched by adding trifluoroacetic acid (TFA) until the pH was less than 3.0. The resultant acidified peptides were desalted using $C_{18}$ OMIX Tips (Agilent Technologies). The tips were conditioned prior to use with LC-MS grade methanol and subsequently equilibrated with Solvent 1 (50:50 water:acetonitrile supplemented with 0.1 %

TFA) followed by Solvent 2 (98:2 water: acetonitrile supplemented with 0.1 % TFA). The peptides were bound to the tips by repeated aspiration and dispensing, desalted using Solvent 2, and eluted using Solvent 1. The recovered peptides were dried in a vacuum concentrator and reconstituted in Solvent 2 (1 µg/µL) for analysis via LC-MS/MS.

### 2.2.7 PEM isolation and processing

The PEMs were removed from each well and were treated with trypsin (0.25% EDTA) for seven minutes to remove the LSECs and rinsed in 0.1X PBS, (pH = 7.4). PEMs were subsequently snap frozen in liquid nitrogen and stored at -80°C until further processing. PEMs from each culture condition (3DHL and 3DH) as well as fresh, unused PEMs, referred to as fresh PEMs (FPs) all of identical surface area, were suspended in freshly prepared 8 M urea in 100 mM AmBic and heated at 95°C overnight. PEMs were subsequently subjected to the same reduction, alkylation, digestion, and desalting steps as described in the previous section.

### 2.2.8 LC-MS analysis

Approximately 3 µg of each peptide sample was loaded onto an Acquity UPLC I-class system equipped with a CSH130 $C_{18}$ 1.7 µm, 1.0 x 150 mm column maintained at 45°C (Waters Corporation, Milford, MA). The mobile phases were 0.1% formic acid in water (Solvent A) and 0.1% formic acid in acetonitrile (Solvent B). Separations were performed at a flow rate of 50 µL/min, using a 110 minute gradient from 3-40% solvent B, with all samples analyzed in duplicate. The column effluent was sprayed directly into a Synapt G2-S mass spectrometer using the high definition mass spectrometry ($HDMS^E$) mode (continuum, positive-ion, "resolution" MS settings). Source conditions were as follows: capillary voltage, 3.0 kV; source temperature, 120˚C; sampling cone, 60 V; desolvation temperature, 350˚C; cone gas flow, 50 L/hr; desolvation gas flow, 500 L/hr; nebulizer gas flow, 6 bar. Both low energy (4 and 2 V in the trap

and transfer regions, respectively) and elevated energy (4 V in the trap and ramped from 20 to 50 V in the transfer region) scans were 1.2 seconds each for the *m/z* range of 50 to 1800. For the ion mobility separation (IMS), the IMS and transfer wave velocities were 600 and 1200 m/sec, respectively. Wave height within the ion mobility cell was ramped from 10 to 40 V. For lock mass correction, a 1.2 second low energy scan was acquired every 30 seconds from a 100 fmol/μL [Glu1]-fibrinopeptide B solution (50:50 acetonitrile: water supplemented with 0.1 % formic acid). The infusion rate on the lock spray was 10 μL/min, and introduced into the mass spectrometer at a capillary voltage of 3.0 kV. Lock mass correction was invoked during the data analysis phase of the work.

**2.2.9 Data analysis**

Raw data files were analyzed using Protein Lynx Global Server (PLGS, Version. 3.0, Waters™ Corporation). LC-MS data was queried against a combined rat and bovine proteome concatenated with a randomized decoy database, allowing for two missed trypsin cleavages. A minimum peptide length was set to five amino acids, with carbamidomethylation of cysteine set as a fixed modification. Oxidation of methionine, proline (*i.e*., hydroxyproline) and lysine (*i.e*. hydroxylysine) were set as variable modifications. Additionally, galactosylation and glucosylgalactosylation of lysine, glycosylation of proline, conversion of N-terminal glutamine to pyro-glutamate and deamidation of asparagine and glutamine were also set as variable modifications. The criteria used for protein identification utilized both a false discovery rate (FDR) of less than 5% and required at least two peptides per protein. The raw PLGS output was then processed using ISOQuant's TOP3 method [141], where the sum of the three most intense peptides was compared across culture conditions. Proteins that were significantly changing in each of the liver cultures were analyzed both manually and computationally via

Protein Analysis Through Evolutionary Relationships (Panther) [173] and The Database for Annotation, Visualization and Integrated Discovery (DAVID) [174] to assess enriched KEGG pathways. PEM protein identification was performed in the same way as the lysates with the addition of allysine and hydroxyallysine, and carbamylation of lysine and the N-terminus as variable modification and enrichment of oxidation of proline. The protein identifications for the PEMs were performed against two different databases. The first database contained the combined rat and contaminants proteome. The second database contained the contaminants list and the rat proteome limited to those associated with the extracellular matrix (392 proteins) to aid in studying changes in ECM [175]. This database was derived using the following criteria in UniProt; Gene ontology (GO) term, go:0031012, which corresponds to the extracellular matrix and both the organism Rattus norvegicus (Rat) [10116] and proteome:up000002494 were used to limit the search to rat proteins. Both of these databases contained randomized decoy sequences that allowed for determination of a false discovery rate. The mass spectrometry proteomics data for the hepatocyte lysates have been deposited to the ProteomeXchange Consortium [176] via the PRIDE partner repository with the dataset identifier PXD002491.

**2.2.10 Ketone body measurements**

LC-MS grade methanol (800 μL) was added to spent cell culture media (200 μL) and incubated at -80°C overnight. Centrifugation (13,000 *x g*, 20 min) was subsequently performed and the supernatant was collected for LC-MS/MS analysis. Samples (5 μL) were injected into a Agilent 1100c-ABSciex 3200 Qtrap LC-MS/MS (Agilent Technologies, Santa Clara, CA), which was operated in negative ion mode. Separations were accomplished via hydrophilic interaction liquid chromatography (HILIC; Kinetex 2.6 μm, 100 Å, 100 x 2.1 mm, Phenomenex, Torrence, CA). The column was equilibrated using 100% mobile phase A (95:5, acetonitrile:50 mM ammonium

formate, pH 3.2) for 20 minutes. Gradient conditions: 0-8 min, 100% A; 8-16 min, linear gradient up to 30% B (50:40:10 acetonitrile:water:ammonium formate, pH = 3.2); 16-18 min, linear gradient up to 100 % B; 18-24 min, 100% B; 24-34 min, linear gradient to 100 % A. The column was then re-equilibrated for 20 minutes with mobile phase A before the injection of the next sample.

Multiple reaction monitoring (MRM) was used in negative ion mode to detect the precursor/product ion pairs of 103.1/58.9 and 101.1/56.9 for β-hydroxybutyrate and acetoacetate, respectively. The mass spectrometer acquisition parameters were set as follows: Source temperature 300 °C; ion spray voltage, -4000.0 V; declustering potential, -17.0 V, entrance potential, -7.0 V, collision energy, -30.0 V, and collision cell exit potential, -5.0 V. The results were quantified by comparing the peak areas of known concentrations of β-hydroxybutyrate and acetoacetate in Analyst (v.1.6). Concentrations used for quantification ranged from 1 μM – 60 μM, prepared in fresh unused hepatocyte media.

### 2.2.11 Glucose measurements

Concentrations were determined with a glucose analyzer (YSI 2700, Yellow Springs Instruments), maintained at the Virginia Tech Metabolic Phenotyping Core Facility. Spent media samples from the 3DHL, 3DH and HM cultures were measured for glucose levels and compared against fresh un-used hepatocyte media.

### 2.2.12 Statistical analyses

All data are reported as mean ± standard deviation and are n = 3 unless otherwise specified. Statistical significance was determined using a two-tailed Student's t-test. The Benjamini-Hochberg correction was applied to account for multiple hypotheses testing with corrected $p$ values ($p < 0.05$) being considered significant.

## 2.3 Results

### 2.3.1 Overview and liver model functions

The process by which samples were prepared as well as global functional data are provided in **Figure 5A**. Liver models containing primary rat hepatocytes, LSECs and PEMs were assembled forming the 3DHL and 3DH liver models. HMs served as controls. After 72 hours after, hepatocytes and PEMs were separated and subjected to processing to peptides that were amenable to bottom-up proteomic analyses.

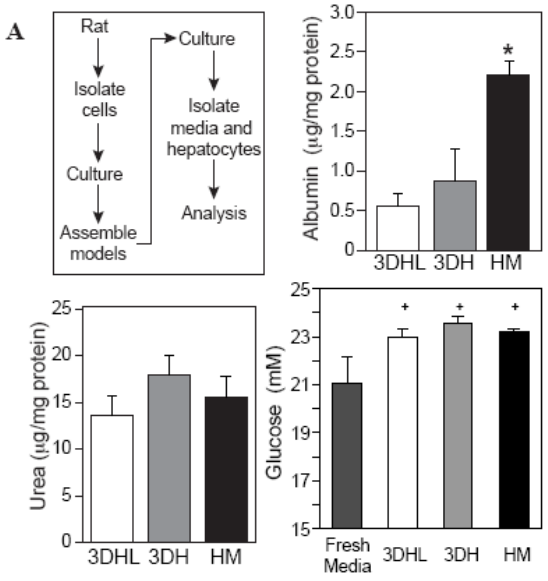

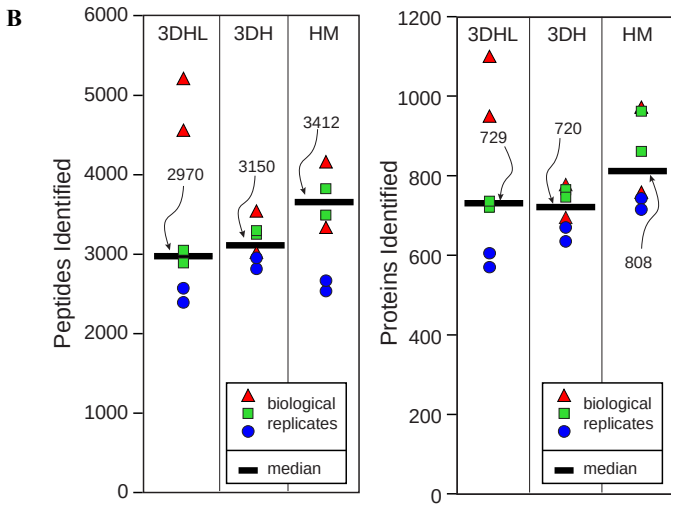


**Figure 5: Culture characterization and proteomic overview A, Experimental overview, extracellular albumin (*, p < 0.01, HM vs. 3DHL and 3DH), urea and glucose levels for each culture condition at the time of hepatocyte harvest. B, Proteins and peptides identified from hepatocyte lysates for each construct. Biological and technical replicates are indicated as well as the median number for each.**

Albumin secretion, urea production and glucose metabolism were measured to assess liver model function at the end of the culture period (**Figure 5A**). Albumin secretion was ~4 fold and 2.5 fold higher in the HM as compared the 3DHL and 3DH liver models respectively. This trend can be attributed to hepatocyte stabilization which takes approximately 2-3 days after introduction of the PEMs as previous results have shown [89]. Urea production and glucose levels were comparable across cultures conditions with glucose concentrations slightly higher than that of basal media (22.3 mM), which is suggestive of hepatocytes in a gluconeogenic state. The untargeted, bottom-up LC-MS analyses using data-independent acquisition (DIA) [177] and ISOQuant processing [141] provided identification and relative abundances ratios of the proteins from each construct. Overall, ~2500-5000 peptides were used to identify ~600-1000 proteins across the three culture conditions **(Figure 5B**).

### 2.3.2 PEM-containing liver constructs and hepatocyte monolayers have different proteomic signatures favoring β-oxidation and ketogenesis

The results from the initial identifications and subsequent label-free quantification by ISOQuant led to 474 proteins with relative abundance ratios between hepatocytes from the three models. These proteins are depicted in **Figure 6,** where proteins that exhibited a fold change of at least 20% and were considered significant ($p < 0.05$) are highlighted. This was deemed to be an acceptable cutoff based on other experiments performed using *in vitro* hepatocyte cultures [148, 178]. In the case of the 3DHL *vs*. 3DH comparison (**Figure 6A**), 79 proteins exhibited at least a 20% fold change (those marked in blue and red), with 66 proteins exhibiting higher levels in 3DHL relative to the 3DH liver models and 13 proteins exhibited higher levels in 3DH relative to 3DHL. Results from the other pairwise comparisons are shown in **Figure 6B** and **Figure 6C**. Based on these distributions and their Pearson's correlation coefficients, the 3DHL and 3DH samples are the most similar, whereas the 3DH and HM samples are most dissimilar.

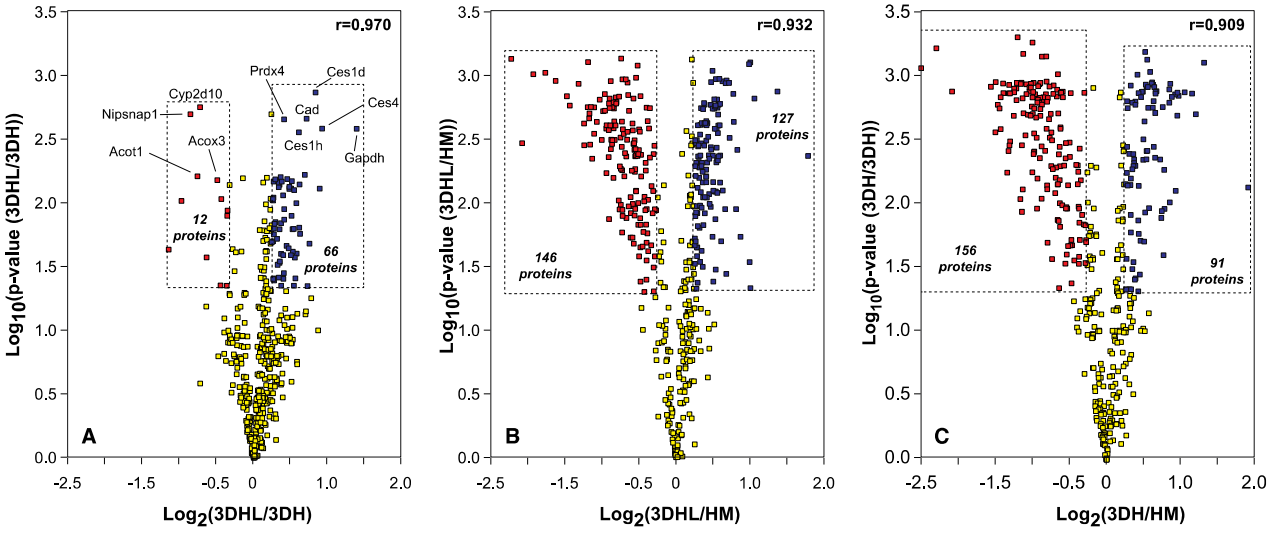


**Figure 6: Volcano plots illustrating proteins that are significantly different in each construct. A, 3DHL *vs.* 3DH; B, 3DHL *vs.* HM; C, 3DH *vs.* HM. Proteins that are in higher abundance for each comparison are in blue and those in lower abundance are in red. Selected proteins are indicated for the 3DHL *vs.* 3DH comparison. Pearson correlations for each comparison are indicated in the upper right of each plot.**

The proteins that changed significantly in relative levels in each comparison were next evaluated for statistically overrepresented KEGG pathways using DAVID [174]. The results are indicative of fatty acid/branched chain amino acid metabolism in the 3D liver models, glycolysis/gluconeogenesis in HMs and drug metabolism in 3DHL liver models (**Table 1**).

**Table 1: DAVID analysis of enriched KEGG pathways. Only terms exhibiting *p*-values less than 0.05 are shown.**

| KEGG pathway | Proteins | *p*-value | Enrichment | Comparison |
|---|---|---|---|---|
| Ribosome | 33 | 1.50E-34 | HM | 3DHL vs HM |
| Ribosome | 30 | 7.30E-29 | HM | 3DH vs HM |
| Valine, leucine and isoleucine degradation | 18 | 4.90E-20 | 3DHL | 3DHL vs HM |
| Fatty acid metabolism | 15 | 7.60E-16 | 3DHL | 3DHL vs HM |
| Valine, leucine and isoleucine degradation | 13 | 1.00E-13 | 3DH | 3DH vs HM |
| Butanoate metabolism | 12 | 1.80E-12 | 3DHL | 3DHL vs HM |
| Fatty acid metabolism | 11 | 3.80E-11 | 3DH | 3DH vs HM |
| Butanoate metabolism | 8 | 1.80E-07 | 3DH | 3DH vs HM |
| Glycolysis / Gluconeogenesis | 13 | 8.40E-07 | HM | 3DHL vs HM |
| Tryptophan metabolism | 8 | 1.30E-05 | 3DHL | 3DHL vs HM |
| Glycolysis / Gluconeogenesis | 12 | 1.40E-05 | HM | 3DH vs HM |
| Ascorbate and aldarate metabolism | 6 | 1.90E-05 | 3DHL | 3DHL vs HM |
| Drug metabolism | 7 | 2.60E-05 | 3DHL | 3DHL vs 3DH |
| Drug metabolism | 9 | 2.80E-05 | 3DHL | 3DHL vs HM |
| PPAR signaling pathway | 8 | 3.30E-05 | 3DH | 3DH vs HM |
| beta-Alanine metabolism | 6 | 5.50E-05 | 3DHL | 3DHL vs HM |
| Limonene and pinene degradation | 5 | 5.70E-05 | 3DHL | 3DHL vs HM |
| Metabolism of xenobiotics by cytochrome P450 | 8 | 5.90E-05 | 3DHL | 3DHL vs HM |
| Lysine degradation | 7 | 6.40E-05 | 3DHL | 3DHL vs HM |
| Primary bile acid biosynthesis | 5 | 7.30E-05 | 3DH | 3DH vs HM |
| Drug metabolism | 7 | 8.90E-05 | 3DHL | 3DHL vs HM |
| PPAR signaling pathway | 8 | 1.40E-04 | 3DHL | 3DHL vs HM |
| Glycine, serine and threonine metabolism | 6 | 2.10E-04 | 3DHL | 3DHL vs HM |
| Arginine and proline metabolism | 7 | 2.10E-04 | 3DHL | 3DHL vs HM |
| Propanoate metabolism | 6 | 2.10E-04 | 3DHL | 3DHL vs HM |
| Retinol metabolism | 7 | 3.40E-04 | 3DHL | 3DHL vs HM |
| Fatty acid elongation in mitochondria | 4 | 3.80E-04 | 3DHL | 3DHL vs HM |
| Glutathione metabolism | 8 | 9.10E-04 | HM | 3DH vs HM |
| Primary bile acid biosynthesis | 4 | 2.80E-03 | 3DHL | 3DHL vs HM |
| Pentose and glucuronate interconversions | 4 | 2.80E-03 | 3DHL | 3DHL vs HM |
| Drug metabolism | 6 | 3.60E-03 | 3DHL | 3DHL vs 3DH |

| | | | | |
|---|---|---|---|---|
| Ascorbate and aldarate metabolism | 4 | 3.80E-03 | 3DHL | 3DHL vs 3DH |
| Tryptophan metabolism | 5 | 4.60E-03 | 3DH | 3DH vs HM |
| beta-Alanine metabolism | 4 | 6.70E-03 | 3DH | 3DH vs HM |
| Arginine and proline metabolism | 5 | 7.60E-03 | 3DH | 3DH vs HM |
| Propanoate metabolism | 4 | 1.50E-02 | 3DH | 3DH vs HM |
| Pentose phosphate pathway | 5 | 1.50E-02 | HM | 3DH vs HM |
| Glycine, serine and threonine metabolism | 4 | 1.60E-02 | 3DH | 3DH vs HM |
| Porphyrin and chlorophyll metabolism | 4 | 1.70E-02 | 3DHL | 3DHL vs 3DH |
| Drug metabolism | 5 | 1.70E-02 | 3DH | 3DH vs HM |
| Limonene and pinene degradation | 3 | 1.70E-02 | 3DH | 3DH vs HM |
| Metabolism of xenobiotics by cytochrome P450 | 7 | 1.70E-02 | HM | 3DH vs HM |
| Synthesis and degradation of ketone bodies | 3 | 1.80E-02 | 3DHL | 3DHL vs HM |
| Pyruvate metabolism | 4 | 1.90E-02 | 3DH | 3DH vs HM |
| Lysine degradation | 4 | 2.00E-02 | 3DH | 3DH vs HM |
| Porphyrin and chlorophyll metabolism | 4 | 2.10E-02 | 3DHL | 3DHL vs HM |
| Pentose phosphate pathway | 5 | 2.20E-02 | HM | 3DHL vs HM |
| Drug metabolism | 7 | 2.90E-02 | HM | 3DH vs HM |
| Starch and sucrose metabolism | 4 | 3.30E-02 | 3DHL | 3DHL vs HM |
| Ascorbate and aldarate metabolism | 3 | 3.30E-02 | 3DH | 3DH vs HM |
| Antigen processing and presentation | 5 | 3.50E-02 | 3DHL | 3DHL vs 3DH |
| Glutathione metabolism | 4 | 3.90E-02 | 3DHL | 3DHL vs 3DH |
| Pentose and glucuronate interconversions | 3 | 4.40E-02 | 3DHL | 3DHL vs 3DH |
| Steroid hormone biosynthesis | 4 | 4.70E-02 | 3DHL | 3DHL vs HM |
| Tyrosine metabolism | 5 | 6.10E-02 | HM | 3DHL vs HM |

Ribosomes were also an enriched term but require detailed isolation in order to obtain actively translating ribosomes required for accurate proteomic analysis [179]. For example, a recent study showed that in order to obtain actively translating ribosome for quantification, addition of cyclohexamide is necessary to halt translation and should be performed before cell lysis [180]. This step was not performed and is not within the scope of this study and therefore will not be discussed. Proteins associated with mitochondrial fatty acid β-oxidation and ketone body formation (**Figure 7A**) were enriched in the PEM-containing liver models (**Figure 7B**). For example, two acyl-CoA ligases required for fatty acid activation (Acsl1 and Acsl5) were present in higher abundance in 3DHL liver models over the HMs, with similar increases in the 3DH *vs.*

HM comparison. The acyl-CoA dehydrogenase enzymes short chain (Acads), short and branched chain (Acadsb) and very long chain (Acadvl) also exhibited increases in the 3DHL and 3DH liver models as compared to HMs. While the enoyl-CoA hydratase (Echs1) was more abundant in the 3DHL model relative to HMs, there was no significant difference when 3DH was compared to HM. Both identified enoyl-CoA isomerases (Eci1 and Eci2) exhibited greater abundances in 3DHL liver models as compared to HM, while only Eci2 showed significant increase in 3DH liver models. Hydroxyacyl-CoA dehydrogenase (Hadh) and subunits of the trifunctional enzyme (Hadha and Hadhb) all exhibited significant increases in the 3DHL liver models. Further interrogation of the lipid metabolism proteins also indicated increases in Acyl-CoA oxidase (Acox3), bifunctional enzyme (Ehhadh) and peroxisomal 3 ketoacyl-CoA thiolase (Acaa1a) in the 3DHL and 3DH liver models as compared to HMs (**Figure 8**) indicating that both mitochondrial and peroxisomal processes are contributing to β-oxidation in the PEM containing liver models.

The formation of ketone bodies or ketogenesis is supported by significant increases in three of the four proteins that make up this energy-generating pathway: hydroxymethylglutaryl-CoA synthase (Hmgcs2), hydroxymethylglutaryl-CoA lyase (Hmgcl) and β-hydroxybutyrate dehydrogenase (Bdh1) (**Figure 7A**). Hmgcs2, Hmgcl, and Bdh1 all show increases in 3DHL as compared to HM (**Figure 7C)**, although only Hmgcs2 and Bdh1 showed significant increases in 3DH over HM. The changes in proteins associated with ketone body production prompted us to determine presence and concentrations of ketone bodies in the cell culture media using a targeted LC-MS/MS approach [181]. Contrary to protein abundances where the PEM containing liver models exhibited higher levels of these proteins, concentrations of acetoacetate and β-hydroxybutyrate in the cell culture media were significantly higher in the HMs (**Figure 7C**).

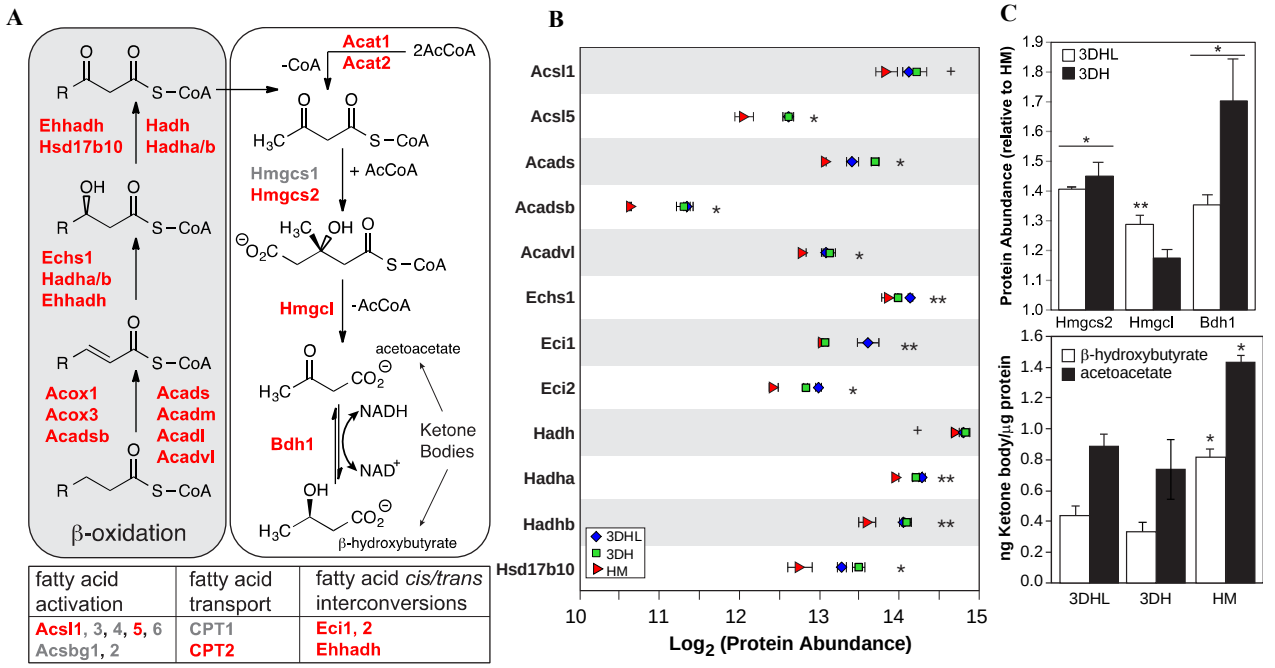


**Figure 7: Fatty acid metabolism and ketogenesis pathways are modulated by the local environment. A, Schematic of the main steps in fatty acid β-oxidation. Proteins identified in this study are shown in bold. B, Relative protein abundances for proteins associated with fatty acid β-oxidation that change significantly based upon the culture conditions (+, $p < 0.05$ HM vs. 3DHL and 3DH; *, $p < 0.01$ HM vs. 3DHL and 3DH; **, $p < 0.05$ 3DHL vs. 3DH). C, Protein abundance ratios for proteins associated with ketogenesis (top; *, $p < 0.01$ HM vs. 3DHL and 3DH; **, $p < 0.01$ HM vs. 3DHL) and levels of the two main ketone bodies, acetoacetate and b-hydroxybutyrate (bottom) as measured by LC-MS (*, $p < 0.01$ HM vs. 3DHL and 3DH for individual metabolites).**

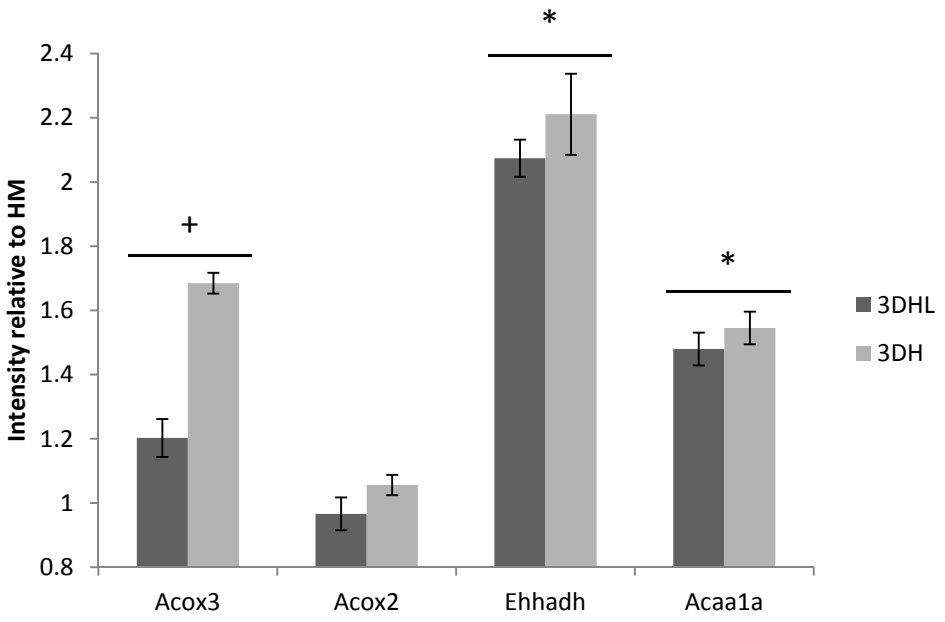


**Figure 8: Peroxisomal processes are also modulated by the local environment. Relative protein abundance ratios for enzymes associated with peroxisomal fatty acid β-oxidation that change significantly based upon the culture conditions (+, $p < 0.05$ HM vs. 3DHL and 3DH; *, $p < 0.01$ HM vs. 3DHL).**

### 2.3.3 HMs contain higher levels of several glycolytic and gluconeogenic enzymes

Glucose concentrations in conditioned media were higher than that of fresh media (**Figure 5A**), indicative of a gluconeogenic state. Eleven enzymes involved in glycolysis and gluconeogenesis exhibited significantly increased levels in the HM cultures (**Figure 9A and B**), including glucose 6 phosphate isomerase (Gpi), fructose-1,6-bisphosphatase (Fbp1), a key regulatory enzyme for gluconeogenesis, fructose bisphosphate aldolase A and B (Aldoa and Aldob), triosephosphate isomerase (Tpi1), glyceraldehyde 3 phosphate dehydrogenase (Gapdh), phosphoglycerate kinase 1 (Pgk1), phosphoglycerate mutase 1 (Pgam1), alpha-enolase (Eno1), pyruvate kinase isozymes R/L (Pklr) and L-lactate dehydrogenase A (Ldha). While the proteomic data would suggest higher glucose levels in HMs as compared to both the 3DHL and 3DH liver models, glucose production rates are under control of both allosteric effectors as well as thermodynamic constraints [182]. Thus, as with the ketone body measurements, the extracellular glucose concentrations obtained by measurement do not directly correlate with what

would be predicted based upon protein abundance measures. Nonetheless, all constructs provide local environments where the hepatocytes synthesize glucose even though the extracellular glucose concentrations present in the media are four times higher than what is observed *in vivo*.

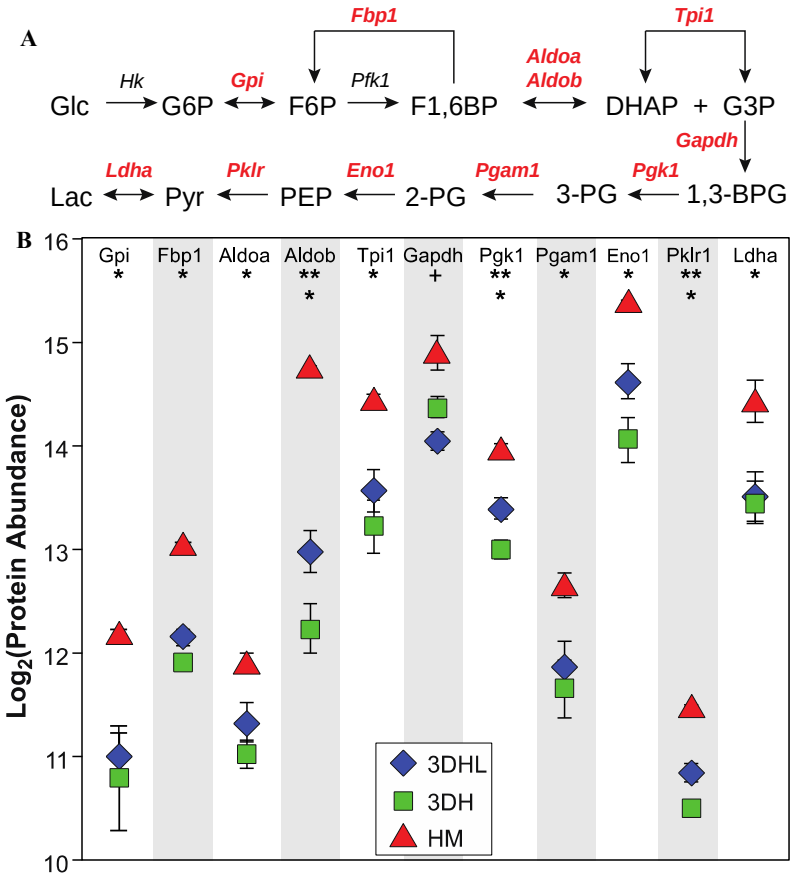


**Figure 9: Proteins associated with glucose processing are more abundant in hepatocyte monolayers. A, Pathway with proteins identified in this study are shown in bold. B, Proteins abundances, n = 3 (+ $p < 0.05$ HM *vs.* both 3DHL and 3DH; * $p < 0.01$ HM *vs.* both 3DHL and 3DH; ** $p < 0.05$ 3DHL *vs.* 3DH). Note that the rate-limiting enzyme for gluconeogenesis fructose-1,6-bisphosphatase 1 (Fbp1) is more abundant in monolayers than the conditions that utilize a PEM.**

### 2.3.4 Structural and trafficking proteins in HMs are indicative of dedifferentiation

A hallmark of hepatocyte dedifferentiation is the modification of cell shape and structure [70, 71, 89]. Several structural and trafficking proteins were found in higher abundance in HMs relative to the other two constructs (**Figure 10**). Actin (Act1 and Actc1), annexins (Anxa 2, 3, and 5), S100 proteins (S100-A10 and S100-A11), keratins (Krt 8 and Krt18), myosins (Myl6 and

Myh9), tropomyosins (Tpm4), transgelins (Tagln and Tagln2), cofilin (Cfl1), destrin (Dstn) and profilin (Pfn1) all exhibited increased levels in HM. As a whole, the increased levels of structural proteins observed in the HM cultures are indicative of changes in hepatocyte morphology and migration, both of which being key features of the dedifferentiation process. These results support the claim that the PEM slows the dedifferentiation process regardless of the presence of the LSECs.

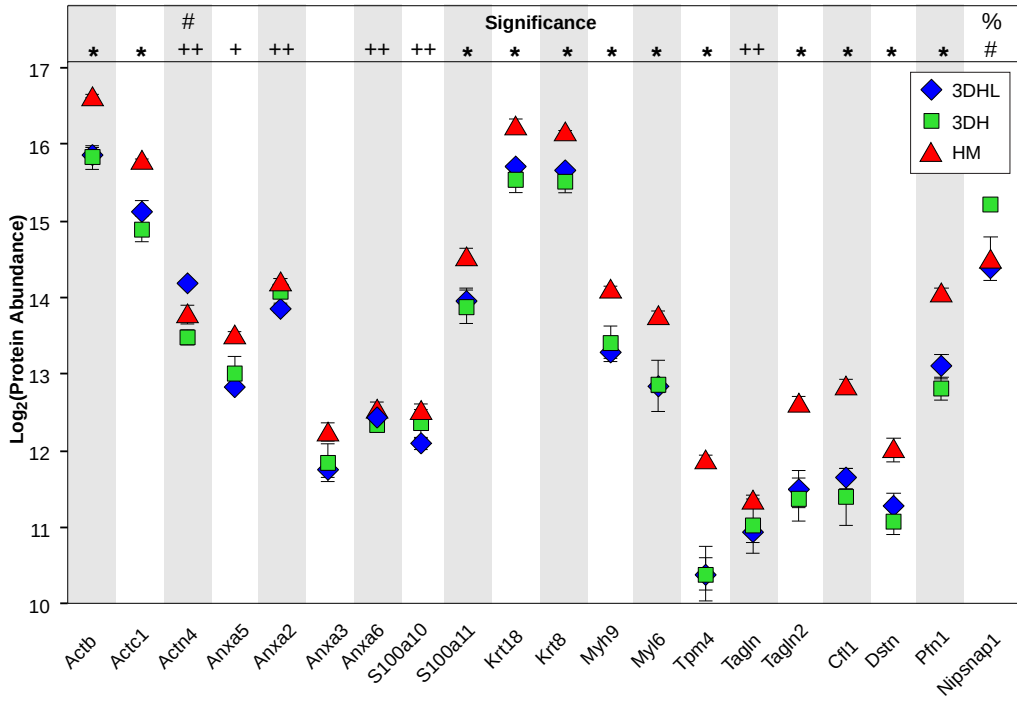


**Figure 10: PEMs and LSECs mitigate production of proteins associated with hepatocyte dedifferentiation. Protein abundances comparisons across culture conditions (+ $p < 0.05$, HM *vs.* both 3DHL and 3DH; * $p < 0.01$, HM *vs.* both 3DHL and 3DH; ++ $p < 0.01$, HM *vs.* 3DHL; # $p < 0.01$, 3DHL *vs.* 3DH; % $p < 0.01$, HM *vs.*3DH).**

### 2.3.5 3DHL liver models exhibit higher levels of proteins associated with drug metabolism

KEGG pathways related to drug metabolism were highly enriched in the 3DHL liver models (**Table 1 and Figure 11**). Several of the Phase I and Phase II detoxification enzymes quantified exhibited significantly increased levels in 3DHL as compared to HM (**Figure 11A**) and as compared to 3DH (**Figure 11C**), including, UDP-glucuronosyltransferases (Ugt), glutathione-S-transferses (Gst), peroxidases (Gpx), carboxylesterases (Ces and Est), cytochrome

p450s (Cyp), and epoxide hydrolases (Ephx). However, only 3 of the 16 enzymes (Ugt2b15, Ces1e, and Cyp2d10) exhibited increased abundance in 3DH as compared to HMs (**Figure 11B).** These results support the claim that detoxification enzyme abundance within the liver models is enhanced by the presence of LSECs.

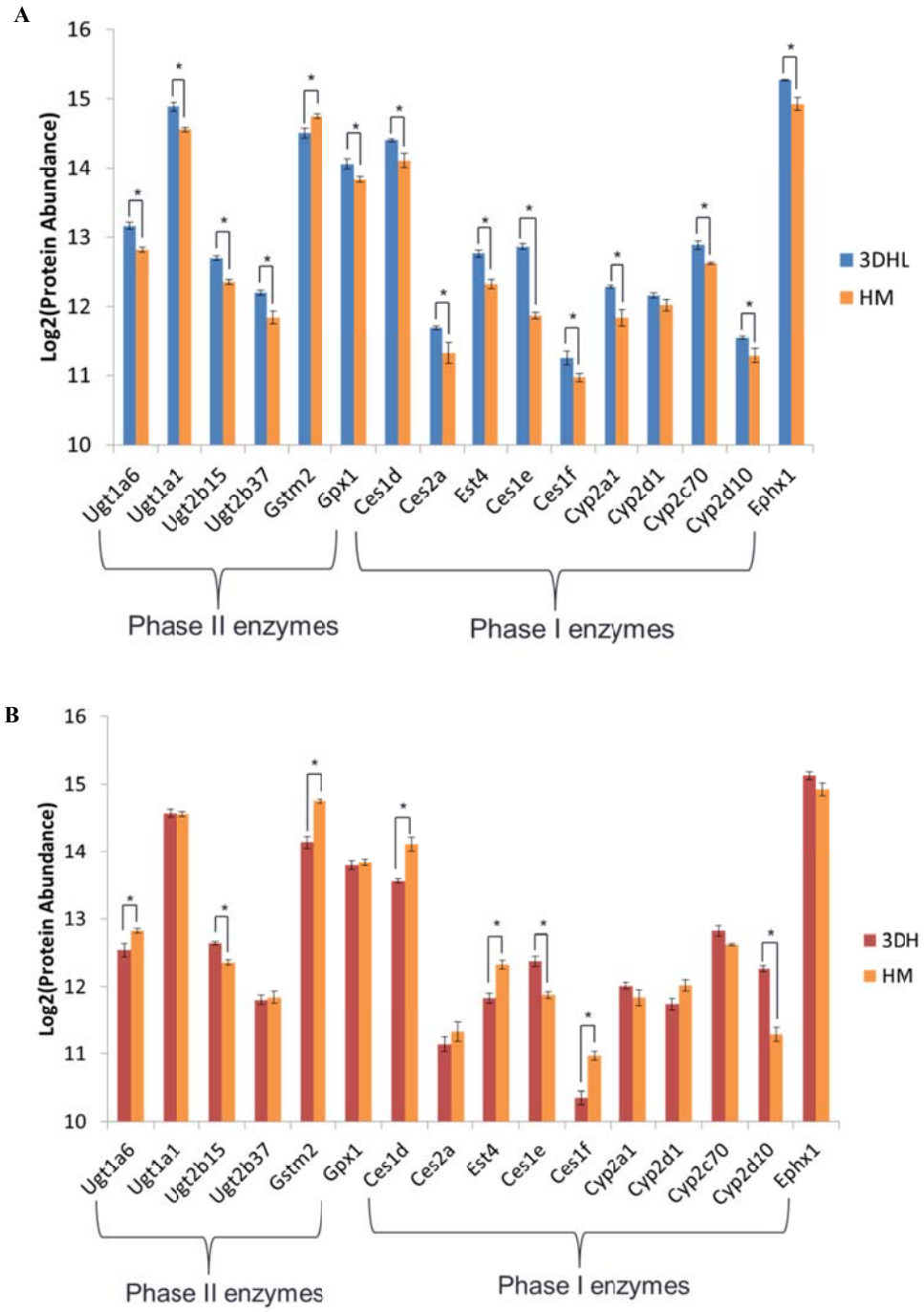

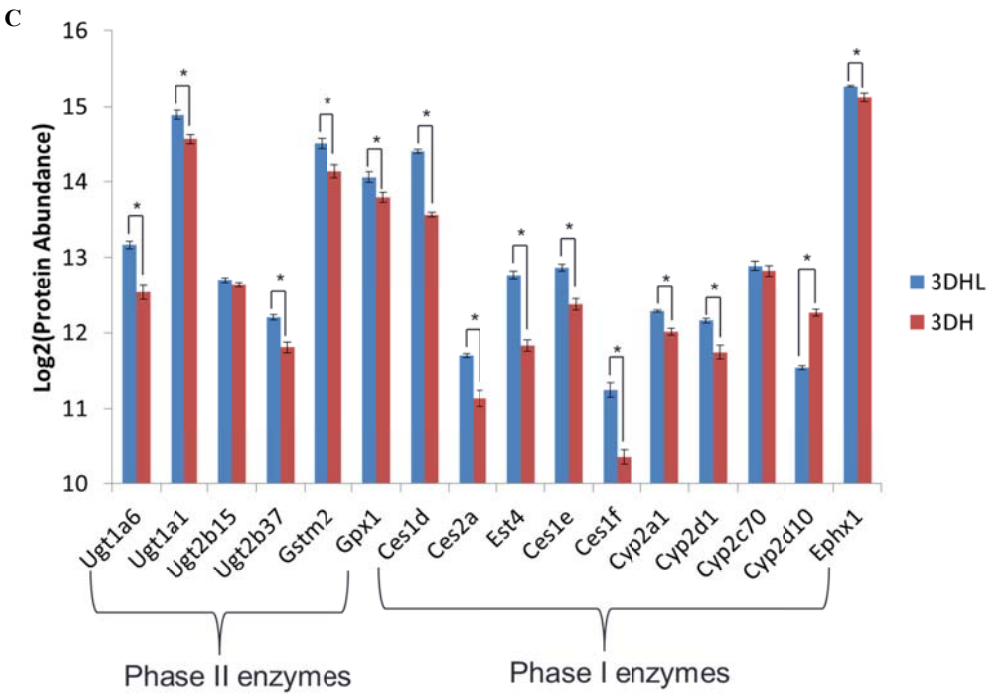


**Figure 11: Drug metabolism-related proteins are higher in abundance in 3DHL as compared to HM (A). Proteins abundances were also compared in 3DH as compared to HM (B) and 3DHL as compared to 3DH (C). Proteins are organized based upon class: Phase I and II enzymes (* $p < 0.01$).**

### 2.3.6 Proteomic analysis of the PEMs show limited matrix remodeling

PEMs were isolated from each liver model at the same time point as the hepatocytes and LC-MS/MS analysis was performed and analyzed using ISOQuant. Protein identifications were performed using two different databases, one that contained proteins associated with the ECM in the Uniprot database and one that contained the entire rat proteome. **Table 2** lists the proteins that were identified from the analysis of the PEMs using the ECM database ordered by the intensities of their top 3 peptides in both 3DHL and 3DH.

**Table 2: Changes in ECM protein abundances are limited at this time point. Proteins identified in PEMs from 3DHL and 3DH liver models were compared against fresh unused PEMs (FP).**

| Description | UniProt ID | 3DHL/FP | *p*-value (3DHL/FP) | Top3 intensity in 3DHL | 3DH/FP | *p*-value (3DH/FP) | Top3 intensity in 3DH |
|---|---|---|---|---|---|---|---|
| Collagen alpha-1(I) chain | P02454 | 1.34 ± 0.18 | 0.64 | 1647494 | 1.30 ± 0.06 | 0.46 | 1601713 |
| Collagen alpha-2(I) chain | P02466 | 1.06 ± 0.08 | 0.72 | 948819 | 1.08 ± 0.05 | 0.59 | 960251 |
| Protein Col28a1 | D3ZN64 | 1.36 ± 0.08 | 0.63 | 578870 | 1.56 ± 0.21 | 0.76 | 664470 |
| Collagen alpha-1(II) chain | P05539 | 1.21 ± 0.02 | 0.82 | 621105 | 1.21 ± 0.14 | 0.94 | 621505 |
| Protein Col4a2 | F1M6Q3 | 1.43 ± 0.07 | 0.58 | 591665 | 1.35 ± 0.08 | 0.49 | 558587 |
| Collagen alpha-1(III) chain | P13941 | 1.07 ± 0.06 | 0.78 | 435902 | 1.17 ± 0.13 | 0.56 | 475615 |
| Collagen alpha-1(XI) chain | P20909 | 1.03 ± 0.18 | 0.92 | 413335 | 1.19 ± 0.49 | 0.70 | 474677 |
| Protein Col10a1 | D3ZGL7 | 1.16 ± 0.05 | 0.70 | 314566 | 1.21 ± 0.01 | 0.54 | 327520 |
| Procollagen, type XI, alpha 2 | Q6MGB2 | 1.50 ± 0.16 | 0.67 | 305476 | 1.58 ± 0.16 | 0.44 | 321260 |
| Collagen alpha-1(V) chain | G3V763 | 1.47 ± 0.11 | 0.63 | 279135 | 1.53 ± 0.10 | 0.44 | 291147 |
| Procollagen, type VII, alpha 1 (Predicted) | D3ZE04 | 0.71 ± 0.33 | 0.63 | 182346 | 0.80 ± 0.45 | 0.69 | 206414 |
| Protein Col4a5 | F1LUN5 | 1.26 ± 0.02 | 0.76 | 187260 | 1.24 ± 0.03 | 0.62 | 184668 |
| Protein Col5a2 | F1LQ00 | 0.66 ± 0.58 | 0.66 | 197287 | 0.40 ± 0.52 | 1.05 | 118631 |
| Protein Col4a1 | F1MA59 | 0.74 ± 0.18 | 0.65 | 113061 | 0.73 ± 0.23 | 0.57 | 112147 |
| Collagen alpha-1(XXVII) chain | Q80ZF0 | 0.95 ± 0.17 | 0.78 | 31720 | 0.94 ± 0.02 | 0.57 | 31217 |
| Procollagen, type XI, alpha 2 (Mapped) | F6T0B3 | 0.58 ± 0.07 | 0.72 | 15466 | 0.65 ± 0.10 | 0.67 | 17065 |
| Fibromodulin | P50609 | 0.32 ± 0.06 | 0.95 | 16696 | 0.29 ± 0.02 | 0.83 | 14989 |
| Protein Col14a1 | D3ZZT9 | 0.51 ± 0.09 | 0.70 | 16525 | 0.44 ± 0.06 | 0.52 | 14457 |

Using this database, no significant differences were observed between PEMs from 3DHL or 3DH as compared to a fresh PEM (FP) among any of the proteins identified. These results indicate that changes in the ECM proteins in the PEMs as a result of cell culture are limited but detectable after 3 days. In order to verify that cellular contamination was not contributing to these trends, PEMs were re-analyzed using the entire rat proteome and the results are shown in **Table 3.**

**Table 3: Results from the analysis performed using the entire rat proteome. Changes in PEM protein abundances are limited at this time point. Proteins identified in PEMs from 3DHL and 3DH liver models were compared against fresh unused PEMs (FP) * indicates a significant change ($p < 0.05$).**

| Description | UniProt ID | 3DHL/FP | *p*-value (3DHL/FP) | Top3 intensity in 3DHL | 3DH/FP | *p*-value (3DH/FP) | Top3 intensity in 3DH |
|---|---|---|---|---|---|---|---|
| Collagen alpha-1(I) chain | P02454 | 1.60 ± 0.56 | 0.10 | 1494775 | 1.48 ± 0.41 | 0.11 | 1405701 |
| Collagen alpha-2(I) chain | P02466 | 1.65 ± 0.13 | 0.04* | 185584 | 1.64 ± 0.06 | 5.57E-04* | 183974 |
| Protein Chmp4bl1 | D4A9Z8 | 1.61 ± 0.50 | 0.22 | 83035 | 1.69 ± 0.44 | 0.14 | 89235 |
| Protein Krt78 OS=Rattus norvegicus | F1MAC2 | 6.09 ± 8.88 | 0.64 | 68987 | 5.79 ± 8.31 | 0.67 | 67517 |
| Collagen alpha-1(XXIII) chain | Q810Y4 | 1.52 ± 1.23 | 0.87 | 40250 | 0.80 ± 0.53 | 0.55 | 20842 |
| Unique cartilage matrix-associated protein | B9TQX4 | 2.69 ± 2.63 | 0.28 | 28989 | 2.75 ± 3.10 | 0.55 | 26518 |
| Protein Lbh (Fragment) | F1M635 | 1.42 ± 0.69 | 0.46 | 26136 | 3.47 ± 0.07 | 0.01* | 52299 |
| RE1-silencing transcription factor | O54963 | 1.30 ± 0.08 | 0.42 | 5563 | 0.87 ± 0.18 | 0.85 | 4197 |

These results show very little difference between the 3DHL and 3DH as compared to the FP. The only exceptions to this were in levels of collagen alpha 2(I) chain and protein LBH (limb-bud-and-heart). However, given that this database was not made to specifically identify ECM proteins, accuracy in the quantification of these proteins is limited [175]. Additionally, protein LBH is one of the lower abundant proteins, based on the intensities of the top 3 peptides and thus accurate quantification also becomes difficult. Nonetheless, no other cellular components were identified as significantly changing between PEMs from the liver models as compared to the FPs, suggesting that the cells were sufficiently removed from the PEMs. Further studies such as fluorescent imaging would need to be performed to verify complete removal of the cells.

## 2.4 Discussion

This study was designed to measure the effect of the local environment on the primary rat hepatocyte proteome. The local environments employed differed in the presence and absence of PEMs and LSECs. Distinct proteomic profiles were observed with hepatocytes from both the 3DHL and 3DH models relative to HMs (**Figure 5 and Figure 6**), with the most dramatic

difference related to lipid (**Figure 7 and Figure 8**), glucose (**Figure 9),** and drug (**Figure 11**) metabolism. Hepatocyte dedifferentiation was also evaluated (**Figure 10**) where it was determined that structural and trafficking proteins served as potential markers for this process.

The majority of proteins in the fatty acid β-oxidation (mitochondrial and peroxisomal) and ketogenesis pathways were found in higher abundances in the 3DHL and 3DH liver models when compared to HMs (**Figure 7A-C and Figure 8**). When intracellular concentrations of glucose in the liver are low, increases in fatty acid β-oxidation occur resulting in production of acetyl-CoA. Ketone bodies are subsequently produced and transported to extrahepatic tissues where conversion back to acetyl-CoA occurs for utilization as an energy source [183]. Changes in proteins associated with ketogenesis prompted the quantification of ketone bodies in the cell culture media. The investigation confirmed the presence of ketone bodies in spent media, although in contrast to the protein abundance data, HMs exhibited higher levels of both acetoacetate and β-hydroxybutyrate when compared to the 3DHL and 3DH liver models (**Figure 7C**). This discrepancy is not surprising considering that protein abundances do not account for changes in enzyme activity due to changes in protein-protein interactions and/or post-translational modifications. Bdh1, for example, requires lipid binding for full enzymatic activity [184], and is also known to be O-GlcNAcylated [185]. Nonetheless, the organotypic liver models are producing ketone bodies and utilizing fatty acid β-oxidation as an energy source. This occurs despite the fact that the extracellular glucose concentration was in excess of 20 mM, more than twice the normal blood glucose concentrations [186].

Previous studies have demonstrated the enrichment of fatty acid β-oxidation [151, 153-155] and ketogenesis [187-189] pathways during liver regeneration. In addition to these studies, freshly isolated primary hepatocytes have also been shown to up-regulate fatty acid metabolism

along with the simultaneous down-regulation of glycolytic pathways when compared to a hepatoma cell line (Hepa1-6) [136]. Based on the results from this study, hepatocytes from the 3DHL and 3DH liver models are exhibiting some similarities to what has been observed during liver regeneration. This also correlates with the previous observation of proliferation in both the 3DHL and 3DHLK liver models [19]. It is also worthy to note that while ketone body levels were lower in the PEM containing cultures, the ratio of acetoacetate to β-hydroxybutyrate for all constructs was maintained at levels similar to what has been observed after a partial hepatectomy [190]. This observation supports the concept that the liver models do not disrupt ketogenesis product ratios.

While lipid metabolism was shown to be favored in the 3DHL and 3DH liver models, the HM proteome exhibited higher levels of proteins related to glycolysis/gluconeogenesis (**Figure 9**). While very few *in vitro* liver model studies measure glucose, two recent studies showed that HM and CS cultures lost their ability to perform gluconeogenesis and glycolysis even when stimulated with insulin and glucagon after 3-4 days in culture [191, 192]. One significant difference between the aforementioned studies and this work is the composition of the cell culture media, an extremely important consideration in organotypic liver models. The hepatocyte medium used in this study contained FBS, glucagon and insulin throughout the culture period with daily media exchanges. This environment led to slightly increased glucose levels after three days of culture, suggesting that the glucagon supplement is overriding the effects of insulin and potentially placing the cells in a state perceived as starvation. However, enzyme activity will need to be verified to test this hypothesis. Additionally, while protein abundances for glucose metabolism were higher in the HMs, when comparing 3DHL and 3DH, there were measurable differences in protein abundances for two key steps in glycolysis and gluconeogenesis, including

Pklr and Fbp1 (**Figure 9**). Based on these observations, we hypothesize that the 3DHL liver models are initiating a shift towards glucose metabolism, and that this is due to the presence of LSECs. Studies utilizing longer culture times will be needed to confirm this hypothesis. In the very least, organotypic liver model studies should routinely include glucose measurements to assess the temporal status of glucose metabolism.

It has been shown that genomic changes in hepatocyte monolayers occur as early as 4 hours, essentially marking the beginning of dedifferentiation [69]. In addition to changes in the genome, previous studies have also shown that after seven days in culture, alterations in hepatocyte morphology are observed, resulting from increases in actin stress fibers [70, 71, 89]. Although very few studies have characterized the proteomic changes associated with this process [147, 148], we identified several proteins that exhibited increased protein abundances in HMs as compared to 3DHL and 3DH (**Figure 10**). Azimifar *et al.* evaluated hepatocyte proteomes at time points similar to those used in our work [158]. The proteomic changes reported as being related to dedifferentiation were increases in structural and trafficking proteins [158]. Annexins are multifunctional proteins often associated with cancer growth and membrane trafficking [193]. In our study, annexin A2, A3 and A5 levels in the HM was higher relative to the 3DH and 3DHL, suggestive of dedifferentiation. Additionally, S100 proteins (S100-A10 and S100-A11), which facilitate cell-cell contact through annexin proteins [194], were also identified as being significantly increased in HMs as compared to 3DHL and 3DH. Other structural proteins identified in this study and those that were also identified in our own were keratins (Krt 8), actins (Act1 and Actc1) and alpha-actinin-4 (Actn4). Krt18 was not identified in the study performed by Azimifar *et al.* Keratins are intermediate filament proteins that are present within the cytoskeleton and have been observed to increase in levels in dedifferentiated hepatocytes [195].

Alpha actinin proteins are involved in the cross linking of actin stress fibers [196], which have been shown to form during dedifferentiation. Proteins related to cell migration and motility were also increased in HM as compared 3DHL and 3DH such as myosins (Myl6 and Myh9), tropomyosins (Tpm4), transgelins (Tagln and Tagln2), cofilin (Cfl1), destrin (Dstn) and profilin (Pfn1). Myosins and tropomyosins regulate the contraction and movement of cells [195]. Silencing of transgelin proteins has been shown to inhibit the migration and invasion of huh7, hepatocarcinoma cells [197]. Cofilin, destrin and profilin are proteins that regulate actin dynamics by initiating and inhibiting the polymerization, de-polymerization and recycling of actin fibers [198-200]. Previous observations have shown that HMs exhibit a flattened and larger morphologies indicative of cell spreading and increased contractility of the cells [70]. Taken together, these results provide a foundation for understanding structural and cell migration proteins and how they contribute to the dedifferentiation in hepatocytes. Such information could be useful for assessing intercellular signaling processes associated with diseases such as cirrhosis and hepatocarcinoma.

The ECM plays a crucial role in maintaining hepatic function [88]. For example, synthesis of collagen by hepatocytes has been shown to contribute to enhancing albumin and urea production [96, 201]. However, in-depth studies on the ECM itself have not been performed on liver models. Proteomic analysis of the PEMs from the 3DHL and 3DH liver models and fresh/unused samples (FPs) was performed to study the effects of the cell culture and any potential ECM remodeling. Current methods used to study ECM are typically inaccurate in part due to the database used from protein identification [202]. While the most abundant proteins are usually identified, the lower abundant ECM components are not usually found due to the fact that many of these databases are too large and thus may assign ECM peptides to other proteins

[203]. Thus, a recent study limited their searches to ECM proteins and also databases that only contained various types of collagen in order to improve accuracy in identification [175]. In this study, we employed the same method where a database limited to ECM proteins was used for protein identification. Upon quantification, the results showed no statistical significance with respect to abundance changes in any ECM component identified (**Table 2**). Additionally, no other cellular components were identified suggesting that any these trends are attributed only to the PEMs (**Table 3**). We conclude from these results, that after 72 hours, only minor changes in the PEMs have occurred. Future studies will focus upon quantifying changes in serum proteins and other small molecules in the PEMs as these could be lend insight into signaling processes.

The biotransformation of drugs, xenobiotics and normal cellular waste products is a critical liver function. The 3DHL liver models exhibited significantly higher levels of phase I and phase II detoxification enzymes as compared to both 3DH and HMs (**Figure 11**), implicating LSECs in modulating the increase. Previous studies in our group have shown preserved activity of CYP1A1 for up to 12 days in culture [19, 89, 166]. Other studies were focused upon genomic changes or changes in enzymatic activity after induction in hepatocyte cultures [81, 86, 88]. Moreover, other studies have also been conducted on HMs cultured for a short period of time (40 hours) or on HepG2 cells treated with acetaminophen, amiodarone and cyclosporin and assessed changes in the drug metabolizing proteome [178, 204]. In our cultures, the presence of multiple cell types and extended culture period is more physiologically relevant. Our results demonstrate increases in levels of CESs, CYPs, UGTs, GSTs, GPXs and EPHXs enzymes. The class of enzymes that was most represented in this data and exhibited the most change between the 3DHL and 3DH cultures was the carboxylesterases enzymes suggesting LSECs modulate their levels. Carboxylesterases are a class of phase I and lipid processing enzymes that hydrolyze

molecules containing esters (such as lipids), amides, thioesters and carbamates [205, 206]. Increased extracellular glucose concentrations (25 mM) in cultured primary mouse hepatocytes leads to increased levels of Ces1d (76% identical to Ces1d in rat), with the increase linked to the farnesoid X receptor, FXR. This transcriptional regulator is typically activated by lipophilic compounds such as bile acids, providing global control of lipid and glucose metabolism [207, 208], where high glucose concentrations favor lipogenesis and glycogen formation. *Ces1g* knockout mice are obese and exhibit non-alcoholic fatty liver disease, a phenotype that can be rescued solely by the addition of polyunsaturated fatty acids [209]. These studies suggest that increased glucose levels in the environment could modulate the levels of carboxylesterase enzymes. As the carboxylesterases were present in significantly higher amounts in the 3DHL models, we propose that the increase was due to the presence of the LSECs. Further studies are needed to determine the signaling molecules and pathways involved.

## 2.5 Conclusions

MS based proteomic analyses were performed to assess the effects of PEMs and LSECs on hepatocyte function in organotypic liver models. The systems evaluated were shown to produce urea, albumin and glucose. Shifts to fatty acid metabolism and ketone body production were shown by both proteomics as well as a quantitative assessment of ketone body concentrations. Liver models that included PEMs and/or LSECs exhibited higher levels of proteins associated with lipid metabolism, and more specifically fatty acid β-oxidation and ketogenesis. Although minimal changes in the PEM were found, they served a critical role in maintaining differentiated hepatocytes. Several carboxylesterases exhibited a dependence on the presence of LSECs demonstrating their effect on the levels of detoxification enzymes present in these liver models.

# Chapter 3: Investigation of the liver sinusoidal endothelial cell proteome

## 3.1 Introduction

The liver is a core organ that performs many essential metabolic functions including biotransformation of xenobiotics, synthesis of blood plasma proteins, and cholesterol, steroid and bile acid metabolism [1, 4, 8, 12, 210, 211] The majority of these functions are carried out by the hepatocytes, the parenchymal cells that make up ~70% of the liver by volume [1]. The non-parenchymal cells (NPCs); the liver sinusoidal endothelial cells (LSECs), Kupffer cells (KCs) and hepatic stellate cells (HSCs) make up ~ 10%, ~5% and ~5% of the liver by volume respectively [1, 3]. All of these cells make up the sinusoid, the basic functional unit of the liver, and are arranged in a stratified, three-dimensional architecture, where the NPCs are separated from the hepatocytes by the Space of Disse.

Sinusoids are essentially capillary vessels that make up the hepatic cords that radiate from the central vein as described in **Chapter 1**. LSECs line the sinusoid walls and exhibit features known as fenestrae, which are pores on the surface of LSECs [32, 38]. Fenestrae structures and rapid endocytic uptake mechanisms endow LSECs with a scavenger role. Hence, LSECs play a crucial role in protein turnover and clearance of foreign and waste substances [34, 212] such as albumin [27, 28], low density lipoproteins [29, 213-216], ECM components [25, 32-34, 217], viral particles and endotoxins [34, 35] and immune complexes [26, 218]. To perform this role, LSECs utilize scavenger receptors (SRs) [22] such as SR-A [23], SR-B[24] SR-H [25] and also FC-λRIIb2 (Commonly referred to as SE-1) [26] as described in **Chapter 1**.

LSECs also play a role in maintaining balanced glucose and lipid levels in the liver via their scavenging abilities [32, 219, 220]. However, very few studies have investigated these mechanisms beyond endocytosis to specifically address how LSECs contribute to liver

metabolism. Studies have been performed using primary porcine NPCs cultured in a bioreactor to investigate their contribution to ammonia metabolism in the liver [221]. NPCs consumed ~ 4-fold higher glutamine within the first 24 hours of culture which correlated with ~ 2-fold increase ammonia production as compared to hepatocytes cultured under the same condition. This study highlights the roles of NPCs in core metabolism. Nedredal *et al.* extended this work by investigating the contributions of LSECs to ammonia metabolism [222]. They showed that porcine LSECs cultured in a bioreactor exhibited ~6-fold increase in ammonia production along with ~3-fold increase in consumption of glutamine by LSECs. These results highlight the role of LSECs in amino acid metabolism.

Interactions between the hepatocytes and the NPCs are essential for maintenance of a functional liver [3, 84, 223]. *In vitro* liver models that mimic the *in vivo* architecture have recently been developed [19, 89, 90, 92-94, 96, 101]. These models incorporate the hepatocytes as well as a combination of NPCs and all have shown enhanced hepatic functions as compared to their monocellular counterparts. Transcriptome analysis has been used to study the effects of intercellular communication on various types of co-cultures [81, 88]. These studies also investigated the effects of clinically relevant drugs on phase I and phase II enzyme expression but give no further insight into other physiological processes. Additionally, an in depth analysis of the proteomes of each cell type in these models has not been performed.

While the function of LSECs have been widely studied, to the best of our knowledge, there has only been one investigation that has evaluated their proteomes [158]. Freshly isolated primary murine LSECs, were shown to be enriched in cytoskeletal proteins such as actins, myosins and tropomyosins and asialoglycoprotein receptors, highlighting their roles in transducing mechanical forces and membrane trafficking [158]. However, no further analysis of

the LSEC proteome was performed. In this study, we sought to evaluate the LSEC proteome from cells cultured in monolayer format for 72 hours and provide preliminary data on the LSEC proteome when cultured with hepatocytes in a 3D liver model.

## 3.2 Materials and methods

### 3.2.1 Chemicals and reagents

Cell culture supplies including Dulbecco's Modified Eagle Medium (DMEM), phosphate-buffered saline (PBS), penicillin, streptomycin and human plasma fibronectin and trypsin (0.25% EDTA) were purchased from Life Technologies (Grand Island, NY). 4-[2-hydroxyethyl] piperazine-1-ethanesulfonic acid (HEPES), glucagon, glutaraldehyde, ethylenediaminetetraacetic acid (EDTA), hyaluronic acid (HA), hydrocortisone, Percoll, Type IV collagenase, chloroform, ammonium bicarbonate (AmBic), urea, trifluoroacetic acid (TFA), and mass spectrometry grade trypsin and endothelial cell growth supplement were purchased from Sigma Aldrich (St. Louis, MO). Mass spectrometry grade lysyl endopeptidase (Lys-C) was purchased from Wako (Richmond, VA). LC-MS grade solvents were purchased from Spectrum Chemicals (New Brunswick, NJ). All other chemicals, unless noted otherwise, were purchased from Fisher Scientific (Pittsburgh, PA).

### 3.2.2 Isolation and culture of hepatocytes

The primary hepatocytes were harvested from six adult female Lewis rats (Harlan, Dublin, VA) that weighed between 170 and 200 grams. Animal care and surgical procedures were conducted as per procedures approved by Virginia Polytechnic Institute and State University's Institutional Animal Care and Use Committee. Hepatocytes were isolated using a two-step collagenase perfusion as previously described [19, 89, 90, 171]. Viability of isolated hepatocytes were $\geq$ 97% and was determined via trypan blue exclusion. Hepatocytes were

cultured on a type I collagen coated 12-well plates at a density of 500,000 cells per well. Hepatocyte cultures were maintained in high glucose (25mM) DMEM supplemented with 10% (v/v) heat inactivated fetal bovine serum (FBS), 200 U/mL penicillin and 200 μg/mL streptomycin, 0.5 U/mL insulin, 4 nM glucagon, and 16 μM hydrocortisone. Media exchange was performed daily.

### 3.2.3 LSEC monolayer isolation

LSECs were also harvested from six adult female Lewis rats. LSECs were purified from the total NPC fraction using a differential adhesion method [19, 90] and were cultured on a fibronectin-coated flask. LSECs were maintained in endothelial cell medium consisting of Media 199 supplemented with 10% (v/v) heat inactivated FBS, 100 U/mL penicillin and 100 μg/mL streptomycin, and 30 μg/mL endothelial cell growth supplement. Endothelial cell media was exchanged daily. After 72 hours, isolation of the LSECs was performed. LSECs in the flask was washed three times with 1X PBS and treated with trypsin (0.25% EDTA) for 7 minutes. 15 mL of hepatocyte media, which corresponds to three times the volume of trypsin used, was subsequently added to neutralize the trypsin activity. LSECs were collected by centrifugation at 900 *x g* for 7 minutes, lysed and treated with a protease inhibitor cocktail. The lysis buffer used contained the following components: 4.3 mM Tris-HCl, 660 μM Tris, 500 μM EDTA, 15 mM NaCl, 350 μM SDS, 0.1% (v/v) Triton X-100, 310 μM sodium azide and 150 μM sodium vanadate and was supplemented with a protease inhibitor (PI) cocktail. This PI cocktail contained 104mM 4-(2-Aminoethyl) benzenesulfonyl fluoride hydrochloride (AEBSF), 80 μM Aprotinin, 4 mM Bestatin, 1.4 mM epoxide 64 (E-64), 2 mM Leupeptin and 1.5 mM Pepstatin A (Sigma-Aldrich). Lysates were snap frozen in liquid nitrogen and stored at -80°C until further processing.

### 3.2.4 Type I collagen isolation

Type I collagen was isolated from rat tail tendons as previously reported [71, 172]. Briefly, tendons were dissected from tails and dissolved in a 3% acetic acid solution overnight at 4°C. The solution was subsequently passed through cheesecloth filters and centrifuged at 13,000 *x g* for 2 hours at 4°C. The supernatant was precipitated using 30% (w/v) sodium chloride and the resultant precipitate was dissolved in 0.6% (v/v) acetic acid for 48 hours at 4°C. The solution was dialyzed against 1 mM hydrochloric acid and sterilized by chloroform. The concentration of collagen was determined by measuring the optical density at 280 nm.

### 3.2.5 Polyelectrolyte multilayer (PEM) assembly

Type I Collagen (cationic) and HA (anionic) were used for the assembly of PEMs using methods as previously described [19, 106]. Collagen was diluted in 1% (v/v) acetic acid and HA was dissolved in 18 MΩ cm water. Both solutions were maintained at a concentration of 1.5 mg/mL and a pH of 4.0. PEMs were assembled on a hydrophobic polytetrafluoroethylene (PTFE) substrate (McMaster-Carr, Atlanta, GA) using a robotic deposition system (NanoStrata Tallahassee, FL). The PTFE substrates were sonicated in toluene for one hour, rinsed in 18 MΩ cm water, and dried overnight. Water contact angle measurements were used to verify the hydrophobicity of the substrate and ranged between 110°-115° (Averaged over 10 measurements per substrate). Deposition times of 30 min were used for each polyelectrolyte with a 10 minute rinse in 18 MΩ cm water maintained at a pH of 4.0 between each deposition. The PEMs used in these studies consisted of 15 bilayers (BL). A BL is defined as the deposition of one cationic and one anionic layer. PEMs were cross-linked with 8% (w/v) glutaraldehyde for 30 seconds, rinsed in deionized (DI) water for 48 hours, dried and stored at room temperature. Prior to cell culture, PEMs were sterilized under germicidal UV for 1 hour.

### 3.2.6 Liver model assembly

Hepatocytes were cultured on a type I collagen gel for 72 hours. The PEMs were overlaid above the hepatocytes and were hydrated with hepatocyte media for 1 hour at 37°C. LSECs were then seeded above the PEMs at a density of 25,000 cells per well to form the three-dimensional liver model, which will be referred to as 3DHL throughout. “H” and “L” refer to the hepatocytes and LSECs respectively.

### 3.2.7 LSEC isolation and processing of lysates

LSECs were isolated from the liver models by removing the PEMs from the culture and treated with trypsin (0.25% EDTA) for 7 minutes. 15 mL of hepatocyte media, which corresponds to three times the volume of trypsin used, was subsequently added to neutralize the trypsin activity. LSECs were collected by centrifugation at 900 *x g* for 7 minutes, lysed and treated with a protease inhibitor cocktail as described in section 3.2.3. Protein concentrations were determined using a commercial BCA protein assay kit (ThermoFisher). Lysates were snap frozen in liquid nitrogen and stored at -80°C until further processing. Hepatocytes and PEMs were also isolated as described in **Chapter 2**. LSEC lysates from both the monolayers and 3DHL liver models were also processed using the same methods as described in **Chapter 2**. LC-MS grade methanol was added to 20 µg of LSEC lysate and incubated at -80°C overnight. Samples were centrifuged (13,000 *x g*, 20 min) and the protein pellets were dried in a vacuum concentrator and re-suspended in freshly prepared 8 M urea in 100 mM ammonium bicarbonate (AmBic) to a concentration of approximately 1 mg/mL. The proteins were reduced using dithiothreitol (DTT, 45 mM in 100 mM AmBic) for 1 hour at 37°C and subsequently alkylated at room temperature in the dark for 30 minutes with iodoacetamide (100 mM in 100 mM AmBic). Excess

iodoacetamide was quenched with DTT/100 mM AmBic, which also diluted the urea to approximately 2M.

Protein digestion utilized a two-step procedure [120]. Lys-C was added at a ratio of 1:50 (Lys-C:protein) and incubated overnight at 37°C with shaking. After dilution with 100 mM AmBic, trypsin was added at the same ratio as was used with Lys-C. Incubation was performed for 4 hours at 37°C with shaking, at which time the digestion was quenched by adding trifluoroacetic acid (TFA) until the pH was less than 3.0. The resultant acidified peptides were desalted using $C_{18}$ OMIX Tips (Agilent Technologies). The tips were conditioned prior to use with LC-MS grade methanol and subsequently equilibrated with Solvent 1 (50:50 water:acetonitrile supplemented with 0.1 % TFA) followed by Solvent 2 (98:2 water: acetonitrile supplemented with 0.1 % TFA). The peptides were bound to the tips by repeated aspiration and dispensing, desalted using Solvent 2, and eluted using Solvent 1. The recovered peptides were dried in a vacuum concentrator and reconstituted in Solvent 2 (1 µg/µL) for analysis via LC-MS/MS.

### 3.2.8 LC-MS analysis

Approximately 7 µg of each peptide sample was loaded onto an Acquity UPLC I-class system equipped with a CSH130 $C_{18}$ 1.7 µm, 1.0 x 150 mm column maintained at 45°C (Waters Corporation, Milford, MA). The mobile phases were 0.1% formic acid in water (Solvent A) and 0.1% formic acid in acetonitrile (Solvent B). Separations were performed at a flow rate of 50 µL/min, using a 110 minute gradient from 3-40% solvent B, with all samples analyzed in duplicate. The column effluent was sprayed directly into a Synapt G2-S mass spectrometer using the high definition mass spectrometry ($HDMS^E$) mode (continuum, positive-ion, "resolution" MS settings). Source conditions were as follows: capillary voltage, 3.0 kV; source temperature,

120˚C; sampling cone, 60 V; desolvation temperature, 350˚C; cone gas flow, 50 L/hr; desolvation gas flow, 500 L/hr; nebulizer gas flow, 6 bar. Both low energy (4 and 2 V in the trap and transfer regions, respectively) and elevated energy (4 V in the trap and ramped from 20 to 50 V in the transfer region) scans were 1.2 seconds each for the m/z range of 50 to 1800. For the ion mobility separation (IMS), the IMS and transfer wave velocities were 600 and 1200 m/sec, respectively. Wave height within the ion mobility cell was ramped from 10 to 40 V. For lock mass correction, a 1.2 second low energy scan was acquired every 30 seconds from a 100 fmol/μL [Glu1]-fibrinopeptide B solution (50:50 acetonitrile: water supplemented with 0.1 % formic acid). The infusion rate on the lock spray was 10 μL/min, and introduced into the mass spectrometer at a capillary voltage of 3.0 kV. Lock mass correction was invoked during the data analysis phase of the work.

**3.2.9 Data analysis**

Raw data files were analyzed using Protein Lynx Global Server (PLGS, Version. 3.0, Waters™ Corporation). LC-MS data was queried against a combined rat and bovine proteome concatenated with a randomized decoy database, allowing for two missed trypsin cleavages. A minimum peptide length was set to five amino acids, with carbamidomethylation of cysteine set as a fixed modification. Oxidation of methionine, proline (*i.e*., hydroxyproline) and lysine (*i.e*. hydroxylysine) were set as variable modifications. Additionally, galactosylation and glucosylgalactosylation of lysine, glycosylation of proline, conversion of N-terminal glutamine to pyro-glutamate and deamidation of asparagine and glutamine were also set as variable modifications. The criteria used for protein identification utilized both a false discovery rate (FDR) of less than 5% and required at least two peptides per protein. The raw PLGS output was then quantified using PLGS expression analysis using the TOP3 method [141], where the sum of

the three most intense peptides was compared across culture conditions (*i.e.* LSEC monolayers vs 3DHL LSECs). This allows for relative quantification of protein abundances between the two experimental conditions. Categorical annotation was performed on the results from the LSEC monolayers to assess statistically significant pathways as compared to the rat proteome [158, 174].

## 3.3 Results

### 3.3.1 Characterization of LSEC monolayers

In this study, LSECs were isolated and cultured as monolayers for 72 hours and proteomes were characterized.

**Table 4: Comparison of the number of proteins identified in both LSECs from monolayers and those from 3DHL liver models. Confidently identified proteins were derived using a false discovery rate of less than 1%.**

| Culture_replicate | Number of confidently identified proteins |
|---|---|
| LSEC monolayer_1 | 127 |
| LSEC monolayer_2 | 324 |
| LSEC monolayer_3 | 356 |
| 3DHL_1 | 10 |
| 3DHL_2 | 37 |
| 3DHL_3 | 28 |

Overall, in the LSEC monolayers, 127-356 rat proteins were confidently identified in the three replicates (**Table 4**). This list was limited to proteins that were confidently identified by employing a false discovery rate (FDR) of less than 1%. One replicate resulted in significantly less identifications which could potentially be due to biological variation between samples. The list of proteins from each replicate is presented in Appendix A, **Tables A1-A3**, of this dissertation. To determine statistically over-represented processes, as compared to the rat genome, categorical annotation using DAVID was employed [158].

**Table 5** only lists select KEGG pathways that were statistically significant in all three replicates of LSECs. The complete list of statistically significant processes is presented in Appendix A, **Table A4**. Other statistically significant processes included Parkinson's disease and Huntington's disease. These KEGG pathways were not included in Table 5 because many of the proteins annotated to these pathways were also included in Oxidative phosphorylation. These proteins included those that were part of the electron transport chain (Complexes I- IV).

**Table 5: Metabolic functions are performed by LSECs. List of KEGG pathways that were enriched in all three replicates of LSEC monolayers.**

| KEGG Pathway | *p*-value |
|---|---|
| Valine, leucine and isoleucine degradation | 7.20E-33 |
| Fatty acid metabolism | 3.60E-19 |
| Oxidative phosphorylation | 2.30E-11 |
| Drug metabolism | 3.80E-07 |

The most enriched KEGG pathways in LSECs are branched chain amino acid metabolism (valine, leucine and isoleucine degradation), fatty acid metabolism, oxidative phosphorylation and drug metabolism. This suggests that some of the key functions performed by LSECs are related to core metabolism. Proteins in at least two of the three replicates that were identified in this study and were part of the enriched pathways of the catabolism of valine, leucine and isoleucine are presented in **Table 6** and **Figure 12**

**Table 6: Proteins related to branched chain amino acid degradation were identified in LSEC monolayers.**

| UniProt ID | Gene ID | Protein description |
|---|---|---|
| P35738 | Bckdhb | branched chain keto acid dehydrogenase E1, beta polypeptide |
| P11960 | Bckdha | branched chain ketoacid dehydrogenase E1, alpha polypeptide |
| P15651 | Acads | acyl-Coenzyme A dehydrogenase, short chain |
| P08503 | Acadm | acyl-Coenzyme A dehydrogenase, medium chain |
| P70584 | Acadsb | acyl-Coenzyme A dehydrogenase, short/branched chain |
| P14604 | Echs1 | enoyl Coenzyme A hydratase, mitochondrial |
| Q64428 | Hadha | trifunctional protein, alpha subunit |
| Q60587 | Hadhb | trifunctional protein, beta subunit |
| Q5I0C3 | Mccc1 | methylcrotonoyl-Coenzyme A carboxylase 1 (alpha) |

| | | |
|---|---|---|
| Q5XIT9 | Mccc2 | methylcrotonoyl-Coenzyme A carboxylase 2 (beta) |
| P07633 | Pccb | propionyl coenzyme A carboxylase, beta polypeptide |
| P14882 | Pcca | propionyl-coenzyme A carboxylase, alpha polypeptide |

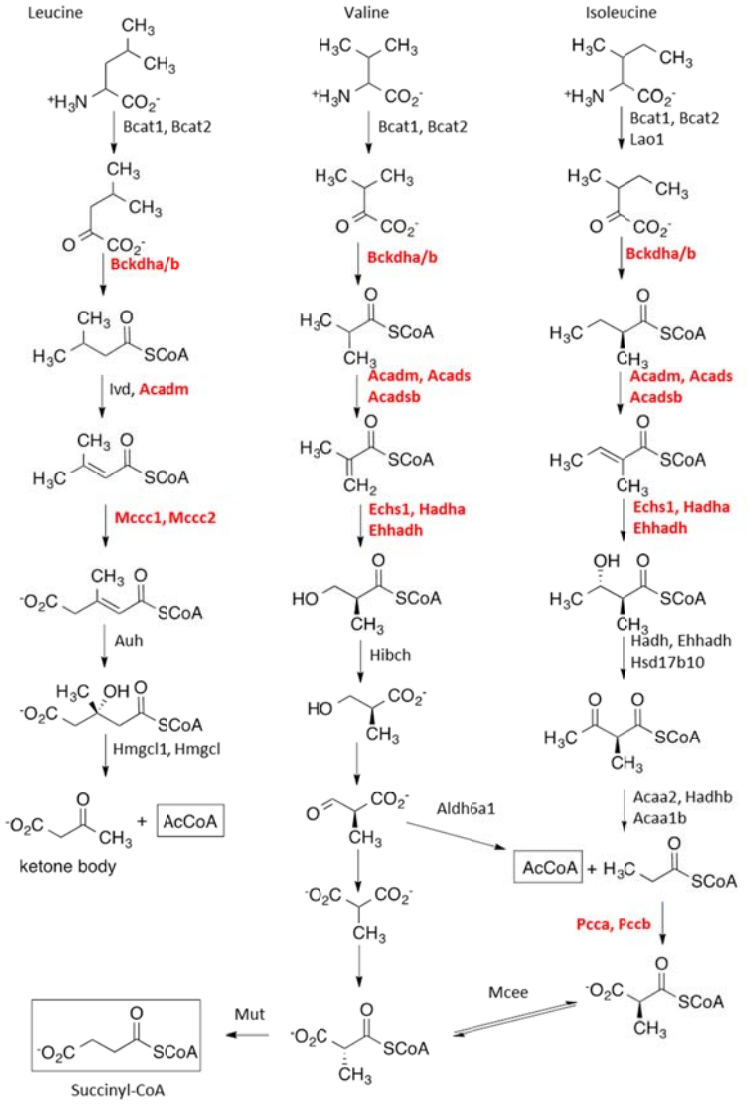


**Figure 12: Valine, leucine, and isoleucine degradation pathway with proteins identified in this study highlighted in red.**

These pathways share many proteins with mitochondrial fatty acid β-oxidation (Acads, Acadm, Acadsb, Echs1, Hadha, and Hadhb) due to the ultimate formation of acetyl-CoA (AcCoA) (**Figure 12**) from branched chain amino acids. Proteins identified in at least two of the three replicates of this study that are involved in fatty acid metabolism are presented in **Table 7**.

**Table 7: Proteins related to mitochondrial fatty acid β-oxidation were identified in LSEC monolayers.**

| UniProt ID | Gene ID | Protein description |
|---|---|---|
| P18163 | Acsl1 | acyl-CoA synthetase long-chain family member 1 |
| O88813 | Acsl5 | acyl-CoA synthetase long-chain family member 5 |
| P18886 | Cpt2 | carnitine palmitoyltransferase 2 |
| P15651 | Acads | acyl-Coenzyme A dehydrogenase, short chain |
| P08503 | Acadm | acyl-Coenzyme A dehydrogenase, medium chain |
| P15650 | Acadl | acyl-Coenzyme A dehydrogenase, long-chain |
| P70584 | Acadsb | acyl-Coenzyme A dehydrogenase, short/branched chain |
| P45953 | Acadvl | acyl-Coenzyme A dehydrogenase, very long chain |
| P14604 | Echs1 | enoyl Coenzyme A hydratase, mitochondrial |
| Q64428 | Hadha | trifunctional protein, alpha subunit |
| Q60587 | Hadhb | trifunctional protein, beta subunit |

Proteins in this list are related to the formation of fatty acyl-CoA (Acsl1 and Acsl5), transport of fatty acids into the mitochondria (Cpt2) and the steps of β-oxidation (Acads, Acadm, Acadsb, Acadvl, Echs1, Hadha. And Hadhb) were identified in LSEC monolayers. This suggests LSECs could be utilizing lipids and amino acids as metabolic inputs for derivation of energy. Future studies will need to be performed to verify this hypothesis. In addition to proteins related to the metabolism of amino acids and lipids being present in LSECs, proteins related to oxidative phosphorylation were also identified and is shown in **Table 8**.

**Table 8: Proteins related to oxidative phosphorylation were identified in LSEC monolayers.**

| UniProt ID | Gene ID | Protein description |
|---|---|---|
| Q6P6W6 | Ndufa10 | NADH dehydrogenase (ubiquinone) 1 alpha subcomplex 10-like 1; NADH dehydrogenase (ubiquinone) 1 alpha subcomplex 10 |
| Q66HF1 | Ndufs1 | NADH dehydrogenase (ubiquinone) Fe-S protein 1 |
| Q641Y2 | Ndufs2 | NADH dehydrogenase (ubiquinone) Fe-S protein 2 |
| P19234 | Ndufv2 | NADH dehydrogenase (ubiquinone) flavoprotein 2 |
| Q920L2 | Sdha | succinate dehydrogenase complex, subunit A, flavoprotein (Fp) |
| P21913 | Sdhb | succinate dehydrogenase complex, subunit B, iron sulfur (Ip) |
| P32551 | Uqcrc2 | ubiquinol cytochrome c reductase core protein 2 |
| Q68FY0 | Uqcrc1 | ubiquinol-cytochrome c reductase core protein I |
| Q5M9I5 | Uqcrh | ubiquinol-cytochrome c reductase hinge protein |
| P20788 | Uqcrfs1 | ubiquinol-cytochrome c reductase, Rieske iron-sulfur polypeptide 1 |
| P10888 | Cox4i1 | cytochrome c oxidase subunit IV isoform 1 |
| P12075 | Cox5b | cytochrome c oxidase subunit Vb |

| | | |
|---|---|---|
| P11240 | Cox5a | cytochrome c oxidase, subunit Va |
| P10818 | Cox6a1 | cytochrome c oxidase, subunit VIa, polypeptide 1 |
| P11951 | Cox6c2 | cytochrome c oxidase, subunit Vic |
| P19511 | Atp5f1 | ATP synthase, H+ transporting, mitochondrial F0 complex, subunit B1 |
| P31399 | Atp5h | ATP synthase D chain, mitochondrial; ATP synthase, H+ transporting, mitochondrial F0 complex, subunit d |
| P29419 | Atp5i | ATP synthase, H+ transporting, mitochondrial F0 complex, subunit E |
| Q6PDU7 | Atp5l | ATP synthase, H+ transporting, mitochondrial F0 complex, subunit G |
| P15999 | Atp5a1 | ATP synthase, H+ transporting, mitochondrial F1 complex, alpha subunit 1, cardiac muscle |
| P10719 | Atp5b | ATP synthase, H+ transporting, mitochondrial F1 complex, beta polypeptide; similar to ATP synthase beta chain, mitochondrial precursor |
| P35435 | Atp5c1 | ATP synthase, H+ transporting, mitochondrial F1 complex, gamma polypeptide 1 |
| Q06647 | Atp5o | ATP synthase, H+ transporting, mitochondrial F1 complex, O subunit |

Various subunits from each of the proteins of each complex of the electron transport chain were identified. Complex I (NADH dehydrogenase), complex II (Succinate dehydrogenase), complex III (ubiquinol:cytochrome c reductase), complex IV (cytochrome c oxidase) and ATP synthase ($F_0$ and $F_1$ subunits) were identified in LSECs suggesting the presence of oxidative phosphorylation and the synthesis of ATP which are processes involved in fulfilling the energy requirements of the cells.

Another essential function of the liver is the biotransformation of drugs and xenobiotics to substances that are excreted from the body. This data suggests that LSECs play an important role in this process and exhibit proteins related to phase I (cytochrome p450 enzymes, CYPs and flavin containing monooxygenase 3) and phase II detoxification (glutathione s-transferases and UDP glucuronyltransferases) processes as shown in **Table 9.**

**Table 9: Proteins related to drug metabolism were identified in LSEC monolayers. These proteins were arranged by class where Cyp and Fmo enzymes are phase I with the remaining classified as phase II detoxification enzymes.**

| UniProt ID | Gene ID | Protein description |
|---|---|---|
| P11711 | Cyp2a1 | cytochrome P450 2A1 |
| Q64614 | Cyp2c6 | cytochrome P450 2C6 |
| P05179 | Cyp2c7 | cytochrome P450 2C7 |
| P11510 | Cyp2c12 | cytochrome P450 2C12 |
| P05182 | Cyp2e1 | cytochrome P450 2E1 |
| Q9EQ76 | Fmo3 | flavin containing monooxygenase 3 |

| | | |
|---|---|---|
| P24473 | Gstk1 | glutathione S-transferase kappa 1 |
| P57113 | Gstz1 | glutathione transferase zeta 1 |
| P08011 | Mgst1 | microsomal glutathione S-transferase 1 |
| P20720 | Ugt1a2 | UDP glucuronosyltransferase 1A2 |
| P08430 | Ugt1a6 | UDP glucuronosyltransferase 1A6 |
| P70624 | Ugt1a7 | UDP glucuronosyltransferase 1A7 |
| Q64550 | Ugt1a1 | UDP glucuronosyltransferase 1A1 |
| Q64638 | Ugt1a5 | UDP glucuronosyltransferase 1A5 |
| P09875 | Ugt2b1 | UDP glucuronosyltransferase 2B17 |
| P36511 | Ugt2b15 | UDP glucuronosyltransferase 2B36 |

### 3.3.2 Preliminary analysis of the 3DHL LSECs

Initially, the goal of this study was to characterize the proteomic changes between LSECs cultured as monolayers against those in 3DHL liver models. However, upon analysis of the number of confidently identified proteins between LSEC monolayers and 3DHL LSECs, drastic differences were observed as shown in **Table 4**. Further interrogation of the raw data suggested that the contaminant peptides in the 3DHL LSECs were causing suppression of the rat peptides and thus less proteins identifications resulted. This was verified by examining the differences in the contaminant proteins between the two culture conditions. Select proteins are presented in **Table 10** with the full list of contaminants compared shown in Appendix A, **Table A5**.

**Table 10: List of select contaminant proteins that were compared between LSECs from monolayers and 3DHL liver models.**

| Protein description | Fold change (3DHL/LSEC) |
|---|---|
| Chain B, Porcine E-Trypsin (E.C.3.4.21.4) [Sus scrofa (contaminant)] | 7.69 ± 0.84 |
| Chain A, Crystal Structure Of The First Active Autolysate Form Of The Porcine Alpha Trypsin [Sus scrofa (contaminant)] | 7.77 ± 0.81 |
| Chain A, Crystal Structure Of Porcine Beta Trypsin With 0.01% Polydocanol [Sus scrofa (contaminant)] | 10.59 ± 0.84 |
| Chain A, Trypsin (E.C.3.4.21.4) Complexed With Inhibitor From Bitter Gourd [Sus scrofa (Contaminant)] | 10.70 ± 0.79 |
| Chain A, Complex Of The Second Kunitz Domain Of Tissue Factor Pathway Inhibitor With Porcine Trypsin [Sus scrofa (contaminant)] | 11.02 ± 0.83 |
| Trypsin precursor (EC 3.4.21.4) [Sus scrofa (contaminant)] | 11.13 ± 0.84 |
| Chain A, Porcine E-Trypsin (E.C.3.4.21.4) [Sus scrofa (contaminant)] | 11.59 ± 0.38 |
| Chain E, Leech-Derived Tryptase InhibitorTRYPSIN COMPLEX [Sus scrofa (contaminant)] | 12.55 ± 0.83 |
| Chain C, Porcine E-Trypsin (E.C.3.4.21.4) [Sus scrofa (contaminant)] | 19.69 ± 0.69 |

| | |
|---|---|
| gi\|2190337\|emb\|CAA41735.1\| serum albumin [Bos taurus (contaminant)] | 1.23 ± 0.96 |
| gi\|1351907\|sp\|P02769\|ALBU_BOVIN Serum albumin precursor (Allergen Bos d 6) (BSA) [Bos taurus (contaminant)] | 1.25 ± 0.96 |

The contaminant proteins exhibiting the greatest fold change in 3DHL as compared to LSEC monolayers were components of porcine (*Sus scrofa)* trypsin (~1.5-19.6 fold change). These results indicate that the ion suppression resulted from excess trypsin present in the 3DHL LSECs. The amount of excess trypsin may have been due to experimental error where incomplete aspiration of the media and trypsin occurred after centrifugation during the isolation of the 3DHL LSECs. This did not occur during the isolation of the LSEC monolayers because the size of the resulting cell pellet after centrifugation was large enough so that aspiration could be performed without disruption of cell pellet. During the 3DHL LSEC isolation, the cell pellet was not as clearly defined possible due to a decreased amount of cells. Additionally, levels of bovine serum albumin were also increased in the 3DHL LSECs as compared to LSEC monolayers (~1.2 fold change) suggesting the potential for endocytosis of these contaminants. Additionally, these trends could also be attributed to the residual media and trypsin components left from incomplete aspiration after centrifugation. Future studies will need to be performed in order to test the hypothesis of possible endocytosis of the serum albumin by the LSEC. However, based on these results, it is not possible to accurately quantify the differences in the LSEC monolayers and 3DHL LSEC proteomes between the two culture conditions due to the presence of tryptic proteins that are causing ion suppression.

## 3.4 Discussion

In this study the proteome of LSEC monolayers were characterized in order to gain insight into their physiological processes prior to assembly of a 3D liver model. Based on categorical annotation, valine, leucine and isoleucine degradation (**Table 6**), fatty acid

metabolism (**Table 7**), oxidative phosphorylation (**Table 8**) and drug metabolism (**Table 9**) were among the most significantly enriched KEGG pathways, indicating that these core functions are performed by LSECs monolayers**.** It is worthy to note that categories related to neurodegenerative disorders, such as Parkinson's disease and Huntington disease, were also found to be statistically significant in the LSEC monolayers. Upon further investigation, it was determined that proteins corresponding to oxidative phosphorylation were also annotated to these pathways. Many studies have shown that mitochondrial dysregulation, specifically to Complex I, is implicated in Parkinson's disease patients [224-226]. Similar observations have also been reported for Huntington's disease, where the activities of Complexes II and III have been shown to decrease under diseased states [227-229]. However, since these diseases are not liver specific, annotations to these pathways are not relevant to our studies and therefore are not discussed. Within the context of the liver, catabolism of leucine and isoleucine leads to the formation of acetyl-CoA, the entry point into the tricarboxylic acid (TCA) cycle. Acetyl-CoA is also produced via fatty acid β-oxidation (acyl-Coenzyme A dehydrogenases, enoyl Coenzyme A hydratase and trifunctional enzymes). Additionally, valine and isoleucine are both metabolized and form succinyl-CoA, which also enters the TCA cycle (**Figure 12**). Electrons produced from the TCA cycle are passed into the electron transport chain, which consist of proteins that span between the intermembrane space and the matrix of the mitochondria, where oxidative phosphorylation occurs. Each complex in the electron transport chain performs a separate function and is linked to these metabolic processes [182]. Complex I accepts electrons from the reduced form of nicotinamide adenine dinucleotide (NADH), which serves as the link between processes such as glycolysis, fatty acid β-oxidation, amino acid degradation and the electron transport chain. Complex II accepts electrons from succinyl-CoA which provides a link between the TCA cycle

and the electron transport chain. Ubiquinone, in its reduced form, is produced from Complexes I and II and is a substrate for Complex III where it is oxidized while cytochrome c is reduced. The reduced cytochrome c is passed to Complex IV where reduction of oxygen occurs resulting in the formation of water. As electrons are passed through each complex, protons ($H^+$) are also transported into the mitochondrial intermembrane space. Accumulation of $H^+$ drives the formation of adenosine triphosphate (ATP). As $H^+$ re-enters the matrix side of the mitochondria through the $F_0$ subunit of ATP synthase, ATP is formed. Together this process results in an energy currency (ATP) that the cells will utilize to drive all metabolic processes. Further work will be needed to characterize the activity of each of these electron transport chain complexes, and their roles in the LSECs from monolayers and 3D models.

With regards to drug metabolism, the role that LSECs play has not been investigated in great detail. One study has shown an effect of acetaminophen toxicity on LSECs, but was limited to measuring cell viability and metabolite levels *in vivo* [230]. Only one such study has been performed to date focusing on characterizing the proteome of freshly isolated primary murine LSECs [158]. Their results highlighted the role of LSECs in supporting cellular structure and membrane trafficking. However, results relating to the detoxification abilities of LSECs were not discussed. In terms of phase I detoxification proteins, both our study and that of Azmifar *et al.* identified CYP2E1 and FMO3 [158]. Microsomal glutathione S-transferase, glutathione S-transferase kappa 1, UDP glucuronosyltransferase 2B17, 1A1, 1A7, and 1A6 were among the commonly identified phase II enzymes in both studies. Among the CYP family, CYP 2A1, 2C6, 2C7, 2C12, and 2E1 were identified in this study. This family of enzymes is responsible for performing the biotransformation of drugs, xenobiotics and steroids [1, 231, 232]. For example, CYP2A1 catalyzes the transformation of testerone to 7α-hydroxytestoterone [233, 234]. CYP

2C6 catalyzes the transformation of drugs such as Warfarin, an anticoagulant, and Diclofenac, a nonsteroidal anti-inflammatory drug (NSAID), in rats [235, 236]. CYP2E1 is ethanol inducible and metabolizes low molecular weight compounds such as ethanol, acetaminophen, and carbon tetrachloride [231, 237]. Among the phase II enzymes, GST and UGT enzymes were identified in the LSEC monolayers. This family of enzymes is involved in the conjugation of drugs and xenobiotics, yielding products that are excreted from body [238]. GSTs conjugate glutathione to products from phase I detoxification [239, 240]. For example, n-acetyl-p-benzoquinoneimine, a product formed from the conversion of acetaminophen by CYP2E1, is conjugated to glutathione via GSTs [239]. As a result of this conjugation, glutathione depletion occurs resulting in increased toxicity due to acetaminophen [240]. UGT enzymes perform glucuronidation in which uridine- 5′-diphospho-α-D-glucuronic acid (UDPGA) is conjugated to alcohols, phenols, carboxylic acids, thiols and amines allowing for excretion via the bile or urine [238, 241]. Taken together, these results highlight the role of LSECs in metabolism of amino acid, lipids and oxidative phosphorylation and phase I and phase II detoxification processes.

Preliminary analysis of the LSECs from 3DHL liver models determined that a technical error was performed during the isolation. Incomplete removal of the supernatant after centrifuging occurred leaving a minute, yet significant amount of contaminant proteins along with the cells (**Table 10**). It is possible that the LSECs could be performing endocytosis on the components present within the microenvironment such as HA from the PEMs and bovine proteins from the cell culture media. However, further imaging studies using labeled serum proteins, such as albumin, would be needed to confirm this hypothesis. Nevertheless, given the amount of trypsin present in these samples, accurate quantification was not feasible. Future studies will have to take this into account to ensure accurate quantification and also determine if

it is possible to separate the role of the HA containing PEMs from that of the hepatocytes on LSECs.

## 3.5 Conclusions

The investigation of LSEC proteomes cultured in a monolayer format, as well as in the 3D liver models was performed. LSECs monolayers were enriched in functions related to core metabolism and detoxification, including branched chain amino acid and lipid metabolism. These functions play a critical role in fulfilling the energy needs of the cells. When these cells were cultured for 3 additional days in the 3D liver models, large amounts of serum and trypsin proteins from the media were identified. This technical limitation did not allow for firm conclusions to be made on the differences between LSEC monolayers and those cultured in the 3DHL liver models. It is possible that the LSECs may be performing endocytosis of the serum components, a known role of these cells. Future studies will be needed to confirm this hypothesis. Nonetheless, this study provides the foundation upon which more in-depth analyses can be performed using the 3DHL LSECs.

# Chapter 4: Future work

The work presented in this dissertation evaluated the effects of the PEMs and LSECs on hepatocytes proteomes after six days of culture, permitting 72 hours of assembled liver model functional activity. Proteomic datasets for HMs, 3DH and 3DHL liver models indicated the PEM was the major factor in the resulting proteome. Characterization of the proteome of LSEC monolayers after 72 hours established an initial proteome for this cell type as well. In conjunction with the 3DHL/3DH/HM study, we determined that the hepatocytes at 72 hours are in a physiologically starved state producing both glucose and ketone bodies, even though the media glucose concentration was well above the normal postprandial concentration [186]. While these results provide new insights into organotypic liver model function, they also suggest new testable hypotheses worthy of further exploration.

## 4.1 Functional characterization and media studies

During the time frame evaluated, the hepatocytes were observed to be in a gluconeogenic state, releasing both glucose and ketone bodies to the medium. This does not mimic the metabolic state of a normal functioning liver. Initial evaluation of glucose levels during longer culture periods would determine if the cells begin to function as traditional hepatocytes using the current media formulation. If they do not, then media formulations may need to be modified, starting with a reduction in glucagon levels. Use of a rapid glucose analyzer would permit real time studies to be performed to assess for optimal glucagon levels. The presence and absence of epidermal growth factor (EGF) could also be evaluated as it has been shown to promote DNA synthesis and is commonly used in hepatocyte media [19, 70, 71, 89-91, 101]. However, it was not used in the proteomics investigations discussed in Chapters 2 and 3. These studies will provide a foundation for producing a model that utilizes glucose as feedstocks instead of lipids in

accordance with a normal functioning liver tissue. In addition to glucose measurements, functional markers such as albumin and urea production will also need to be measured to assess liver function

## 4.2 Evaluation of hepatocyte proteomes in the presence of both the LSECs and PEMs utilizing longer culture periods and optimized media conditions

The results from the above projects provide a functional model system that can be re-evaluated at the proteome level. An initial study would center on the 3DH and 3DHL models, and it is recommended that evaluation of the PEMs also occur at these time points as well. This could potentially provide information on matrix remodeling that is conducive to liver function. Future work should also include elucidating the effects of hepatocytes on the LSECs as this was the original aim of Chapter 3. Care should be taken when isolating the cells from the PEMs to make sure all of the components of the media and other possible contaminants are removed. Introduction of an extra wash step after isolation of the cells, but before lysis, possibly with a buffer solution like PBS, would be beneficial. This would allow for more accurate quantification of protein content and proteomic differences between culture conditions. However, it is also possible the contaminants will never be completely eliminated due to the rapid scavenger and endocytotic activities of these cells. Imaging studies using fluorescently labeled albumin may allow a rapid assessment of the extent to which contamination is due to normal LSEC function. Such studies must also bear in mind that rat LSECs are small and thus there will always be the challenge of detection limits for LSEC proteomics.

## 4.3 Proteomics and metabolomics of more complex models

To expand this study further, the addition of the other NPCs types and their effect on the hepatocyte proteome should be evaluated. The first experiment would be to determine the differences between liver models containing hepatocytes, LSECs, and a PEM with and without

the addition of KCs. Standard conditions ascertained previously should be employed, with assessment of urea, albumin and glucose performed as well. If possible, more than one time point should be chosen and the PEMs should be harvested. This would provide insight into how communication among the three cells types influences hepatocyte proteomes. Additionally, in order to gain insight into how KCs are influenced by the other two cell types, comparison to fresh KCs should also be performed. This should also be compared to models where only KCs and hepatocytes are present, but separated by a PEM.

The analyses of hepatocyte proteomes obtained from liver models have begun to yield insight into the effects of cell-ECM and cell-cell interactions. However, metabolite profiles have not been assessed. For example, the data in Chapter 2 suggested increased abundance of proteins related to both mitochondrial and peroxisomal β-oxidation. Therefore, lipid levels in the cell culture media are expected to decrease. Thus analysis of the "lipidome" can be performed where one could selectively separate lipids from the cell culture media using protocols as previously described [242, 243]. These protocols involve liquid-liquid extraction methods with mixtures of methanol, methyl-*tert*-butyl-ether, and water. This mixture induces a phase separation where lipids will be separated into an organic solvent. LC-MS/MS analysis can be performed on this fraction and metabolite identification could be performed using the Lipid Metabolites and Pathways Strategy (LIPID MAPS). This kind of study could serve as a validation or could be in contrast to the proteomic predictions.

### 4.4 Assessment of intercellular signaling processes

One of the initial goals of this work was to ascertain the paracrine signaling process between cell types. These types of studies are always a challenge since signaling molecules are difficult to detect by MS in a media composed of 10% FBS. While cytokines are difficult to

detect unless they are specifically targeted, it should be pointed out that some studies have linked amino acids, such as proline and glutamine, to enhancement of hepatic function [96, 244]. However, no direct link to any intercellular signaling pathway has been elucidated. Evaluation of the more hydrophilic substances in an untargeted way may provide clues as to signaling processes. Another potential intracellular route would be an assessment of the phosphopeptide pools derived from hepatocytes generated under different culture conditions. Changes in the phosphoproteome are essentially related to signaling pathways and could possibly provide a path back to the source of the signal. For example, phosphorylation of the glycoprotein 130 (GP130) receptor plays a role in activation of the janus kinase/signal transducer and activator of transcription (JAK/STAT) or the mitogen activated protein kinase (MAPK) pathways activated by IL-6 [157, 245]. In addition to the phosphoproteome, protein-protein interactions could also be studied using MS based techniques coupled with affinity purification [246]. Such interactions exist in many pathways such as those activated by transforming growth factor-β (TGF-β), where a complex known as the apoptosome, which consists of cytochrome C, apoptotic protease activating factor -1 (APAF-1) and caspase 9 forms. The formation of the apoptosome leads to the activation of caspase 3 and consequently apoptosis of hepatocytes [247, 248]. Thus, coupling results from both of these studies together could yield great insight into signaling processes.

## References


1. Arias, I.M., J.L. Boyer, F.V. Chisary, N. Fausto, D. Schachter, and D. Shafritz, eds. *The Liver:Biology and Pathobiology*. 4 ed. 2001, Lipponcott Williams and Wilkins: Philadelphia, PA.
2. Shan, J., K. Stevens, K. Trehan, G. Underhill, A. Chen, and S. Bhatia, *Hepatic Tissue Engineering*, in *Molecular Pathology of Liver Diseases*, S.P.S. Monga, Editor. 2011, Springer US. p. 321-342.
3. Godoy, P., N.J. Hewitt, U. Albrecht, M.E. Andersen, N. Ansari, S. Bhattacharya, J.G. Bode, J. Bolleyn, C. Borner, J. Bottger, A. Braeuning, R.A. Budinsky, B. Burkhardt, N.R. Cameron, G. Camussi, C.S. Cho, Y.J. Choi, J. Craig Rowlands, U. Dahmen, G. Damm, O. Dirsch, M.T. Donato, J. Dong, S. Dooley, D. Drasdo, R. Eakins, K.S. Ferreira, V. Fonsato, J. Fraczek, R. Gebhardt, A. Gibson, M. Glanemann, C.E. Goldring, M.J. Gomez-Lechon, G.M. Groothuis, L. Gustavsson, C. Guyot, D. Hallifax, S. Hammad, A. Hayward, D. Haussinger, C. Hellerbrand, P. Hewitt, S. Hoehme, H.G. Holzhutter, J.B. Houston, J. Hrach, K. Ito, H. Jaeschke, V. Keitel, J.M. Kelm, B. Kevin Park, C. Kordes, G.A. Kullak-Ublick, E.L. LeCluyse, P. Lu, J. Luebke-Wheeler, A. Lutz, D.J. Maltman, M. Matz-Soja, P. McMullen, I. Merfort, S. Messner, C. Meyer, J. Mwinyi, D.J. Naisbitt, A.K. Nussler, P. Olinga, F. Pampaloni, J. Pi, L. Pluta, S.A. Przyborski, A. Ramachandran, V. Rogiers, C. Rowe, C. Schelcher, K. Schmich, M. Schwarz, B. Singh, E.H. Stelzer, B. Stieger, R. Stober, Y. Sugiyama, C. Tetta, W.E. Thasler, T. Vanhaecke, M. Vinken, T.S. Weiss, A. Widera, C.G. Woods, J.J. Xu, K.M. Yarborough, and J.G. Hengstler, *Recent advances in 2D and 3D in vitro systems using primary hepatocytes, alternative hepatocyte sources and non-parenchymal liver cells and their use in investigating mechanisms of hepatotoxicity, cell signaling and ADME.* Arch Toxicol, 2013. **87**(8): p. 1315-530.
4. Abdel-Misih, S.R. and M. Bloomston, *Liver anatomy.* Surg Clin North Am, 2010. **90**(4): p. 643-53.
5. Lindros, K.O., *Zonation of cytochrome P450 expression, drug metabolism and toxicity in liver.* Gen Pharmacol, 1997. **28**(2): p. 191-6.
6. Jungermann, K. and T. Kietzmann, *Oxygen: modulator of metabolic zonation and disease of the liver.* Hepatology, 2000. **31**(2): p. 255-60.
7. Domansky, K., W. Inman, J. Serdy, A. Dash, M.H. Lim, and L.G. Griffith, *Perfused multiwell plate for 3D liver tissue engineering.* Lab Chip, 2010. **10**(1): p. 51-8.
8. Hijmans, B.S., A. Greffiorst, M.H. Oosterveer, and A.K. Groen, *Zonation of glucose and fatty acid metabolism in the liver: Mechanism and metabolic consequences.* Biochimie, 2014. **96C**: p. 121-129.
9. Gebhardt, R., *Metabolic zonation of the liver: regulation and implications for liver function.* Pharmacol Ther, 1992. **53**(3): p. 275-354.
10. Gebhardt, R., *Metabolic Zonation of the Liver - Regulation and Implications for Liver-Function.* Pharmacology & Therapeutics, 1992. **53**(3): p. 275-354.
11. Jungermann, K. and T. Kietzmann, *Zonation of parenchymal and nonparenchymal metabolism in liver.* Annual Review of Nutrition, 1996. **16**: p. 179-203.
12. Jungermann, K., *Metabolic zonation of liver parenchyma: significance for the regulation of glycogen metabolism, gluconeogenesis, and glycolysis.* Diabetes Metab Rev, 1987. **3**(1): p. 269-93.

13. Guzmán, M. and J. Castro, *Zonation of fatty acid metabolism in rat liver.* Biochemical Journal, 1989. **264**(1): p. 107-113.
14. Katz, N.R., W. Fischer, and S. Giffhorn, *Distribution of enzymes of fatty acid and ketone body metabolism in periportal and perivenous rat-liver tissue.* Eur J Biochem, 1983. **135**(1): p. 103-7.
15. Guzman, M., C. Bijleveld, and M.J. Geelen, *Flexibility of zonation of fatty acid oxidation in rat liver.* Biochem J, 1995. **311 ( Pt 3)**: p. 853-60.
16. Treyer, A. and A. Musch, *Hepatocyte polarity.* Compr Physiol, 2013. **3**(1): p. 243-87.
17. Reid, L.M., A.S. Fiorino, S.H. Sigal, S. Brill, and P.A. Holst, *Extracellular matrix gradients in the space of disse: Relevance to liver biology.* Hepatology, 1992. **15**(6): p. 1198-1203.
18. Martinez-Hernandez, A. and P.S. Amenta, *The hepatic extracellular matrix. I. Components and distribution in normal liver.* Virchows Arch A Pathol Anat Histopathol, 1993. **423**(1): p. 1-11.
19. Larkin, A.L., R.R. Rodrigues, T.M. Murali, and P. Rajagopalan, *Designing a multicellular organotypic 3D liver model with a detachable, nanoscale polymeric Space of Disse.* Tissue Eng Part C Methods, 2013. **19**(11): p. 875-84.
20. Martinez-Hernandez, A., F.M. Delgado, and P.S. Amenta, *The extracellular matrix in hepatic regeneration. Localization of collagen types I, III, IV, laminin, and fibronectin.* Lab Invest, 1991. **64**(2): p. 157-66.
21. Martinez-Hernandez, A. and P.S. Amenta, *The extracellular matrix in hepatic regeneration.* FASEB J, 1995. **9**(14): p. 1401-10.
22. Sorensen, K.K., P. McCourt, T. Berg, C. Crossley, D. Le Couteur, K. Wake, and B. Smedsrod, *The scavenger endothelial cell: a new player in homeostasis and immunity.* Am J Physiol Regul Integr Comp Physiol, 2012. **303**(12): p. R1217-30.
23. Hughes, D.A., I.P. Fraser, and S. Gordon, *Murine macrophage scavenger receptor: in vivo expression and function as receptor for macrophage adhesion in lymphoid and non-lymphoid organs.* Eur J Immunol, 1995. **25**(2): p. 466-73.
24. Malerod, L., K. Juvet, T. Gjoen, and T. Berg, *The expression of scavenger receptor class B, type I (SR-BI) and caveolin-1 in parenchymal and nonparenchymal liver cells.* Cell Tissue Res, 2002. **307**(2): p. 173-80.
25. Hansen, B., P. Longati, K. Elvevold, G.I. Nedredal, K. Schledzewski, R. Olsen, M. Falkowski, J. Kzhyshkowska, F. Carlsson, S. Johansson, B. Smedsrod, S. Goerdt, and P. McCourt, *Stabilin-1 and stabilin-2 are both directed into the early endocytic pathway in hepatic sinusoidal endothelium via interactions with clathrin/AP-2, independent of ligand binding.* Exp Cell Res, 2005. **303**(1): p. 160-73.
26. Mousavi, S.A., M. Sporstol, C. Fladeby, R. Kjeken, N. Barois, and T. Berg, *Receptor-mediated endocytosis of immune complexes in rat liver sinusoidal endothelial cells is mediated by FcgammaRIIb2.* Hepatology, 2007. **46**(3): p. 871-84.
27. Blomhoff, R., W. Eskild, and T. Berg, *Endocytosis of formaldehyde-treated serum albumin via scavenger pathway in liver endothelial cells.* Biochem J, 1984. **218**(1): p. 81-6.
28. Tavassoli, M., T. Kishimoto, R. Soda, M. Kataoka, and K. Harjes, *Liver endothelium mediates the uptake of iron-transferrin complex by hepatocytes.* Exp Cell Res, 1986. **165**(2): p. 369-79.

29. Irving, M.G., F.J. Roll, S. Huang, and D.M. Bissell, *Characterization and culture of sinusoidal endothelium from normal rat liver: lipoprotein uptake and collagen phenotype.* Gastroenterology, 1984. **87**(6): p. 1233-47.
30. Fraser, R., B.R. Dobbs, and G.W. Rogers, *Lipoproteins and the liver sieve: the role of the fenestrated sinusoidal endothelium in lipoprotein metabolism, atherosclerosis, and cirrhosis.* Hepatology, 1995. **21**(3): p. 863-74.
31. Elvevold, K., J. Simon-Santamaria, H. Hasvold, P. McCourt, B. Smedsrod, and K.K. Sorensen, *Liver sinusoidal endothelial cells depend on mannose receptor-mediated recruitment of lysosomal enzymes for normal degradation capacity.* Hepatology, 2008. **48**(6): p. 2007-15.
32. Smedsrod, B., H. Pertoft, S. Gustafson, and T.C. Laurent, *Scavenger functions of the liver endothelial cell.* Biochem J, 1990. **266**(2): p. 313-27.
33. Wisse, E., R.B. De Zanger, K. Charels, P. Van Der Smissen, and R.S. McCuskey, *The liver sieve: considerations concerning the structure and function of endothelial fenestrae, the sinusoidal wall and the space of Disse.* Hepatology, 1985. **5**(4): p. 683-92.
34. Elvevold, K., B. Smedsrod, and I. Martinez, *The liver sinusoidal endothelial cell: a cell type of controversial and confusing identity.* Am J Physiol Gastrointest Liver Physiol, 2008. **294**(2): p. G391-400.
35. Catala, M., A. Anton, and M.T. Portoles, *Characterization of the simultaneous binding of Escherichia coli endotoxin to Kupffer and endothelial liver cells by flow cytometry.* Cytometry, 1999. **36**(2): p. 123-30.
36. Breiner, K.M., H. Schaller, and P.A. Knolle, *Endothelial cell-mediated uptake of a hepatitis B virus: a new concept of liver targeting of hepatotropic microorganisms.* Hepatology, 2001. **34**(4 Pt 1): p. 803-8.
37. Simon-Santamaria, J., C.H. Rinaldo, P. Kardas, R. Li, I. Malovic, K. Elvevold, P. McCourt, B. Smedsrod, H.H. Hirsch, and K.K. Sorensen, *Efficient uptake of blood-borne BK and JC polyomavirus-like particles in endothelial cells of liver sinusoids and renal vasa recta.* PLoS One, 2014. **9**(11): p. e111762.
38. Braet, F. and E. Wisse, *Structural and functional aspects of liver sinusoidal endothelial cell fenestrae: a review.* Comp Hepatol, 2002. **1**(1): p. 1.
39. Bilzer, M., F. Roggel, and A.L. Gerbes, *Role of Kupffer cells in host defense and liver disease.* Liver Int, 2006. **26**(10): p. 1175-86.
40. Willekens, F.L.A., J.M. Werre, J.K. Kruijt, B. Roerdinkholder-Stoelwinder, Y.A.M. Groenen-Döpp, A.G. van den Bos, G.J.C.G.M. Bosman, and T.J.C. van Berkel, *Liver Kupffer cells rapidly remove red blood cell–derived vesicles from the circulation by scavenger receptors*. Vol. 105. 2005. 2141-2145.
41. Terpstra, V. and T.J.C. van Berkel, *Scavenger receptors on liver Kupffer cells mediate the in vivo uptake of oxidatively damaged red blood cells in mice*. Vol. 95. 2000. 2157-2163.
42. Naito, M., G. Hasegawa, Y. Ebe, and T. Yamamoto, *Differentiation and function of Kupffer cells.* Med Electron Microsc, 2004. **37**(1): p. 16-28.
43. Fox, E.S., P. Thomas, and S.A. Broitman, *Comparative studies of endotoxin uptake by isolated rat Kupffer and peritoneal cells.* Infection and Immunity, 1987. **55**(12): p. 2962-2966.
44. Su, G.L., *Lipopolysaccharides in liver injury: molecular mechanisms of Kupffer cell activation.* Am J Physiol Gastrointest Liver Physiol, 2002. **283**(2): p. G256-65.

45. Ojaniemi, M., M. Liljeroos, K. Harju, R. Sormunen, R. Vuolteenaho, and M. Hallman, *TLR-2 is upregulated and mobilized to the hepatocyte plasma membrane in the space of Disse and to the Kupffer cells TLR-4 dependently during acute endotoxemia in mice.* Immunol Lett, 2006. **102**(2): p. 158-68.
46. Scott, M.J., S. Liu, G.L. Su, Y. Vodovotz, and T.R. Billiar, *Hepatocytes enhance effects of lipopolysaccharide on liver nonparenchymal cells through close cell interactions.* Shock, 2005. **23**(5): p. 453-8.
47. Hoebe, K.H., R.F. Witkamp, J. Fink-Gremmels, A.S. Van Miert, and M. Monshouwer, *Direct cell-to-cell contact between Kupffer cells and hepatocytes augments endotoxin-induced hepatic injury.* Am J Physiol Gastrointest Liver Physiol, 2001. **280**(4): p. G720-8.
48. Steib, C. and A. Gerbes, *Signaling Pathways in Liver Diseases Kupffer Cells*, in *Signaling Pathways in Liver Diseases*, J.-F. Dufour and P.-A. Clavien, Editors. 2010, Springer Berlin Heidelberg. p. 69-78.
49. Malik, R., C. Selden, and H. Hodgson, *The role of non-parenchymal cells in liver growth.* Semin Cell Dev Biol, 2002. **13**(6): p. 425-31.
50. Ramadori, G. and T. Armbrust, *Cytokines in the liver.* Eur J Gastroenterol Hepatol, 2001. **13**(7): p. 777-84.
51. Decker, K., *The response of liver macrophages to inflammatory stimulation.* Keio J Med, 1998. **47**(1): p. 1-9.
52. Yin, S., H. Wang, O. Park, W. Wei, J. Shen, and B. Gao, *Enhanced liver regeneration in IL-10-deficient mice after partial hepatectomy via stimulating inflammatory response and activating hepatocyte STAT3.* Am J Pathol, 2011. **178**(4): p. 1614-21.
53. Michalopoulos, G.K., *Liver regeneration.* J Cell Physiol, 2007. **213**(2): p. 286-300.
54. Vansaun, M.N., A.M. Mendonsa, and D. Lee Gorden, *Hepatocellular proliferation correlates with inflammatory cell and cytokine changes in a murine model of nonalchoholic fatty liver disease.* PLoS One, 2013. **8**(9): p. e73054.
55. Kinoshita, T. and A. Miyajima, *Cytokine regulation of liver development.* Biochim Biophys Acta, 2002. **1592**(3): p. 303-12.
56. Senoo, H., K. Yoshikawa, M. Morii, M. Miura, K. Imai, and Y. Mezaki, *Hepatic stellate cell (vitamin A-storing cell) and its relative--past, present and future.* Cell Biol Int, 2010. **34**(12): p. 1247-72.
57. Geerts, A., *History, heterogeneity, developmental biology, and functions of quiescent hepatic stellate cells.* Semin Liver Dis, 2001. **21**(3): p. 311-35.
58. Arthur, M.J., A. Stanley, J.P. Iredale, J.A. Rafferty, R.M. Hembry, and S.L. Friedman, *Secretion of 72 kDa type IV collagenase/gelatinase by cultured human lipocytes. Analysis of gene expression, protein synthesis and proteinase activity.* Biochem J, 1992. **287 ( Pt 3)**: p. 701-7.
59. Milani, S., H. Herbst, D. Schuppan, C. Grappone, G. Pellegrini, M. Pinzani, A. Casini, A. Calabro, G. Ciancio, F. Stefanini, and et al., *Differential expression of matrix-metalloproteinase-1 and -2 genes in normal and fibrotic human liver.* Am J Pathol, 1994. **144**(3): p. 528-37.
60. Han, Y.P., C. Yan, L. Zhou, L. Qin, and H. Tsukamoto, *A matrix metalloproteinase-9 activation cascade by hepatic stellate cells in trans-differentiation in the three-dimensional extracellular matrix.* J Biol Chem, 2007. **282**(17): p. 12928-39.

61. Friedman, S.L., *Molecular regulation of hepatic fibrosis, an integrated cellular response to tissue injury.* J Biol Chem, 2000. **275**(4): p. 2247-50.
62. Iredale, J.P., *Hepatic stellate cell behavior during resolution of liver injury.* Semin Liver Dis, 2001. **21**(3): p. 427-36.
63. Friedman, S.L., *Mechanisms of hepatic fibrogenesis.* Gastroenterology, 2008. **134**(6): p. 1655-69.
64. Iredale, J.P., *Models of liver fibrosis: exploring the dynamic nature of inflammation and repair in a solid organ.* J Clin Invest, 2007. **117**(3): p. 539-48.
65. Friedman, S.L., *Hepatic stellate cells: protean, multifunctional, and enigmatic cells of the liver.* Physiol Rev, 2008. **88**(1): p. 125-72.
66. Karsdal, M.A., T. Manon-Jensen, F. Genovese, J.H. Kristensen, M.J. Nielsen, J.M.B. Sand, N.-U.B. Hansen, A.-C. Bay-Jensen, C.L. Bager, A. Krag, A. Blanchard, H. Krarup, D.J. Leeming, and D. Schuppan, *Novel insights into the function and dynamics of extracellular matrix in liver fibrosis*. Vol. 308. 2015. G807-G830.
67. Gressner, A.M. and R. Weiskirchen, *Modern pathogenetic concepts of liver fibrosis suggest stellate cells and TGF-beta as major players and therapeutic targets.* J Cell Mol Med, 2006. **10**(1): p. 76-99.
68. Veidal, S.S., M.J. Nielsen, D.J. Leeming, and M.A. Karsdal, *Phosphodiesterase inhibition mediates matrix metalloproteinase activity and the level of collagen degradation fragments in a liver fibrosis ex vivo rat model.* BMC Res Notes, 2012. **5**(1): p. 686.
69. Baker, T.K., M.A. Carfagna, H. Gao, E.R. Dow, Q. Li, G.H. Searfoss, and T.P. Ryan, *Temporal gene expression analysis of monolayer cultured rat hepatocytes.* Chem Res Toxicol, 2001. **14**(9): p. 1218-31.
70. Dunn, J.C., R.G. Tompkins, and M.L. Yarmush, *Long-term in vitro function of adult hepatocytes in a collagen sandwich configuration.* Biotechnol Prog, 1991. **7**(3): p. 237-45.
71. Dunn, J.C., M.L. Yarmush, H.G. Koebe, and R.G. Tompkins, *Hepatocyte function and extracellular matrix geometry: long-term culture in a sandwich configuration.* FASEB J, 1989. **3**(2): p. 174-7.
72. Anada, T., J. Fukuda, Y. Sai, and O. Suzuki, *An oxygen-permeable spheroid culture system for the prevention of central hypoxia and necrosis of spheroids.* Biomaterials, 2012. **33**(33): p. 8430-41.
73. Glicklis, R., J.C. Merchuk, and S. Cohen, *Modeling mass transfer in hepatocyte spheroids via cell viability, spheroid size, and hepatocellular functions.* Biotechnol Bioeng, 2004. **86**(6): p. 672-80.
74. Lan, S.F., B. Safiejko-Mroczka, and B. Starly, *Long-term cultivation of HepG2 liver cells encapsulated in alginate hydrogels: a study of cell viability, morphology and drug metabolism.* Toxicol In Vitro, 2010. **24**(4): p. 1314-23.
75. Tran, N.M., M. Dufresne, G. Duverlie, S. Castelain, C. Defarge, P. Paullier, and C. Legallais, *An appropriate selection of a 3D alginate culture model for hepatic Huh-7 cell line encapsulation intended for viral studies.* Tissue Eng Part A, 2013. **19**(1-2): p. 103-13.
76. Bhattacharya, M., M.M. Malinen, P. Lauren, Y.R. Lou, S.W. Kuisma, L. Kanninen, M. Lille, A. Corlu, C. GuGuen-Guillouzo, O. Ikkala, A. Laukkanen, A. Urtti, and M.

Yliperttula, *Nanofibrillar cellulose hydrogel promotes three-dimensional liver cell culture.* Journal of Controlled Release, 2012. **164**(3): p. 291-298.
77. Lan, S.-F. and B. Starly, *Alginate based 3D hydrogels as an in vitro co-culture model platform for the toxicity screening of new chemical entities.* Toxicology and Applied Pharmacology, 2011. **256**(1): p. 62-72.
78. Tran, N.M., M. Dufresne, G. Duverlie, S. Castelain, C. Defarge, P. Paullier, and C. Legallais, *An Appropriate Selection of a 3D Alginate Culture Model for Hepatic Huh-7 Cell Line Encapsulation Intended for Viral Studies.* Tissue Engineering Part A, 2013. **19**(1-2): p. 103-113.
79. Curcio, E., S. Salerno, G. Barbieri, L. De Bartolo, E. Drioli, and A. Bader, *Mass transfer and metabolic reactions in hepatocyte spheroids cultured in rotating wall gas-permeable membrane system.* Biomaterials, 2007. **28**(36): p. 5487-97.
80. March, S., E.E. Hui, G.H. Underhill, S. Khetani, and S.N. Bhatia, *Microenvironmental regulation of the sinusoidal endothelial cell phenotype in vitro.* Hepatology, 2009. **50**(3): p. 920-8.
81. Khetani, S.R. and S.N. Bhatia, *Microscale culture of human liver cells for drug development.* Nat Biotechnol, 2008. **26**(1): p. 120-6.
82. Ukairo, O., C. Kanchagar, A. Moore, J. Shi, J. Gaffney, S. Aoyama, K. Rose, S. Krzyzewski, J. McGeehan, M.E. Andersen, S.R. Khetani, and E.L. Lecluyse, *Long-term stability of primary rat hepatocytes in micropatterned cocultures.* J Biochem Mol Toxicol, 2013. **27**(3): p. 204-12.
83. Bader, A., E. Knop, A. Kern, K. Boker, N. Fruhauf, O. Crome, H. Esselmann, C. Pape, G. Kempka, and K.F. Sewing, *3-D coculture of hepatic sinusoidal cells with primary hepatocytes-design of an organotypical model.* Exp Cell Res, 1996. **226**(1): p. 223-33.
84. Bhatia, S.N., U.J. Balis, M.L. Yarmush, and M. Toner, *Effect of cell-cell interactions in preservation of cellular phenotype: cocultivation of hepatocytes and nonparenchymal cells.* FASEB J, 1999. **13**(14): p. 1883-900.
85. Yip, D. and C.H. Cho, *A multicellular 3D heterospheroid model of liver tumor and stromal cells in collagen gel for anti-cancer drug testing.* Biochem Biophys Res Commun, 2013. **433**(3): p. 327-32.
86. Li, C.Y., K.R. Stevens, R.E. Schwartz, B.S. Alejandro, J.H. Huang, and S.N. Bhatia, *Micropatterned cell-cell interactions enable functional encapsulation of primary hepatocytes in hydrogel microtissues.* Tissue Eng Part A, 2014. **20**(15-16): p. 2200-12.
87. Lee, S.A., Y. No da, E. Kang, J. Ju, D.S. Kim, and S.H. Lee, *Spheroid-based three-dimensional liver-on-a-chip to investigate hepatocyte-hepatic stellate cell interactions and flow effects.* Lab Chip, 2013. **13**(18): p. 3529-37.
88. Chen, A.A., D.K. Thomas, L.L. Ong, R.E. Schwartz, T.R. Golub, and S.N. Bhatia, *Humanized mice with ectopic artificial liver tissues.* Proc Natl Acad Sci U S A, 2011. **108**(29): p. 11842-7.
89. Kim, Y., A.L. Larkin, R.M. Davis, and P. Rajagopalan, *The design of in vitro liver sinusoid mimics using chitosan-hyaluronic acid polyelectrolyte multilayers.* Tissue Eng Part A, 2010. **16**(9): p. 2731-41.
90. Kim, Y. and P. Rajagopalan, *3D Hepatic Cultures Simultaneously Maintain Primary Hepatocyte and Liver Sinusoidal Endothelial Cell Phenotypes.* Plos One, 2010. **5**(11): p. e15456.

91. Detzel, C.J., Y. Kim, and P. Rajagopalan, *Engineered three-dimensional liver mimics recapitulate critical rat-specific bile acid pathways.* Tissue Eng Part A, 2011. **17**(5-6): p. 677-89.
92. Kasuya, J., R. Sudo, T. Mitaka, M. Ikeda, and K. Tanishita, *Spatio-temporal control of hepatic stellate cell-endothelial cell interactions for reconstruction of liver sinusoids in vitro.* Tissue Eng Part A, 2012. **18**(9-10): p. 1045-56.
93. Kim, K., K. Ohashi, R. Utoh, K. Kano, and T. Okano, *Preserved liver-specific functions of hepatocytes in 3D co-culture with endothelial cell sheets.* Biomaterials, 2012. **33**(5): p. 1406-13.
94. Kasuya, J., R. Sudo, T. Mitaka, M. Ikeda, and K. Tanishita, *Hepatic stellate cell-mediated three-dimensional hepatocyte and endothelial cell triculture model.* Tissue Eng Part A, 2011. **17**(3-4): p. 361-70.
95. Kasuya, J. and K. Tanishita, *Microporous membrane-based liver tissue engineering for the reconstruction of three-dimensional functional liver tissues in vitro.* Biomatter, 2012. **2**(4): p. 290-5.
96. Jindal, R., Y. Nahmias, A.W. Tilles, F. Berthiaume, and M.L. Yarmush, *Amino acid-mediated heterotypic interaction governs performance of a hepatic tissue model.* Faseb Journal, 2009. **23**(7): p. 2288-2298.
97. Jindal, R., S.J. Patel, and M.L. Yarmush, *Tissue-Engineered Model for Real-Time Monitoring of Liver Inflammation.* Tissue Eng Part C Methods, 2010.
98. Kasuya, J., R. Sudo, T. Mitaka, M. Ikeda, and K. Tanishita, *Hepatic Stellate Cell-Mediated Three-Dimensional Hepatocyte and Endothelial Cell Triculture Model.* Tissue Engineering Part A, 2011. **17**(3-4): p. 361-370.
99. Kasuya, J., R. Sudo, T. Mitaka, M. Ikeda, and K. Tanishita, *Spatio-Temporal Control of Hepatic Stellate Cell-Endothelial Cell Interactions for Reconstruction of Liver Sinusoids In Vitro.* Tissue Engineering Part A, 2012. **18**(9-10): p. 1045-1056.
100. Connolly, J.O., N. Simpson, L. Hewlett, and A. Hall, *Rac regulates endothelial morphogenesis and capillary assembly.* Mol Biol Cell, 2002. **13**(7): p. 2474-85.
101. Bale, S.S., I. Golberg, R. Jindal, W.J. McCarty, M. Luitje, M. Hegde, A. Bhushan, O.B. Usta, and M.L. Yarmush, *Long-term coculture strategies for primary hepatocytes and liver sinusoidal endothelial cells.* Tissue Eng Part C Methods, 2015. **21**(4): p. 413-22.
102. Decher, G., M. Eckle, J. Schmitt, and B. Struth, *Layer-by-layer assembled multicomposite films.* Current Opinion in Colloid & Interface Science, 1998. **3**(1): p. 32-39.
103. Decher, G. and J. Schlenoff, eds. *Multilayer Thin Films : Sequential Assembly of Nanocomposite Materials*. 2003, Wiley-VCH.
104. Decher, G., *Fuzzy Nanoassemblies: Toward Layered Polymeric Multicomposites.* Science, 1997. **277**(5330): p. 1232-1237.
105. Schlenoff, J.B. and S.T. Dubas, *Mechanism of Polyelectrolyte Multilayer Growth: Charge Overcompensation and Distribution.* Macromolecules, 2001. **34**(3): p. 592-598.
106. Larkin, A.L., R.M. Davis, and P. Rajagopalan, *Biocompatible, detachable, and free-standing polyelectrolyte multilayer films.* Biomacromolecules, 2010. **11**(10): p. 2788-96.
107. Mendelsohn, J.D., C.J. Barrett, V.V. Chan, A.J. Pal, A.M. Mayes, and M.F. Rubner, *Fabrication of Microporous Thin Films from Polyelectrolyte Multilayers.* Langmuir, 2000. **16**(11): p. 5017-5023.

108. Detzel, C.J., A.L. Larkin, and P. Rajagopalan, *Polyelectrolyte multilayers in tissue engineering.* Tissue Eng Part B Rev, 2011. **17**(2): p. 101-13.
109. Kinter, M. and N.E. Sherman, *Protein Sequencing and Identification Using Tandem Mass Spectrometry*, ed. D.M. Desiderio and N.M.M. Nibbering. 2000: John Wiley & Sons, Inc.
110. Cox, J. and M. Mann, *Quantitative, high-resolution proteomics for data-driven systems biology.* Annu Rev Biochem, 2011. **80**: p. 273-99.
111. Bensimon, A., A.J. Heck, and R. Aebersold, *Mass spectrometry-based proteomics and network biology.* Annu Rev Biochem, 2012. **81**: p. 379-405.
112. Aebersold, R. and M. Mann, *Mass spectrometry-based proteomics.* Nature, 2003. **422**(6928): p. 198-207.
113. Geromanos, S.J., J.P. Vissers, J.C. Silva, C.A. Dorschel, G.Z. Li, M.V. Gorenstein, R.H. Bateman, and J.I. Langridge, *The detection, correlation, and comparison of peptide precursor and product ions from data independent LC-MS with data dependant LC-MS/MS.* PROTEOMICS, 2009. **9**(6): p. 1683-95.
114. Becker, C.H. and M. Bern, *Recent developments in quantitative proteomics.* Mutation Research/Genetic Toxicology and Environmental Mutagenesis, 2011. **722**(2): p. 171-182.
115. Zhang, Y., M. Li, L. Wei, L. Zhu, S. Hu, S. Wu, S. Ma, and Y. Gao, *Differential protein expression in perfusates from metastasized rat livers.* Proteome Sci, 2013. **11**(1): p. 37.
116. McCormack, A.L., D.M. Schieltz, B. Goode, S. Yang, G. Barnes, D. Drubin, and J.R. Yates, 3rd, *Direct analysis and identification of proteins in mixtures by LC/MS/MS and database searching at the low-femtomole level.* Anal Chem, 1997. **69**(4): p. 767-76.
117. Hervey, M.B. Strader, and G.B. Hurst, *Comparison of Digestion Protocols for Microgram Quantities of Enriched Protein Samples.* Journal of Proteome Research, 2007. **6**(8): p. 3054-3061.
118. Wada, Y. and M. Kadoya, *In-gel digestion with endoproteinase LysC.* Journal of Mass Spectrometry, 2003. **38**(1): p. 117-118.
119. Nagaraj, N., A. Lu, M. Mann, and J.R. Wiśniewski, *Detergent-Based but Gel-Free Method Allows Identification of Several Hundred Membrane Proteins in Single LC-MS Runs.* Journal of Proteome Research, 2008. **7**(11): p. 5028-5032.
120. Wisniewski, J.R. and M. Mann, *Consecutive proteolytic digestion in an enzyme reactor increases depth of proteomic and phosphoproteomic analysis.* Anal Chem, 2012. **84**(6): p. 2631-7.
121. Glatter, T., C. Ludwig, E. Ahrne, R. Aebersold, A.J. Heck, and A. Schmidt, *Large-scale quantitative assessment of different in-solution protein digestion protocols reveals superior cleavage efficiency of tandem Lys-C/trypsin proteolysis over trypsin digestion.* J Proteome Res, 2012. **11**(11): p. 5145-56.
122. Klammer, A.A. and M.J. MacCoss, *Effects of Modified Digestion Schemes on the Identification of Proteins from Complex Mixtures.* Journal of Proteome Research, 2006. **5**(3): p. 695-700.
123. McDonald, W.H., R. Ohi, D.T. Miyamoto, T.J. Mitchison, and J.R. Yates Iii, *Comparison of three directly coupled HPLC MS/MS strategies for identification of proteins from complex mixtures: single-dimension LC-MS/MS, 2-phase MudPIT, and 3-phase MudPIT.* International Journal of Mass Spectrometry, 2002. **219**(1): p. 245-251.
124. Gordon, J.A. and W.P. Jencks, *The relationship of structure to the effectiveness of denaturing agents for proteins.* Biochemistry, 1963. **2**: p. 47-57.

125. Greene, R.F., Jr. and C.N. Pace, *Urea and guanidine hydrochloride denaturation of ribonuclease, lysozyme, alpha-chymotrypsin, and beta-lactoglobulin.* J Biol Chem, 1974. **249**(17): p. 5388-93.
126. Raijmakers, R., P. Neerincx, S. Mohammed, and A.J. Heck, *Cleavage specificities of the brother and sister proteases Lys-C and Lys-N.* Chem Commun (Camb), 2010. **46**(46): p. 8827-9.
127. Wisniewski, J.R., A. Zougman, N. Nagaraj, and M. Mann, *Universal sample preparation method for proteome analysis.* Nat Methods, 2009. **6**(5): p. 359-62.
128. Nagaraj, N., A. Lu, M. Mann, and J.R. Wisniewski, *Detergent-based but gel-free method allows identification of several hundred membrane proteins in single LC-MS runs.* J Proteome Res, 2008. **7**(11): p. 5028-32.
129. Proc, J.L., M.A. Kuzyk, D.B. Hardie, J. Yang, D.S. Smith, A.M. Jackson, C.E. Parker, and C.H. Borchers, *A quantitative study of the effects of chaotropic agents, surfactants, and solvents on the digestion efficiency of human plasma proteins by trypsin.* J Proteome Res, 2010. **9**(10): p. 5422-37.
130. Swaney, D.L., C.D. Wenger, and J.J. Coon, *Value of using multiple proteases for large-scale mass spectrometry-based proteomics.* J Proteome Res, 2010. **9**(3): p. 1323-9.
131. Saveliev, S., M. Bratz, R. Zubarev, M. Szapacs, H. Budamgunta, and M. Urh, *Trypsin/Lys-C protease mix for enhanced protein mass spectrometry analysis.* Nat Meth, 2013. **10**(11).
132. Arike, L., K. Valgepea, L. Peil, R. Nahku, K. Adamberg, and R. Vilu, *Comparison and applications of label-free absolute proteome quantification methods on Escherichia coli.* Journal of Proteomics, 2012. **75**(17): p. 5437-5448.
133. Ong, S.E. and M. Mann, *Mass spectrometry-based proteomics turns quantitative.* Nature Chemical Biology, 2005. **1**(5): p. 252-262.
134. Chahrour, O., D. Cobice, and J. Malone, *Stable isotope labelling methods in mass spectrometry-based quantitative proteomics.* Journal of Pharmaceutical and Biomedical Analysis, 2015. **113**: p. 2-20.
135. Ong, S.-E., B. Blagoev, I. Kratchmarova, D.B. Kristensen, H. Steen, A. Pandey, and M. Mann, *Stable Isotope Labeling by Amino Acids in Cell Culture, SILAC, as a Simple and Accurate Approach to Expression Proteomics.* Molecular & Cellular Proteomics, 2002. **1**(5): p. 376-386.
136. Pan, C., C. Kumar, S. Bohl, U. Klingmueller, and M. Mann, *Comparative proteomic phenotyping of cell lines and primary cells to assess preservation of cell type-specific functions.* Mol Cell Proteomics, 2009. **8**(3): p. 443-50.
137. Ross, P.L., Y.N. Huang, J.N. Marchese, B. Williamson, K. Parker, S. Hattan, N. Khainovski, S. Pillai, S. Dey, S. Daniels, S. Purkayastha, P. Juhasz, S. Martin, M. Bartlet-Jones, F. He, A. Jacobson, and D.J. Pappin, *Multiplexed Protein Quantitation in Saccharomyces cerevisiae Using Amine-reactive Isobaric Tagging Reagents.* Molecular & Cellular Proteomics, 2004. **3**(12): p. 1154-1169.
138. Neilson, K.A., N.A. Ali, S. Muralidharan, M. Mirzaei, M. Mariani, G. Assadourian, A. Lee, S.C. van Sluyter, and P.A. Haynes, *Less label, more free: Approaches in label-free quantitative mass spectrometry.* PROTEOMICS, 2011. **11**(4): p. 535-553.
139. Levin, Y., E. Hradetzky, and S. Bahn, *Quantification of proteins using data-independent analysis (MSE) in simple andcomplex samples: a systematic evaluation.* PROTEOMICS, 2011. **11**(16): p. 3273-87.

140. Li, G.Z., J.P. Vissers, J.C. Silva, D. Golick, M.V. Gorenstein, and S.J. Geromanos, *Database searching and accounting of multiplexed precursor and product ion spectra from the data independent analysis of simple and complex peptide mixtures.* PROTEOMICS, 2009. **9**(6): p. 1696-719.
141. Kuharev, J., P. Navarro, U. Distler, O. Jahn, and S. Tenzer, *In-depth evaluation of software tools for data-independent acquisition based label-free quantification.* PROTEOMICS, 2015: p. n/a-n/a.
142. Carroll, K.M., D.M. Simpson, C.E. Eyers, C.G. Knight, P. Brownridge, W.B. Dunn, C.L. Winder, K. Lanthaler, P. Pir, N. Malys, D.B. Kell, S.G. Oliver, S.J. Gaskell, and R.J. Beynon, *Absolute quantification of the glycolytic pathway in yeast: deployment of a complete QconCAT approach.* Mol Cell Proteomics, 2011. **10**(12): p. M111 007633.
143. Villavicencio-Diaz, T.N., A. Rodriguez-Ulloa, O. Guirola-Cruz, and Y. Perez-Riverol, *Bioinformatics tools for the functional interpretation of quantitative proteomics results.* Curr Top Med Chem, 2014. **14**(3): p. 435-49.
144. Shi, R., C. Kumar, A. Zougman, Y. Zhang, A. Podtelejnikov, J. Cox, J.R. Wisniewski, and M. Mann, *Analysis of the mouse liver proteome using advanced mass spectrometry.* J Proteome Res, 2007. **6**(8): p. 2963-72.
145. Liao, C.C., Y.L. Lin, and C.F. Kuo, *Effect of High-Fat Diet on Hepatic Proteomics of Hamsters.* J Agric Food Chem, 2015.
146. Low, T.Y., S. van Heesch, H. van den Toorn, P. Giansanti, A. Cristobal, P. Toonen, S. Schafer, N. Hubner, B. van Breukelen, S. Mohammed, E. Cuppen, A.J. Heck, and V. Guryev, *Quantitative and qualitative proteome characteristics extracted from in-depth integrated genomics and proteomics analysis.* Cell Rep, 2013. **5**(5): p. 1469-78.
147. Rowe, C., D.T. Gerrard, R. Jenkins, A. Berry, K. Durkin, L. Sundstrom, C.E. Goldring, B.K. Park, N.R. Kitteringham, K.P. Hanley, and N.A. Hanley, *Proteome-wide analyses of human hepatocytes during differentiation and dedifferentiation.* Hepatology, 2013. **58**(2): p. 799-809.
148. Rowe, C., C.E. Goldring, N.R. Kitteringham, R.E. Jenkins, B.S. Lane, C. Sanderson, V. Elliott, V. Platt, P. Metcalfe, and B.K. Park, *Network analysis of primary hepatocyte dedifferentiation using a shotgun proteomics approach.* J Proteome Res, 2010. **9**(5): p. 2658-68.
149. Slany, A., V.J. Haudek, H. Zwickl, N.C. Gundacker, M. Grusch, T.S. Weiss, K. Seir, C. Rodgarkia-Dara, C. Hellerbrand, and C. Gerner, *Cell characterization by proteome profiling applied to primary hepatocytes and hepatocyte cell lines Hep-G2 and Hep-3B.* J Proteome Res, 2010. **9**(1): p. 6-21.
150. Li, L., D.Z. Lu, Y.M. Li, X.Q. Zhang, X.X. Zhou, and X. Jin, *Proteomic analysis of liver mitochondria from rats with nonalcoholic steatohepatitis.* World J Gastroenterol, 2014. **20**(16): p. 4778-86.
151. Guo, Y., M. Darshi, Y. Ma, G.A. Perkins, Z. Shen, K.J. Haushalter, R. Saito, A. Chen, Y.S. Lee, H.H. Patel, S.P. Briggs, M.H. Ellisman, J.M. Olefsky, and S.S. Taylor, *Quantitative proteomic and functional analysis of liver mitochondria from high fat diet (HFD) diabetic mice.* Mol Cell Proteomics, 2013. **12**(12): p. 3744-58.
152. Forner, F., L.J. Foster, S. Campanaro, G. Valle, and M. Mann, *Quantitative Proteomic Comparison of Rat Mitochondria from Muscle, Heart, and Liver.* Molecular & Cellular Proteomics, 2006. **5**(4): p. 608-619.

153. Kumar, S., Y. Zou, Q. Bao, M. Wang, and G. Dai, *Proteomic analysis of immediate-early response plasma proteins after 70% and 90% partial hepatectomy.* Hepatol Res, 2013. **43**(8): p. 876-89.
154. Yuan, X., S. Yan, J. Zhao, D. Shi, B. Yuan, W. Dai, B. Jiao, W. Zhang, and M. Miao, *Lipid metabolism and peroxisome proliferator-activated receptor signaling pathways participate in late-phase liver regeneration.* J Proteome Res, 2011. **10**(3): p. 1179-90.
155. Sun, Y., X. Deng, W. Li, Y. Yan, H. Wei, Y. Jiang, and F. He, *Liver proteome analysis of adaptive response in rat immediately after partial hepatectomy.* PROTEOMICS, 2007. **7**(23): p. 4398-4407.
156. Guo, F., H. Nian, H. Zhang, L. Huang, Y. Tang, X. Xiao, and D. He, *Proteomic analysis of the transition from quiescent to proliferating stages in rat liver hepatectomy model.* PROTEOMICS, 2006. **6**(10): p. 3075-86.
157. Streetz, K.L., T. Luedde, M.P. Manns, and C. Trautwein, *Interleukin 6 and liver regeneration.* Gut, 2000. **47**(2): p. 309-12.
158. Azimifar, S.B., N. Nagaraj, J. Cox, and M. Mann, *Cell-Type-Resolved Quantitative Proteomics of Murine Liver.* Cell Metabolism, 2014. **20**(6): p. 1076-1087.
159. Sharma, N.S., D. Nagrath, and M.L. Yarmush, *Metabolic profiling based quantitative evaluation of hepatocellular metabolism in presence of adipocyte derived extracellular matrix.* PLoS One, 2011. **6**(5): p. e20137.
160. Reid, L.M., A.S. Fiorino, S.H. Sigal, S. Brill, and P.A. Holst, *Extracellular matrix gradients in the space of Disse: relevance to liver biology.* Hepatology, 1992. **15**(6): p. 1198-203.
161. Klingmuller, U., A. Bauer, S. Bohl, P.J. Nickel, K. Breitkopf, S. Dooley, S. Zellmer, C. Kern, I. Merfort, T. Sparna, J. Donauer, G. Walz, M. Geyer, C. Kreutz, M. Hermes, F. Gotschel, A. Hecht, D. Walter, L. Egger, K. Neubert, C. Borner, M. Brulport, W. Schormann, C. Sauer, F. Baumann, R. Preiss, S. MacNelly, P. Godoy, E. Wiercinska, L. Ciuclan, J. Edelmann, K. Zeilinger, M. Heinrich, U.M. Zanger, R. Gebhardt, T. Maiwald, R. Heinrich, J. Timmer, F. von Weizsacker, and J.G. Hengstler, *Primary mouse hepatocytes for systems biology approaches: a standardized in vitro system for modelling of signal transduction pathways.* Syst Biol (Stevenage), 2006. **153**(6): p. 433-47.
162. Lan, S.F. and B. Starly, *Alginate based 3D hydrogels as an in vitro co-culture model platform for the toxicity screening of new chemical entities.* Toxicol Appl Pharmacol, 2011. **256**(1): p. 62-72.
163. Li, C.Y., K.R. Stevens, R.E. Schwartz, B.S. Alejandro, J.H. Huang, and S.N. Bhatia, *Micropatterned Cell-Cell Interactions Enable Functional Encapsulation of Primary Hepatocytes in Hydrogel Microtissues.* Tissue Engineering Part A, 2014. **20**(15-16): p. 2200-2212.
164. Underhill, G.H., A.A. Chen, D.R. Albrecht, and S.N. Bhatia, *Assessment of hepatocellular function within PEG hydrogels.* Biomaterials, 2007. **28**(2): p. 256-70.
165. Vu, L.T., R.R. Less, and P. Rajagopalan, *The promise of organotypic hepatic and gastrointestinal models.* Trends Biotechnol, 2014. **32**(8): p. 406-13.
166. Kim, Y., C.D. Lasher, L.M. Milford, T.M. Murali, and P. Rajagopalan, *A comparative study of genome-wide transcriptional profiles of primary hepatocytes in collagen sandwich and monolayer cultures.* Tissue Eng Part C Methods, 2010. **16**(6): p. 1449-60.

167. Khetani, S.R., G. Szulgit, J.A. Del Rio, C. Barlow, and S.N. Bhatia, *Exploring interactions between rat hepatocytes and nonparenchymal cells using gene expression profiling.* Hepatology, 2004. **40**(3): p. 545-54.
168. Nagaraj, N., J.R. Wisniewski, T. Geiger, J. Cox, M. Kircher, J. Kelso, S. Paabo, and M. Mann, *Deep proteome and transcriptome mapping of a human cancer cell line.* Mol Syst Biol, 2011. **7**: p. 548.
169. Schwanhausser, B., D. Busse, N. Li, G. Dittmar, J. Schuchhardt, J. Wolf, W. Chen, and M. Selbach, *Global quantification of mammalian gene expression control.* Nature, 2011. **473**(7347): p. 337-342.
170. Maier, T., M. Güell, and L. Serrano, *Correlation of mRNA and protein in complex biological samples.* FEBS Letters, 2009. **583**(24): p. 3966-3973.
171. Seglen, P.O., *Chapter 4 Preparation of Isolated Rat Liver Cells*, in *Methods in Cell Biology*, M.P. David, Editor. 1976, Academic Press. p. 29-83.
172. Elsdale, T. and J. Bard, *Collagen substrata for studies on cell behavior.* J Cell Biol, 1972. **54**(3): p. 626-37.
173. Mi, H., A. Muruganujan, and P.D. Thomas, *PANTHER in 2013: modeling the evolution of gene function, and other gene attributes, in the context of phylogenetic trees.* Nucleic Acids Res, 2013. **41**(Database issue): p. D377-86.
174. Huang, D.W., B.T. Sherman, and R.A. Lempicki, *Systematic and integrative analysis of large gene lists using DAVID bioinformatics resources.* Nature Protocols, 2009. **4**(1): p. 44-57.
175. Hansen, K.C., L. Kiemele, O. Maller, J. O'Brien, A. Shankar, J. Fornetti, and P. Schedin, *An in-solution ultrasonication-assisted digestion method for improved extracellular matrix proteome coverage.* Mol Cell Proteomics, 2009. **8**(7): p. 1648-57.
176. Vizcaino, J.A., E.W. Deutsch, R. Wang, A. Csordas, F. Reisinger, D. Rios, J.A. Dianes, Z. Sun, T. Farrah, N. Bandeira, P.A. Binz, I. Xenarios, M. Eisenacher, G. Mayer, L. Gatto, A. Campos, R.J. Chalkley, H.J. Kraus, J.P. Albar, S. Martinez-Bartolome, R. Apweiler, G.S. Omenn, L. Martens, A.R. Jones, and H. Hermjakob, *ProteomeXchange provides globally coordinated proteomics data submission and dissemination.* Nat Biotechnol, 2014. **32**(3): p. 223-6.
177. Distler, U., J. Kuharev, P. Navarro, Y. Levin, H. Schild, and S. Tenzer, *Drift time-specific collision energies enable deep-coverage data-independent acquisition proteomics.* Nat Methods, 2014. **11**(2): p. 167-70.
178. Van Summeren, A., J. Renes, F.G. Bouwman, J.P. Noben, J.H. van Delft, J.C. Kleinjans, and E.C. Mariman, *Proteomics investigations of drug-induced hepatotoxicity in HepG2 cells.* Toxicol Sci, 2011. **120**(1): p. 109-22.
179. Yan, G. and X. Yan, *Ribosomal proteomics: Strategies, approaches, and perspectives.* Biochimie, 2015. **113**(0): p. 69-77.
180. He, S.L. and R. Green, *Polysome analysis of mammalian cells.* Methods Enzymol, 2013. **530**: p. 183-92.
181. Sunny, N.E., S. Satapati, X. Fu, T. He, R. Mehdibeigi, C. Spring-Robinson, J. Duarte, M.J. Potthoff, J.D. Browning, and S.C. Burgess, *Progressive adaptation of hepatic ketogenesis in mice fed a high-fat diet.* Am J Physiol Endocrinol Metab, 2010. **298**(6): p. E1226-35.
182. Nelson, D.L., A.L. Lehninger, and M.M. Cox, *Lehninger principles of biochemistry*. 2008, New York: W.H. Freeman.

183. Newman, J.C. and E. Verdin, *Ketone bodies as signaling metabolites.* Trends Endocrinol Metab, 2014. **25**(1): p. 42-52.
184. Churchill, P., J.O. McIntyre, H. Eibl, and S. Fleischer, *Activation of D-beta-hydroxybutyrate apodehydrogenase using molecular species of mixed fatty acyl phospholipids.* J Biol Chem, 1983. **258**(1): p. 208-14.
185. Cao, W., J. Cao, J. Huang, J. Yao, G. Yan, H. Xu, and P. Yang, *Discovery and confirmation of O-GlcNAcylated proteins in rat liver mitochondria by combination of mass spectrometry and immunological methods.* PLoS One, 2013. **8**(10): p. e76399.
186. Iori, E., B. Vinci, E. Murphy, M.C. Marescotti, A. Avogaro, and A. Ahluwalia, *Glucose and fatty acid metabolism in a 3 tissue in-vitro model challenged with normo- and hyperglycaemia.* PLoS One, 2012. **7**(4): p. e34704.
187. Schofield, P.S., T.J. French, and M.C. Sugden, *Ketone-body metabolism after surgical stress or partial hepatectomy. Evidence for decreased ketogenesis and a site of control distal to carnitine palmitoyltransferase I.* Biochem J, 1987. **241**(2): p. 475-81.
188. Schofield, P.S., D.J. McLees, D.D. Myles, and M.C. Sugden, *Ketone-body metabolism after partial hepatectomy in the rat.* Biochem J, 1985. **231**(1): p. 225-8.
189. Huang, J. and D.A. Rudnick, *Elucidating the metabolic regulation of liver regeneration.* Am J Pathol, 2014. **184**(2): p. 309-21.
190. Higashi, S., N. Tabata, K.H. Kondo, M. Kai, K. Miyamoto, Y. Maeda, and T. Setoguchi, *A predominant increase of arterial beta-hydroxybutyrate concentration during partial hepatectomies in patients with impaired indocyanine green clearance test.* J Surg Res, 1999. **81**(2): p. 243-8.
191. Davidson, M.D., M. Lehrer, and S.R. Khetani, *Hormone and Drug-Mediated Modulation of Glucose Metabolism in a Microscale Model of the Human Liver.* Tissue Eng Part C Methods, 2014.
192. Lu, Y., G. Zhang, C. Shen, K. Uygun, M.L. Yarmush, and Q. Meng, *A novel 3D liver organoid system for elucidation of hepatic glucose metabolism.* Biotechnol Bioeng, 2012. **109**(2): p. 595-604.
193. Wang, C.Y. and C.F. Lin, *Annexin A2: its molecular regulation and cellular expression in cancer development.* Dis Markers, 2014. **2014**: p. 308976.
194. Myrvang, H.K., X. Guo, C. Li, and L.V. Dekker, *Protein interactions between surface annexin A2 and S100A10 mediate adhesion of breast cancer cells to microvascular endothelial cells.* FEBS Letters, 2013. **587**(19): p. 3210-3215.
195. Blaheta, R.A., B. Kronenberger, D. Woitaschek, M.K. Auth, M. Scholz, S. Weber, H. Schuldes, A. Encke, and B.H. Markus, *Dedifferentiation of human hepatocytes by extracellular matrix proteins in vitro: quantitative and qualitative investigation of cytokeratin 7, 8, 18, 19 and vimentin filaments.* J Hepatol, 1998. **28**(4): p. 677-90.
196. Sjöblom, B., A. Salmazo, and K. Djinović-Carugo, *α-Actinin structure and regulation.* Cellular and Molecular Life Sciences, 2008. **65**(17): p. 2688-2701.
197. Lee, E.-K., G.-Y. Han, H.W. Park, Y.-J. Song, and C.-W. Kim, *Transgelin Promotes Migration and Invasion of Cancer Stem Cells.* Journal of Proteome Research, 2010. **9**(10): p. 5108-5117.
198. Bravo-Cordero, J.J., M.A.O. Magalhaes, R.J. Eddy, L. Hodgson, and J. Condeelis, *Functions of cofilin in cell locomotion and invasion.* Nat Rev Mol Cell Biol, 2013. **14**(7): p. 405-415.

199. Van Troys, M., L. Huyck, S. Leyman, S. Dhaese, J. Vandekerkhove, and C. Ampe, *Ins and outs of ADF/cofilin activity and regulation.* European Journal of Cell Biology, 2008. **87**(8–9): p. 649-667.
200. Blanchoin, L., R. Boujemaa-Paterski, C. Sykes, and J. Plastino, *Actin dynamics, architecture, and mechanics in cell motility.* Physiol Rev, 2014. **94**(1): p. 235-63.
201. Hegde, M., R. Jindal, A. Bhushan, S.S. Bale, W.J. McCarty, I. Golberg, O.B. Usta, and M.L. Yarmush, *Dynamic interplay of flow and collagen stabilizes primary hepatocytes culture in a microfluidic platform.* Lab Chip, 2014. **14**(12): p. 2033-9.
202. Byron, A., J.D. Humphries, and M.J. Humphries, *Defining the extracellular matrix using proteomics.* Int J Exp Pathol, 2013. **94**(2): p. 75-92.
203. Naba, A., K.R. Clauser, H. Ding, C.A. Whittaker, S.A. Carr, and R.O. Hynes, *The extracellular matrix: Tools and insights for the "omics" era.* Matrix Biol, 2015.
204. Van Summeren, A., J. Renes, D. Lizarraga, F.G. Bouwman, J.P. Noben, J.H. van Delft, J.C. Kleinjans, and E.C. Mariman, *Screening for drug-induced hepatotoxicity in primary mouse hepatocytes using acetaminophen, amiodarone, and cyclosporin a as model compounds: an omics-guided approach.* OMICS, 2013. **17**(2): p. 71-83.
205. Laizure, S.C., V. Herring, Z. Hu, K. Witbrodt, and R.B. Parker, *The role of human carboxylesterases in drug metabolism: have we overlooked their importance?* Pharmacotherapy, 2013. **33**(2): p. 210-22.
206. Holmes, R.S., M.W. Wright, S.J. Laulederkind, L.A. Cox, M. Hosokawa, T. Imai, S. Ishibashi, R. Lehner, M. Miyazaki, E.J. Perkins, P.M. Potter, M.R. Redinbo, J. Robert, T. Satoh, T. Yamashita, B. Yan, T. Yokoi, R. Zechner, and L.J. Maltais, *Recommended nomenclature for five mammalian carboxylesterase gene families: human, mouse, and rat genes and proteins.* Mamm Genome, 2010. **21**(9-10): p. 427-41.
207. Claudel, T., B. Staels, and F. Kuipers, *The Farnesoid X receptor: a molecular link between bile acid and lipid and glucose metabolism.* Arterioscler Thromb Vasc Biol, 2005. **25**(10): p. 2020-30.
208. Xu, J., Y. Li, W.D. Chen, Y. Xu, L. Yin, X. Ge, K. Jadhav, L. Adorini, and Y. Zhang, *Hepatic carboxylesterase 1 is essential for both normal and farnesoid X receptor-controlled lipid homeostasis.* Hepatology, 2014. **59**(5): p. 1761-71.
209. Quiroga, A.D., L. Li, M. Trotzmuller, R. Nelson, S.D. Proctor, H. Kofeler, and R. Lehner, *Deficiency of carboxylesterase 1/esterase-x results in obesity, hepatic steatosis, and hyperlipidemia.* Hepatology, 2012. **56**(6): p. 2188-98.
210. Godoy, P., M. Schug, A. Bauer, and J.G. Hengstler, *Reversible Manipulation of Apoptosis Sensitivity in Cultured Hepatocytes by Matrix-Mediated Manipulation of Signaling Activities*, in *Hepatocytes: Methods and Protocols*, P. Maurel, Editor. 2010, Humana Press Inc: Totowa. p. 139-155.
211. Diehl-Jones, W.L. and D.F. Askin, *The neonatal liver, Part 1: embryology, anatomy, and physiology.* Neonatal Netw, 2002. **21**(2): p. 5-12.
212. Smedsrod, B., *Clearance function of scavenger endothelial cells.* Comp Hepatol, 2004. **3 Suppl 1**: p. S22.
213. Li, R., A. Oteiza, K.K. Sorensen, P. McCourt, R. Olsen, B. Smedsrod, and D. Svistounov, *Role of liver sinusoidal endothelial cells and stabilins in elimination of oxidized low-density lipoproteins.* Am J Physiol Gastrointest Liver Physiol, 2011. **300**(1): p. G71-81.
214. Ohgami, N., A. Miyazaki, M. Sakai, A. Kuniyasu, H. Nakayama, and S. Horiuchi, *Advanced glycation end products (AGE) inhibit scavenger receptor class B type I-*

*mediated reverse cholesterol transport: a new crossroad of AGE to cholesterol metabolism.* J Atheroscler Thromb, 2003. **10**(1): p. 1-6.
215. Ohgami, N., R. Nagai, M. Ikemoto, H. Arai, A. Kuniyasu, S. Horiuchi, and H. Nakayama, *CD36, a member of class B scavenger receptor family, is a receptor for advanced glycation end products.* Ann N Y Acad Sci, 2001. **947**: p. 350-5.
216. Ling, W., M. Lougheed, H. Suzuki, A. Buchan, T. Kodama, and U.P. Steinbrecher, *Oxidized or acetylated low density lipoproteins are rapidly cleared by the liver in mice with disruption of the scavenger receptor class A type I/II gene.* J Clin Invest, 1997. **100**(2): p. 244-52.
217. McCourt, P.A., B.H. Smedsrod, J. Melkko, and S. Johansson, *Characterization of a hyaluronan receptor on rat sinusoidal liver endothelial cells and its functional relationship to scavenger receptors.* Hepatology, 1999. **30**(5): p. 1276-86.
218. Muro, H., H. Shirasawa, I. Kosugi, and S. Nakamura, *Defect of Fc receptors and phenotypical changes in sinusoidal endothelial cells in human liver cirrhosis.* Am J Pathol, 1993. **143**(1): p. 105-20.
219. Tsuchiya, K. and D. Accili, *Liver sinusoidal endothelial cells link hyperinsulinemia to hepatic insulin resistance.* Diabetes, 2013. **62**(5): p. 1478-89.
220. De Leeuw, A.M., A. Brouwer, and D.L. Knook, *Sinusoidal endothelial cells of the liver: fine structure and function in relation to age.* J Electron Microsc Tech, 1990. **14**(3): p. 218-36.
221. Nedredal, G.I., K. Elvevold, L.M. Ytrebø, O.-M. Fuskevåg, I. Pettersen, K. Bertheussen, B. Langbakk, B. Smedsrød, and A. Revhaug, *Significant contribution of liver nonparenchymal cells to metabolism of ammonia and lactate and cocultivation augments the functions of a bioartificial liver.* American Journal of Physiology - Gastrointestinal and Liver Physiology, 2007. **293**(1): p. G75-G83.
222. Nedredal, G.I., K. Elvevold, L.M. Ytrebø, O.-M. Fuskevåg, I. Pettersen, P.A.G. McCourt, K. Bertheussen, B. Smedsrød, and A. Revhaug, *Porcine liver sinusoidal endothelial cells contribute significantly to intrahepatic ammonia metabolism.* Hepatology, 2009. **50**(3): p. 900-908.
223. Arias, I., J. Boyer, F. Chisari, N. Fausto, D. Schachter, and D. Shafritz, eds. *The Liver Biology and Pathobiology*. 4 ed. 2001, Lippincott Williams & Wilkins: Philadelphia, PA.
224. Haelterman, N.A., W.H. Yoon, H. Sandoval, M. Jaiswal, J.M. Shulman, and H.J. Bellen, *A mitocentric view of Parkinson's disease.* Annu Rev Neurosci, 2014. **37**: p. 137-59.
225. Vos, M., P. Verstreken, and C. Klein, *Stimulation of electron transport as potential novel therapy in Parkinson's disease with mitochondrial dysfunction.* Biochemical Society Transactions, 2015. **43**(2): p. 275-279.
226. Zheng, B., Z. Liao, J.J. Locascio, K.A. Lesniak, S.S. Roderick, M.L. Watt, A.C. Eklund, Y. Zhang-James, P.D. Kim, M.A. Hauser, E. Grünblatt, L.B. Moran, S.A. Mandel, P. Riederer, R.M. Miller, H.J. Federoff, U. Wüllner, S. Papapetropoulos, M.B. Youdim, I. Cantuti-Castelvetri, A.B. Young, J.M. Vance, R.L. Davis, J.C. Hedreen, C.H. Adler, T.G. Beach, M.B. Graeber, F.A. Middleton, J.-C. Rochet, and C.R. Scherzer, *PGC-1α, A Potential Therapeutic Target for Early Intervention in Parkinson's Disease.* Science Translational Medicine, 2010. **2**(52): p. 52ra73-52ra73.
227. Damiano, M., L. Galvan, N. Déglon, and E. Brouillet, *Mitochondria in Huntington's disease.* Biochimica et Biophysica Acta (BBA) - Molecular Basis of Disease, 2010. **1802**(1): p. 52-61.

228. Mena, N.P., P.J. Urrutia, F. Lourido, C.M. Carrasco, and M.T. Núñez, *Mitochondrial iron homeostasis and its dysfunctions in neurodegenerative disorders.* Mitochondrion, 2015. **21**: p. 92-105.
229. Brennan, W.A., Jr., E.D. Bird, and J.R. Aprille, *Regional mitochondrial respiratory activity in Huntington's disease brain.* J Neurochem, 1985. **44**(6): p. 1948-50.
230. DeLeve, L.D., X. Wang, N. Kaplowitz, H.M. Shulman, J.A. Bart, and A. van der Hoek, *Sinusoidal endothelial cells as a target for acetaminophen toxicity. Direct action versus requirement for hepatocyte activation in different mouse strains.* Biochem Pharmacol, 1997. **53**(9): p. 1339-45.
231. Rich, K.J. and A.R. Boobis, *Expression and inducibility of P450 enzymes during liver ontogeny.* Microscopy Research and Technique, 1997. **39**(5): p. 424-435.
232. Nelson, D.R., T. Kamataki, D.J. Waxman, F.P. Guengerich, R.W. Estabrook, R. Feyereisen, F.J. Gonzalez, M.J. Coon, I.C. Gunsalus, O. Gotoh, and et al., *The P450 superfamily: update on new sequences, gene mapping, accession numbers, early trivial names of enzymes, and nomenclature.* DNA Cell Biol, 1993. **12**(1): p. 1-51.
233. Huang, Y., N. Hu, X. Gao, Z. Yan, S. Li, W. Jing, and R. Yan, *Alterations of testosterone metabolism in microsomes from rats with experimental colitis induced by dextran sulfate sodium.* Chemico-Biological Interactions, 2015. **232**: p. 38-48.
234. Haduch, A., J. Wojcikowski, and W.A. Daniel, *Effect of short- and long-term treatment with antidepressant drugs on the activity of rat CYP2A in the liver.* Pharmacol Rep, 2005. **57**(6): p. 774-81.
235. Zacharova, A., M. Siller, A. Spicakova, E. Anzenbacherova, N. Skottova, P. Anzenbacher, and R. Vecera, *Rosuvastatin suppresses the liver microsomal CYP2C11 and CYP2C6 expression in male Wistar rats.* Xenobiotica, 2012. **42**(8): p. 731-6.
236. Vecera, R., A. Zacharova, M. Siller, Z. Matuskova, N. Skottova, E. Anzenbacherova, and P. Anzenbacher, *The influence of rosuvastatin on liver microsomal CYP2C6 in hereditary hypertriglyceridemic rat.* Neuro Endocrinol Lett, 2012. **33 Suppl 3**: p. 48-52.
237. Cederbaum, A.I., *Cytochrome P450 2E1-dependent oxidant stress and upregulation of anti-oxidant defense in liver cells.* J Gastroenterol Hepatol, 2006. **21 Suppl 3**: p. S22-5.
238. Jancova, P., P. Anzenbacher, and E. Anzenbacherova, *Phase II drug metabolizing enzymes.* Biomed Pap Med Fac Univ Palacky Olomouc Czech Repub, 2010. **154**(2): p. 103-16.
239. Yuan, L. and N. Kaplowitz, *Mechanisms of drug-induced liver injury.* Clin Liver Dis, 2013. **17**(4): p. 507-18, vii.
240. McGill, M.R., C.D. Williams, Y. Xie, A. Ramachandran, and H. Jaeschke, *Acetaminophen-induced liver injury in rats and mice: comparison of protein adducts, mitochondrial dysfunction, and oxidative stress in the mechanism of toxicity.* Toxicol Appl Pharmacol, 2012. **264**(3): p. 387-94.
241. Fisher, M.B., M.F. Paine, T.J. Strelevitz, and S.A. Wrighton, *The role of hepatic and extrahepatic UDP-glucuronosyltransferases in human drug metabolism.* Drug Metab Rev, 2001. **33**(3-4): p. 273-97.
242. Castro-Perez, J.M., J. Kamphorst, J. DeGroot, F. Lafeber, J. Goshawk, K. Yu, J.P. Shockcor, R.J. Vreeken, and T. Hankemeier, *Comprehensive LC-MS E lipidomic analysis using a shotgun approach and its application to biomarker detection and identification in osteoarthritis patients.* J Proteome Res, 2010. **9**(5): p. 2377-89.

243. Matyash, V., G. Liebisch, T.V. Kurzchalia, A. Shevchenko, and D. Schwudke, *Lipid extraction by methyl-tert-butyl ether for high-throughput lipidomics.* J Lipid Res, 2008. **49**(5): p. 1137-46.
244. Lavoinne, A., A. Baquet, and L. Hue, *Stimulation of glycogen synthesis and lipogenesis by glutamine in isolated rat hepatocytes.* Biochem J, 1987. **248**(2): p. 429-37.
245. Eulenfeld, R., A. Dittrich, C. Khouri, P.J. Muller, B. Mutze, A. Wolf, and F. Schaper, *Interleukin-6 signalling: more than Jaks and STATs.* Eur J Cell Biol, 2012. **91**(6-7): p. 486-95.
246. Li, X., W. Wang, and J. Chen, *From pathways to networks: connecting dots by establishing protein-protein interaction networks in signaling pathways using affinity purification and mass spectrometry.* PROTEOMICS, 2015. **15**(2-3): p. 188-202.
247. Cain, K. and C. Freathy, *Liver toxicity and apoptosis: role of TGF-beta1, cytochrome c and the apoptosome.* Toxicol Lett, 2001. **120**(1-3): p. 307-15.
248. Sanchez, A., A.M. Alvarez, M. Benito, and I. Fabregat, *Apoptosis induced by transforming growth factor-beta in fetal hepatocyte primary cultures: involvement of reactive oxygen intermediates.* J Biol Chem, 1996. **271**(13): p. 7416-22.

# Appendix A

**Table A1: Proteins identified in LSEC monolayer replicate 1**

| UniProt ID | Protein description |
|---|---|
| P26772 | 10 kDa heat shock protein_ mitochondrial |
| Q64591 | 2_4-dienoyl-CoA reductase_ mitochondrial |
| Q68G44 | 3-hydroxy-3-methylglutaryl-Coenzyme A synthase 2 (Mitochondrial) |
| O70351 | 3-hydroxyacyl-CoA dehydrogenase type-2 |
| P13437 | 3-ketoacyl-CoA thiolase_ mitochondrial |
| P63039 | 60 kDa heat shock protein_ mitochondrial |
| P06761 | 78 kDa glucose-regulated protein |
| Q7TPI5 | Ac2-281 |
| P17764 | Acetyl-CoA acetyltransferase_ mitochondrial |
| G3V796 | Acetyl-Coenzyme A dehydrogenase_ medium chain |
| P68035 | Actin_ alpha cardiac muscle 1 |
| P68136 | Actin_ alpha skeletal muscle |
| P62738 | Actin_ aortic smooth muscle |
| P60711 | Actin_ cytoplasmic 1 |
| P63269 | Actin_ gamma-enteric smooth muscle |
| Q499N5 | Acyl-CoA synthetase family member 2_ mitochondrial |
| P29410 | Adenylate kinase 2_ mitochondrial |
| Q6P9Y4 | ADP/ATP translocase 1 |
| Q09073 | ADP/ATP translocase 2 |
| G3V7J0 | Aldehyde dehydrogenase family 6_ subfamily A1_ isoform CRA_b |
| Q66HF8 | Aldehyde dehydrogenase X_ mitochondrial |
| Q64057 | Alpha-aminoadipic semialdehyde dehydrogenase |
| P04764 | Alpha-enolase |
| P00507 | Aspartate aminotransferase_ mitochondrial |
| P19511 | ATP synthase F(0) complex subunit B1_ mitochondrial |
| P15999 | ATP synthase subunit alpha_ mitochondrial |
| P10719 | ATP synthase subunit beta_ mitochondrial |
| P31399 | ATP synthase subunit d_ mitochondrial |
| P29419 | ATP synthase subunit e_ mitochondrial |
| D3ZAF6 | ATP synthase subunit f_ mitochondrial |
| Q6PDU7 | ATP synthase subunit g_ mitochondrial |
| P35435 | ATP synthase subunit gamma_ mitochondrial |
| Q06647 | ATP synthase subunit O_ mitochondrial |
| Q7TP24 | Ba1-667 |
| P18418 | Calreticulin |
| P07756 | Carbamoyl-phosphate synthase [ammonia]_ mitochondrial |

| | |
|---|---|
| P97601 | Chaperonin 10 |
| G3V936 | Citrate synthase |
| Q68FY0 | Cytochrome b-c1 complex subunit 1_ mitochondrial |
| P20788 | Cytochrome b-c1 complex subunit Rieske_ mitochondrial |
| P00406 | Cytochrome c oxidase subunit 2 |
| P10888 | Cytochrome c oxidase subunit 4 isoform 1_ mitochondrial |
| P11240 | Cytochrome c oxidase subunit 5A_ mitochondrial |
| Q5EB99 | Cytochrome P450-like |
| Q64614 | Cytochrome P450PB-1 (Fragment) |
| P29147 | D-beta-hydroxybutyrate dehydrogenase_ mitochondrial |
| P0C2X9 | Delta-1-pyrroline-5-carboxylate dehydrogenase_ mitochondrial |
| G3V6P2 | Dihydrolipoamide S-succinyltransferase (E2 component of 2-oxo-glutarate complex)_ isoform CRA_a |
| Q641Y0 | Dolichyl-diphosphooligosaccharide--protein glycosyltransferase 48 kDa subunit |
| P07153 | Dolichyl-diphosphooligosaccharide--protein glycosyltransferase subunit 1 |
| P25235 | Dolichyl-diphosphooligosaccharide--protein glycosyltransferase subunit 2 |
| P13803 | Electron transfer flavoprotein subunit alpha_ mitochondrial |
| Q68FU3 | Electron transfer flavoprotein subunit beta |
| Q66HD0 | Endoplasmin |
| Q5BJ93 | Enolase 1_ (Alpha) |
| P14604 | Enoyl-CoA hydratase_ mitochondrial |
| O88752 | Epsilon 1 globin |
| B0BNJ4 | Ethylmalonic encephalopathy 1 |
| B2RYW9 | Fumarylacetoacetate hydrolase domain-containing protein 2 |
| Q99521 | Gastrin-binding protein (Fragment) |
| P10860 | Glutamate dehydrogenase 1_ mitochondrial |
| P04041 | Glutathione peroxidase 1 |
| P04906 | Glutathione S-transferase P |
| Q5I0P2 | Glycine cleavage system H protein_ mitochondrial |
| Q64599 | Hemiferrin |
| P02091 | Hemoglobin subunit beta-1 |
| P11517 | Hemoglobin subunit beta-2 |
| P15865 | Histone H1.4 |
| Q6I8Q6 | Histone H2A |
| Q00715 | Histone H2B type 1 |
| P62804 | Histone H4 |
| Q9WVK7 | Hydroxyacyl-coenzyme A dehydrogenase_ mitochondrial |
| P22791 | Hydroxymethylglutaryl-CoA synthase_ mitochondrial |
| Q63280 | Keratin K5 (Fragment) |
| A0A0G2K509 | Keratin_ type II cytoskeletal 5 |
| Q4FZU2 | Keratin_ type II cytoskeletal 6A |
| Q498S9 | LOC498793 protein (Fragment) |

| | |
|---|---|
| P15650 | Long-chain specific acyl-CoA dehydrogenase_ mitochondrial |
| P04636 | Malate dehydrogenase_ mitochondrial |
| P08503 | Medium-chain specific acyl-CoA dehydrogenase_ mitochondrial |
| Q4V8K1 | Metalloreductase STEAP4 |
| Q02253 | Methylmalonate-semialdehyde dehydrogenase [acylating]_ mitochondrial |
| Q31266 | MHC class I RT1.Aw3 protein |
| P08011 | Microsomal glutathione S-transferase 1 |
| O89035 | Mitochondrial dicarboxylate carrier |
| P04182 | Ornithine aminotransferase_ mitochondrial |
| P00481 | Ornithine carbamoyltransferase_ mitochondrial |
| P24368 | Peptidyl-prolyl cis-trans isomerase B |
| Q9R063 | Peroxiredoxin-5_ mitochondrial |
| Q9WVK3 | Peroxisomal trans-2-enoyl-CoA reductase |
| Q63412 | Product of unknown function (Fragment) |
| P62963 | Profilin-1 |
| P67779 | Prohibitin |
| Q5XIH7 | Prohibitin-2 |
| D3ZRN3 | Protein Actbl2 |
| D3ZBE6 | Protein Atp5hl1 |
| P11598 | Protein disulfide-isomerase A3 |
| Q63081 | Protein disulfide-isomerase A6 |
| P04785 | Protein disulfide-isomerase |
| D4A2K1 | Protein Hoga1 |
| D3ZFH5 | Protein Itih2 |
| G3V908 | Protein Kb15 |
| M0R4D7 | Protein LOC100910820 |
| D3ZFH6 | Protein Phb-ps1 |
| F1LZW6 | Protein Slc25a13 |
| D3ZB81 | Protein Slc25a31 |
| Q5XI04 | Protein Stom |
| P52873 | Pyruvate carboxylase_ mitochondrial |
| Q63223 | Rat hemoglobin beta-chain (Fragment) |
| Q5RJR9 | Serine (Or cysteine) proteinase inhibitor_ clade H_ member 1_ isoform CRA_b |
| P12346 | Serotransferrin |
| P29457 | Serpin H1 |
| P02770 | Serum albumin |
| P48721 | Stress-70 protein_ mitochondrial |
| P21913 | Succinate dehydrogenase [ubiquinone] iron-sulfur subunit_ mitochondrial |
| F1LPV8 | Succinyl-CoA ligase subunit beta |
| P07895 | Superoxide dismutase [Mn]_ mitochondrial |
| R9PY10 | Taste receptor type 1 member 2 |

| | |
|---|---|
| P24329 | Thiosulfate sulfurtransferase |
| Q64428 | Trifunctional enzyme subunit alpha_ mitochondrial |
| Q60587 | Trifunctional enzyme subunit beta_ mitochondrial |
| P08542 | UDP-glucuronosyltransferase 2B17 |
| P08541 | UDP-glucuronosyltransferase 2B2 |
| D3ZLR6 | UDP-glucuronosyltransferase 2B37 |
| P09118 | Uricase |
| Q9Z2L0 | Voltage-dependent anion-selective channel protein 1 |
| P81155 | Voltage-dependent anion-selective channel protein 2 |

**Table A2: Proteins identified in LSEC monolayer replicate 2**

| UniProt ID | Protein description |
|---|---|
| Q9R1Z0 | Voltage-dependent anion-selective channel protein 3 |
| P81155 | Voltage-dependent anion-selective channel protein 2 |
| Q9Z2L0 | Voltage-dependent anion-selective channel protein 1 |
| P45953 | Very long-chain specific acyl-CoA dehydrogenase_ mitochondrial |
| P09118 | Uricase |
| Q9JJW3 | Up-regulated during skeletal muscle growth protein 5 |
| P70624 | UGT1A7 |
| P19488 | UDP-glucuronosyltransferase 2B37 |
| P08541 | UDP-glucuronosyltransferase 2B2 |
| P08542 | UDP-glucuronosyltransferase 2B17 |
| P36511 | UDP-glucuronosyltransferase 2B15 |
| P09875 | UDP-glucuronosyltransferase 2B1 |
| P08430 | UDP-glucuronosyltransferase 1-6 |
| Q64638 | UDP-glucuronosyltransferase 1-5 |
| P20720 | UDP-glucuronosyltransferase 1-2 |
| Q64550 | UDP-glucuronosyltransferase 1-1 |
| Q60587 | Trifunctional enzyme subunit beta_ mitochondrial |
| Q64428 | Trifunctional enzyme subunit alpha_ mitochondrial |
| P32089 | Tricarboxylate transport protein_ mitochondrial |
| Q5I0E7 | Transmembrane emp24 domain-containing protein 9 |
| Q07984 | Translocon-associated protein subunit delta |
| Q7TPJ0 | Translocon-associated protein subunit alpha |
| Q9Z311 | Trans-2-enoyl-CoA reductase_ mitochondrial |
| P24329 | Thiosulfate sulfurtransferase |
| Q9Z0V6 | Thioredoxin-dependent peroxide reductase_ mitochondrial |
| P97615 | Thioredoxin_ mitochondrial |
| F8WFI0 | Taste receptor type 1 member 2 |
| P07895 | Superoxide dismutase [Mn]_ mitochondrial |
| Q07116 | Sulfite oxidase_ mitochondrial |

| | |
|---|---|
| P70631 | Succinyl-CoA synthetase alpha subunit (Fragment) |
| Q68FT4 | Succinyl-CoA ligase subunit beta (Fragment) |
| P21913 | Succinate dehydrogenase [ubiquinone] iron-sulfur subunit_ mitochondrial |
| Q920L2 | Succinate dehydrogenase [ubiquinone] flavoprotein subunit_ mitochondrial |
| P48721 | Stress-70 protein_ mitochondrial |
| Q4FZT0 | Stomatin-like protein 2_ mitochondrial |
| P17178 | Sterol 26-hydroxylase_ mitochondrial |
| Q6AXV4 | Sorting and assembly machinery component 50 homolog |
| Q4V7D1 | Signal sequence receptor_ alpha |
| Q63965 | Sideroflexin-1 |
| P15651 | Short-chain specific acyl-CoA dehydrogenase_ mitochondrial |
| P70584 | Short/branched chain specific acyl-CoA dehydrogenase_ mitochondrial |
| Q68FP2 | Serum paraoxonase/lactonase 3 |
| P55159 | Serum paraoxonase/arylesterase 1 |
| P02770 | Serum albumin |
| P12346 | Serotransferrin |
| Q5U3Z7 | Serine hydroxymethyltransferase |
| Q64380 | Sarcosine dehydrogenase_ mitochondrial |
| P52759 | Ribonuclease UK114 |
| Q5EB60 | RGD1308874 protein (Fragment) |
| F1LVY2 | Retinol dehydrogenase 7 |
| P55006 | Retinol dehydrogenase 7 |
| P50169 | Retinol dehydrogenase 3 |
| P50170 | Retinol dehydrogenase 2 |
| Q498D5 | Regulator of microtubule dynamics protein 2 |
| Q63223 | Rat hemoglobin beta-chain (Fragment) |
| P49432 | Pyruvate dehydrogenase E1 component subunit beta_ mitochondrial |
| P26284 | Pyruvate dehydrogenase E1 component subunit alpha_ somatic form_ mitochondrial |
| P52873 | Pyruvate carboxylase_ mitochondrial |
| Q68FT3 | Pyridine nucleotide-disulfide oxidoreductase domain-containing protein 2 |
| G3V908 | Protein Kb15 |
| D4A2K1 | Protein Hoga1 |
| Q62902 | Protein ERGIC-53 |
| P04785 | Protein disulfide-isomerase |
| A0A0G2JSZ5 | Protein disulfide-isomerase A6 |
| Q63081 | Protein disulfide-isomerase A6 |
| Q5I0H9 | Protein disulfide-isomerase A5 |
| P38659 | Protein disulfide-isomerase A4 |
| G3V6T7 | Protein disulfide-isomerase A4 |
| P11598 | Protein disulfide-isomerase A3 |
| F1LR47 | Protein Cyp2c6v1 |

| | |
|---|---|
| M0RB90 | Protein Cyp2c6v1 |
| A0A0G2K455 | Protein Ces2 |
| D3ZBE6 | Protein Atp5hl1 |
| M0RA88 | Protein Aldh1l2 |
| A0A0G2K047 | Protein Acss3 |
| D3ZGU2 | Protein Acss3 |
| F1M1W1 | Protein Acsm1 |
| D3ZIQ1 | Protein Acot4 |
| D3ZA93 | Protein Acot13 |
| M0RDK9 | Protein Acad8 |
| P07633 | Propionyl-CoA carboxylase beta chain_ mitochondrial |
| P14882 | Propionyl-CoA carboxylase alpha chain_ mitochondrial |
| Q5XIH7 | Prohibitin-2 |
| P67779 | Prohibitin |
| Q2V057 | Probable proline dehydrogenase 2 |
| Q4KLP0 | Probable 2-oxoglutarate dehydrogenase E1 component DHKTD1_ mitochondrial |
| P16036 | Phosphate carrier protein_ mitochondrial |
| Q9WVK3 | Peroxisomal trans-2-enoyl-CoA reductase |
| P07896 | Peroxisomal bifunctional enzyme |
| P97562 | Peroxisomal acyl-coenzyme A oxidase 2 |
| Q9R063 | Peroxiredoxin-5_ mitochondrial |
| Q9Z0V5 | Peroxiredoxin-4 |
| D3ZZR9 | Peptidyl-prolyl cis-trans isomerase |
| P24368 | Peptidyl-prolyl cis-trans isomerase B |
| P00481 | Ornithine carbamoyltransferase_ mitochondrial |
| P04182 | Ornithine aminotransferase_ mitochondrial |
| Q497B0 | Omega-amidase NIT2 |
| Q8K4G6 | O-acetyl-ADP-ribose deacetylase MACROD1 (Fragment) |
| P19804 | Nucleoside diphosphate kinase B |
| Q05982 | Nucleoside diphosphate kinase A |
| P11915 | Non-specific lipid-transfer protein |
| Q5BJZ3 | Nicotinamide nucleotide transhydrogenase |
| B2RZD6 | Ndufa4 protein |
| P56522 | NADPH:adrenodoxin oxidoreductase_ mitochondrial |
| Q66HF1 | NADH-ubiquinone oxidoreductase 75 kDa subunit_ mitochondrial |
| P20070 | NADH-cytochrome b5 reductase 3 |
| Q641Y2 | NADH dehydrogenase [ubiquinone] iron-sulfur protein 2_ mitochondrial |
| P19234 | NADH dehydrogenase [ubiquinone] flavoprotein 2_ mitochondrial |
| Q6P6W6 | NADH dehydrogenase (Ubiquinone) 1 alpha subcomplex 10 |
| Q1HCL7 | NAD kinase 2_ mitochondrial |
| C8CHS6 | Mitochondrial superoxide dismutase 2 (Fragment) |

| | |
|---|---|
| P38718 | Mitochondrial pyruvate carrier 2 |
| P63031 | Mitochondrial pyruvate carrier 1 |
| Q9WVA1 | Mitochondrial import inner membrane translocase subunit Tim8 A |
| P62076 | Mitochondrial import inner membrane translocase subunit Tim13 |
| O89035 | Mitochondrial dicarboxylate carrier |
| B0BN52 | Mitochondrial carrier 2 |
| P97521 | Mitochondrial carnitine/acylcarnitine carrier protein |
| O88994 | Mitochondrial amidoxime reducing component 2 |
| P97700 | Mitochondrial 2-oxoglutarate/malate carrier protein |
| D4A1W8 | Microsomal triglyceride transfer protein |
| P08011 | Microsomal glutathione S-transferase 1 |
| Q562C4 | Methyltransferase-like protein 7B |
| D4A197 | Methylmalonyl CoA epimerase (Predicted)_ isoform CRA_d |
| Q02253 | Methylmalonate-semialdehyde dehydrogenase [acylating]_ mitochondrial |
| Q5I0C3 | Methylcrotonoyl-CoA carboxylase subunit alpha_ mitochondrial |
| Q5XIT9 | Methylcrotonoyl-CoA carboxylase beta chain_ mitochondrial |
| P0C5H9 | Mesencephalic astrocyte-derived neurotrophic factor |
| P70580 | Membrane-associated progesterone receptor component 1 |
| P08503 | Medium-chain specific acyl-CoA dehydrogenase_ mitochondrial |
| P57113 | Maleylacetoacetate isomerase |
| P04636 | Malate dehydrogenase_ mitochondrial |
| Q7TNX8 | LRP16-like protein |
| O88813 | Long-chain-fatty-acid--CoA ligase 5 |
| P18163 | Long-chain-fatty-acid--CoA ligase 1 |
| P15650 | Long-chain specific acyl-CoA dehydrogenase_ mitochondrial |
| Q924S5 | Lon protease homolog_ mitochondrial |
| Q63010 | Liver carboxylesterase B-1 |
| Q64573 | Liver carboxylesterase 4 |
| P10867 | L-gulonolactone oxidase |
| Q58FK9 | Kynurenine--oxoglutarate transaminase |
| A0A0G2K4P6 | Kynurenine/alpha-aminoadipate aminotransferase_ mitochondrial |
| Q64602 | Kynurenine/alpha-aminoadipate aminotransferase_ mitochondrial |
| Q6IG03 | Keratin_ type II cytoskeletal 73 |
| Q4FZU2 | Keratin_ type II cytoskeletal 6A |
| Q6P6Q2 | Keratin_ type II cytoskeletal 5 |
| Q6IMF3 | Keratin_ type II cytoskeletal 1 |
| P12007 | Isovaleryl-CoA dehydrogenase_ mitochondrial |
| P56574 | Isocitrate dehydrogenase [NADP]_ mitochondrial |
| P22791 | Hydroxymethylglutaryl-CoA synthase_ mitochondrial |
| P17425 | Hydroxymethylglutaryl-CoA synthase_ cytoplasmic |
| P97519 | Hydroxymethylglutaryl-CoA lyase_ mitochondrial |

| | |
|---|---|
| Q9WVK7 | Hydroxyacyl-coenzyme A dehydrogenase_ mitochondrial |
| Q4QQW3 | Hydroxyacid-oxoacid transhydrogenase_ mitochondrial |
| P15865 | Histone H1.4 |
| D4AB01 | Histidine triad nucleotide binding protein 2 (Predicted)_ isoform CRA_a |
| P11517 | Hemoglobin subunit beta-2 |
| P02091 | Hemoglobin subunit beta-1 |
| Q64599 | Hemiferrin |
| P14659 | Heat shock-related 70 kDa protein 2 |
| Q5XHZ0 | Heat shock protein 75 kDa_ mitochondrial |
| P63018 | Heat shock cognate 71 kDa protein |
| P55063 | Heat shock 70 kDa protein 1-like |
| B2RYT7 | Haloacid dehalogenase-like hydrolase domain containing 3 |
| Q9QYU8 | H protein |
| P29411 | GTP:AMP phosphotransferase AK3_ mitochondrial |
| P97576 | GrpE protein homolog 1_ mitochondrial |
| Q5PQT3 | Glycine N-acyltransferase |
| Q5I0P2 | Glycine cleavage system H protein_ mitochondrial |
| Q562C3 | Glycine C-acetyltransferase (2-amino-3-ketobutyrate-coenzyme A ligase) |
| F1LNI0 | Glycerol-3-phosphate dehydrogenase |
| Q0VGK3 | Glycerate kinase |
| P24473 | Glutathione S-transferase kappa 1 |
| P04041 | Glutathione peroxidase 1 |
| D3ZT90 | Glutaryl-Coenzyme A dehydrogenase (Predicted) |
| D4ADD7 | Glutaredoxin 5 homolog (S. cerevisiae) (Predicted)_ isoform CRA_b |
| P28492 | Glutaminase liver isoform_ mitochondrial |
| P10860 | Glutamate dehydrogenase 1_ mitochondrial |
| Q8CJG5 | Gene |
| Q99521 | Gastrin-binding protein (Fragment) |
| B2RYW9 | Fumarylacetoacetate hydrolase domain-containing protein 2 |
| P14408 | Fumarate hydratase_ mitochondrial |
| P30839 | Fatty aldehyde dehydrogenase |
| B0BNJ4 | Ethylmalonic encephalopathy 1 |
| Q6MGB5 | Estradiol 17-beta-dehydrogenase 8 |
| P56571 | ES1 protein homolog_ mitochondrial |
| P07687 | Epoxide hydrolase 1 |
| P14604 | Enoyl-CoA hydratase_ mitochondrial |
| P23965 | Enoyl-CoA delta isomerase 1_ mitochondrial |
| D3ZIL6 | Enoyl Coenzyme A hydratase domain containing 2 (Predicted)_ isoform CRA_a |
| P52555 | Endoplasmic reticulum resident protein 29 |
| P85834 | Elongation factor Tu_ mitochondrial |
| Q66HF3 | Electron transfer flavoprotein-ubiquinone oxidoreductase_ mitochondrial |

| | |
|---|---|
| Q68FU3 | Electron transfer flavoprotein subunit beta |
| P13803 | Electron transfer flavoprotein subunit alpha_ mitochondrial |
| Q6P6S9 | Ectonucleoside triphosphate diphosphohydrolase 5 |
| P61805 | Dolichyl-diphosphooligosaccharide--protein glycosyltransferase subunit DAD1 |
| P25235 | Dolichyl-diphosphooligosaccharide--protein glycosyltransferase subunit 2 |
| P07153 | Dolichyl-diphosphooligosaccharide--protein glycosyltransferase subunit 1 |
| Q641Y0 | Dolichyl-diphosphooligosaccharide--protein glycosyltransferase 48 kDa subunit |
| Q68G41 | Dodecenoyl-Coenzyme A delta isomerase (3_2 trans-enoyl-Coenzyme A isomerase) |
| D0VYQ0 | DLST protein |
| Q63342 | Dimethylglycine dehydrogenase_ mitochondrial |
| Q8K4C0 | Dimethylaniline monooxygenase [N-oxide-forming] 5 |
| Q9EQ76 | Dimethylaniline monooxygenase [N-oxide-forming] 3 |
| Q01205 | Dihydrolipoyllysine-residue succinyltransferase component of 2-oxoglutarate dehydrogenase complex_ mitochondrial |
| P08461 | Dihydrolipoyllysine-residue acetyltransferase component of pyruvate dehydrogenase complex_ mitochondrial |
| Q6P6R2 | Dihydrolipoyl dehydrogenase_ mitochondrial |
| B2GV15 | Dihydrolipoamide branched chain transacylase E2 |
| Q64592 | Delta3_ delta2-enoyl-CoA isomerase |
| Q62651 | Delta(3_5)-Delta(2_4)-dienoyl-CoA isomerase_ mitochondrial |
| Q8VID1 | Dehydrogenase/reductase SDR family member 4 |
| P29147 | D-beta-hydroxybutyrate dehydrogenase_ mitochondrial |
| P84850 | D-2-hydroxyglutarate dehydrogenase_ mitochondrial |
| Q68FS4 | Cytosol aminopeptidase |
| Q64614 | Cytochrome P450PB-1 (Fragment) |
| Q5EB99 | Cytochrome P450-like |
| P05182 | Cytochrome P450 2E1 |
| P05179 | Cytochrome P450 2C7 |
| P05178 | Cytochrome P450 2C6 |
| P24470 | Cytochrome P450 2C23 |
| P11510 | Cytochrome P450 2C12_ female-specific |
| P11711 | Cytochrome P450 2A1 |
| D3ZFQ8 | Cytochrome c-1 (Predicted)_ isoform CRA_c |
| P35171 | Cytochrome c oxidase subunit 7A2_ mitochondrial |
| P11951 | Cytochrome c oxidase subunit 6C-2 |
| D3ZD09 | Cytochrome c oxidase subunit 6B1 |
| P12075 | Cytochrome c oxidase subunit 5B_ mitochondrial |
| P11240 | Cytochrome c oxidase subunit 5A_ mitochondrial |
| P10888 | Cytochrome c oxidase subunit 4 isoform 1_ mitochondrial |
| P00406 | Cytochrome c oxidase subunit 2 |
| P20788 | Cytochrome b-c1 complex subunit Rieske_ mitochondrial |
| B2RYS2 | Cytochrome b-c1 complex subunit 7 |
| Q5M9I5 | Cytochrome b-c1 complex subunit 6_ mitochondrial |

| | |
|---|---|
| P32551 | Cytochrome b-c1 complex subunit 2_ mitochondrial |
| Q68FY0 | Cytochrome b-c1 complex subunit 1_ mitochondrial |
| O35796 | Complement component 1 Q subcomponent-binding protein_ mitochondrial |
| G3V936 | Citrate synthase |
| Q6UPE0 | Choline dehydrogenase_ mitochondrial |
| P97601 | Chaperonin 10 |
| B0K020 | CDGSH iron-sulfur domain-containing protein 1 |
| P04762 | Catalase |
| P18886 | Carnitine O-palmitoyltransferase 2_ mitochondrial |
| Q8K3R0 | Carboxylic ester hydrolase |
| M0R7R1 | Carboxylic ester hydrolase |
| Q63108 | Carboxylesterase 1E |
| P16303 | Carboxylesterase 1D |
| P10959 | Carboxylesterase 1C |
| P07756 | Carbamoyl-phosphate synthase [ammonia]_ mitochondrial |
| A0JN30 | Canopy 2 homolog (Zebrafish) |
| P18418 | Calreticulin |
| P35565 | Calnexin |
| B5DFA3 | Bucs1 protein |
| Q3B8N9 | Biphenyl hydrolase-like (Serine hydrolase) |
| Q9ES38 | Bile acyl-CoA synthetase |
| Q63276 | Bile acid-CoA:amino acid N-acyltransferase |
| Q99NC6 | Beta-actin FE-3 (Fragment) |
| Q5EB89 | Bckdha protein (Fragment) |
| Q7TP24 | Ba1-667 |
| Q7TP27 | Ba1-651 |
| F1LU71 | AU RNA binding protein/enoyl-coenzyme A hydratase (Predicted)_ isoform CRA_a |
| Q5BJQ0 | Atypical kinase ADCK3_ mitochondrial |
| Q06647 | ATP synthase subunit O_ mitochondrial |
| P35435 | ATP synthase subunit gamma_ mitochondrial |
| Q6PDU7 | ATP synthase subunit g_ mitochondrial |
| D3ZAF6 | ATP synthase subunit f_ mitochondrial |
| P29419 | ATP synthase subunit e_ mitochondrial |
| P35434 | ATP synthase subunit delta_ mitochondrial |
| P31399 | ATP synthase subunit d_ mitochondrial |
| P10719 | ATP synthase subunit beta_ mitochondrial |
| P15999 | ATP synthase subunit alpha_ mitochondrial |
| P19511 | ATP synthase F(0) complex subunit B1_ mitochondrial |
| P00507 | Aspartate aminotransferase_ mitochondrial |
| Q5I0N0 | Arylacetamide deacetylase |
| B2RZ09 | Arginine-rich_ mutated in early stage tumors (Predicted)_ isoform CRA_b |

| | |
|---|---|
| Q5XI85 | Aminomethyltransferase |
| P70473 | Alpha-methylacyl-CoA racemase |
| D4ACE9 | Alpha-aminoadipic semialdehyde synthase_ mitochondrial |
| Q64057 | Alpha-aminoadipic semialdehyde dehydrogenase |
| P14046 | Alpha-1-inhibitor 3 |
| P11884 | Aldehyde dehydrogenase_ mitochondrial |
| Q66HF8 | Aldehyde dehydrogenase X_ mitochondrial |
| G3V9W6 | Aldehyde dehydrogenase |
| Q0D2L3 | Agmatinase_ mitochondrial |
| P24483 | Adrenodoxin_ mitochondrial OS=Rattus norvegicus GN=Fdx1 PE=2 SV=1 |
| Q09073 | ADP/ATP translocase 2 |
| Q05962 | ADP/ATP translocase 1 |
| Q7TP48 | Adipocyte plasma membrane-associated protein |
| Q9WUS0 | Adenylate kinase 4_ mitochondrial |
| P29410 | Adenylate kinase 2_ mitochondrial |
| Q6AYQ8 | Acylpyruvase FAHD1_ mitochondrial |
| O55171 | Acyl-coenzyme A thioesterase 2_ mitochondrial |
| G3V7C4 | Acyl-coenzyme A thioesterase 1 |
| Q6AYT9 | Acyl-coenzyme A synthetase ACSM5_ mitochondrial |
| F1LNW3 | Acyl-coenzyme A oxidase |
| Q5M9H2 | Acyl-Coenzyme A dehydrogenase_ very long chain |
| Q499N5 | Acyl-CoA synthetase family member 2_ mitochondrial |
| D3ZF13 | Acyl carrier protein |
| P60711 | Actin_ cytoplasmic 1 |
| P62738 | Actin_ aortic smooth muscle |
| P68035 | Actin_ alpha cardiac muscle 1 |
| Q9ER34 | Aconitate hydratase_ mitochondrial |
| M0RAP9 | Acetyltransferase component of pyruvate dehydrogenase complex |
| G3V796 | Acetyl-Coenzyme A dehydrogenase_ medium chain |
| P17764 | Acetyl-CoA acetyltransferase_ mitochondrial |
| Q7TPA1 | Ab1-114 |
| Q7TMB6 | Aa2-174 |
| P06761 | 78 kDa glucose-regulated protein |
| P63039 | 60 kDa heat shock protein_ mitochondrial |
| Q9JLJ3 | 4-trimethylaminobutyraldehyde dehydrogenase |
| G3V728 | 4-nitrophenylphosphatase domain and non-neuronal SNAP25-like protein homolog 1 (C. elegans)_ isoform CRA_b |
| P50554 | 4-aminobutyrate aminotransferase_ mitochondrial |
| P24008 | 3-oxo-5-alpha-steroid 4-dehydrogenase 1 |
| P97532 | 3-mercaptopyruvate sulfurtransferase |
| P13437 | 3-ketoacyl-CoA thiolase_ mitochondrial |
| P29266 | 3-hydroxyisobutyrate dehydrogenase_ mitochondrial |

| | |
|---|---|
| O70351 | 3-hydroxyacyl-CoA dehydrogenase type-2 |
| P35738 | 2-oxoisovalerate dehydrogenase subunit beta_ mitochondrial |
| P11960 | 2-oxoisovalerate dehydrogenase subunit alpha_ mitochondrial (Fragment) |
| Q5XI78 | 2-oxoglutarate dehydrogenase_ mitochondrial |
| Q64591 | 2_4-dienoyl-CoA reductase_ mitochondrial |
| Q5M875 | 17-beta-hydroxysteroid dehydrogenase 13 |
| D3ZTP0 | 10-formyltetrahydrofolate dehydrogenase |
| P26772 | 10 kDa heat shock protein_ mitochondrial |

**Table A3: Proteins identified in LSEC monolayer replicate 3**

| UniProt ID | Protein description |
|---|---|
| Q9R1Z0 | Voltage-dependent anion-selective channel protein 3 |
| P81155 | Voltage-dependent anion-selective channel protein 2 |
| Q9Z2L0 | Voltage-dependent anion-selective channel protein 1 |
| P45953 | Very long-chain specific acyl-CoA dehydrogenase_ mitochondrial |
| P97524 | Very long-chain acyl-CoA synthetase |
| P09118 | Uricase |
| Q9JJW3 | Up-regulated during skeletal muscle growth protein 5 |
| Q68G32 | Ugt1a7c protein (Fragment) |
| F1LLV5 | UDP-glucuronosyltransferase |
| F1M7N8 | UDP-glucuronosyltransferase 2B37 |
| Q68G19 | UDP-glucuronosyltransferase 2B35 |
| D4A132 | UDP-glucuronosyltransferase 2B10 |
| Q7TT85 | UDP-glucuronosyltransferase 2B |
| Q5EBC8 | UDP-glucuronosyltransferase 2B |
| Q6T5F3 | UDP-glucuronosyltransferase 1A9 |
| Q8VD44 | UDP-glucuronosyltransferase 1A8 |
| Q8VD43 | UDP-glucuronosyltransferase 1A7C |
| Q63662 | UDP-glucuronosyltransferase 1A6 |
| Q8VD45 | UDP-glucuronosyltransferase 1A5 |
| Q6T5F0 | UDP-glucuronosyltransferase 1A5 |
| Q5DT04 | UDP-glucuronosyltransferase 1A1 |
| P97886 | UDP-glucuronosyltransferase 1 |
| Q62789 | UDP-glucuronosyltransferase 2B7 |
| P19488 | UDP-glucuronosyltransferase 2B37 |
| P08541 | UDP-glucuronosyltransferase 2B2 |
| P08542 | UDP-glucuronosyltransferase 2B17 |
| P36511 | UDP-glucuronosyltransferase 2B15 |
| P09875 | UDP-glucuronosyltransferase 2B1 |
| Q91Y43 | UDP-glucuronosyltransferase 1A6 (Fragment) |

| | |
|---|---|
| Q5FWT0 | Ubc protein (Fragment) |
| P69897 | Tubulin beta-5 chain |
| Q6P9T8 | Tubulin beta-4B chain |
| Q4QRB4 | Tubulin beta-3 chain |
| P85108 | Tubulin beta-2A chain |
| Q60587 | Trifunctional enzyme subunit beta_ mitochondrial |
| Q64428 | Trifunctional enzyme subunit alpha_ mitochondrial |
| P32089 | Tricarboxylate transport protein_ mitochondrial |
| Q5I0E7 | Transmembrane emp24 domain-containing protein 9 |
| Q63584 | Transmembrane emp24 domain-containing protein 10 |
| Q07984 | Translocon-associated protein subunit delta |
| Q9Z311 | Trans-2-enoyl-CoA reductase_ mitochondrial |
| P24329 | Thiosulfate sulfurtransferase |
| Q9Z0V6 | Thioredoxin-dependent peroxide reductase_ mitochondrial |
| P11232 | Thioredoxin |
| R9PY10 | Taste receptor type 1 member 2 |
| P07895 | Superoxide dismutase [Mn]_ mitochondrial |
| P70631 | Succinyl-CoA synthetase alpha subunit (Fragment) |
| F1LPV8 | Succinyl-CoA ligase subunit beta |
| P13086 | Succinyl-CoA ligase [ADP/GDP-forming] subunit alpha_ mitochondrial |
| P21913 | Succinate dehydrogenase [ubiquinone] iron-sulfur subunit_ mitochondrial |
| Q920L2 | Succinate dehydrogenase [ubiquinone] flavoprotein subunit_ mitochondrial |
| P48721 | Stress-70 protein_ mitochondrial |
| Q4FZT0 | Stomatin-like protein 2_ mitochondrial |
| P17178 | Sterol 26-hydroxylase_ mitochondrial |
| A1E0X5 | Steroid 5 alpha-reductase (Fragment) |
| Q66HN6 | Solute carrier family 27 (Fatty acid transporter)_ member 2 |
| Q63965 | Sideroflexin-1 |
| P15651 | Short-chain specific acyl-CoA dehydrogenase_ mitochondrial |
| P70584 | Short/branched chain specific acyl-CoA dehydrogenase_ mitochondrial |
| Q68FP2 | Serum paraoxonase/lactonase 3 |
| P55159 | Serum paraoxonase/arylesterase 1 |
| P02770 | Serum albumin |
| P12346 | Serotransferrin |
| Q5U3Z7 | Serine hydroxymethyltransferase |
| Q64380 | Sarcosine dehydrogenase_ mitochondrial |
| P52759 | Ribonuclease UK114 |
| P55006 | Retinol dehydrogenase 7 |
| P49432 | Pyruvate dehydrogenase E1 component subunit beta_ mitochondrial |
| P26284 | Pyruvate dehydrogenase E1 component subunit alpha_ somatic form_ mitochondrial |
| P52873 | Pyruvate carboxylase_ mitochondrial |

| | |
|---|---|
| Q68FT3 | Pyridine nucleotide-disulfide oxidoreductase domain-containing protein 2 |
| P04785 | Protein disulfide-isomerase |
| Q63081 | Protein disulfide-isomerase A6 |
| Q5I0H9 | Protein disulfide-isomerase A5 |
| P38659 | Protein disulfide-isomerase A4 |
| P11598 | Protein disulfide-isomerase A3 |
| P07633 | Propionyl-CoA carboxylase beta chain_ mitochondrial |
| P14882 | Propionyl-CoA carboxylase alpha chain_ mitochondrial |
| Q68FZ8 | Propionyl coenzyme A carboxylase_ beta polypeptide |
| P67779 | Prohibitin |
| P62963 | Profilin-1 |
| Q63412 | Product of unknown function (Fragment) |
| Q2V057 | Probable proline dehydrogenase 2 |
| Q4KLP0 | Probable 2-oxoglutarate dehydrogenase E1 component DHKTD1_ mitochondrial |
| Q63654 | Polyubiquitin (Fragment) |
| Q07969 | Platelet glycoprotein 4 |
| P06765 | Platelet factor 4 |
| P16036 | Phosphate carrier protein_ mitochondrial |
| Q9WVK3 | Peroxisomal trans-2-enoyl-CoA reductase |
| P97852 | Peroxisomal multifunctional enzyme type 2 |
| P07896 | Peroxisomal bifunctional enzyme |
| Q63448 | Peroxisomal acyl-coenzyme A oxidase 3 |
| P97562 | Peroxisomal acyl-coenzyme A oxidase 2 |
| P07872 | Peroxisomal acyl-coenzyme A oxidase 1 |
| Q9R063 | Peroxiredoxin-5_ mitochondrial |
| Q9Z0V5 | Peroxiredoxin-4 |
| P24368 | Peptidyl-prolyl cis-trans isomerase B |
| P10111 | Peptidyl-prolyl cis-trans isomerase A |
| P00481 | Ornithine carbamoyltransferase_ mitochondrial |
| P04182 | Ornithine aminotransferase_ mitochondrial |
| Q497B0 | Omega-amidase NIT2 |
| G3V8V6 | O-acetyl-ADP-ribose deacetylase MACROD1 |
| P19804 | Nucleoside diphosphate kinase B |
| Q05982 | Nucleoside diphosphate kinase A |
| P11915 | Non-specific lipid-transfer protein |
| Q5EBA4 | Nipsnap1 protein (Fragment) |
| Q5BJZ3 | Nicotinamide nucleotide transhydrogenase |
| P56522 | NADPH:adrenodoxin oxidoreductase_ mitochondrial |
| Q66HF1 | NADH-ubiquinone oxidoreductase 75 kDa subunit_ mitochondrial |
| P20070 | NADH-cytochrome b5 reductase 3 |
| D3ZCZ9 | NADH dehydrogenase [ubiquinone] iron-sulfur protein 6_ mitochondrial |

| | |
|---|---|
| Q641Y2 | NADH dehydrogenase [ubiquinone] iron-sulfur protein 2_ mitochondrial |
| P19234 | NADH dehydrogenase [ubiquinone] flavoprotein 2_ mitochondrial |
| B2RYS8 | NADH dehydrogenase [ubiquinone] 1 beta subcomplex subunit 8_ mitochondrial |
| Q5BK63 | NADH dehydrogenase [ubiquinone] 1 alpha subcomplex subunit 9_ mitochondrial |
| Q63362 | NADH dehydrogenase [ubiquinone] 1 alpha subcomplex subunit 5 |
| D3ZS58 | NADH dehydrogenase [ubiquinone] 1 alpha subcomplex subunit 2 |
| Q561S0 | NADH dehydrogenase [ubiquinone] 1 alpha subcomplex subunit 10_ mitochondrial |
| Q5XIH3 | NADH dehydrogenase (Ubiquinone) flavoprotein 1 |
| B0BNE6 | NADH dehydrogenase (Ubiquinone) Fe-S protein 8 (Predicted)_ isoform CRA_a |
| Q5RJN0 | NADH dehydrogenase (Ubiquinone) Fe-S protein 7 |
| B2RYW3 | NADH dehydrogenase (Ubiquinone) 1 beta subcomplex_ 9 |
| D4A565 | NADH dehydrogenase (Ubiquinone) 1 beta subcomplex_ 5 (Predicted)_ isoform CRA_b |
| Q6P6W6 | NADH dehydrogenase (Ubiquinone) 1 alpha subcomplex 10 |
| Q1HCL7 | NAD kinase 2_ mitochondrial |
| B0BN52 | Mitochondrial carrier 2 |
| P97521 | Mitochondrial carnitine/acylcarnitine carrier protein |
| O88994 | Mitochondrial amidoxime reducing component 2 |
| D4A1W8 | Microsomal triglyceride transfer protein 1 |
| P08011 | Microsomal glutathione S-transferase 1 |
| Q562C4 | Methyltransferase-like protein 7B |
| D4A197 | Methylmalonyl CoA epimerase (Predicted)_ isoform CRA_d |
| Q02253 | Methylmalonate-semialdehyde dehydrogenase [acylating]_ mitochondrial |
| Q5I0C3 | Methylcrotonoyl-CoA carboxylase subunit alpha_ mitochondrial |
| Q5XIT9 | Methylcrotonoyl-CoA carboxylase beta chain_ mitochondrial |
| P0C5H9 | Mesencephalic astrocyte-derived neurotrophic factor |
| P70580 | Membrane-associated progesterone receptor component 1 |
| P08503 | Medium-chain specific acyl-CoA dehydrogenase_ mitochondrial |
| P57113 | Maleylacetoacetate isomerase |
| P04636 | Malate dehydrogenase_ mitochondrial |
| Q7TNX8 | LRP16-like protein |
| F1LPB3 | Long-chain-fatty-acid--CoA ligase 5 |
| P18163 | Long-chain-fatty-acid--CoA ligase 1 |
| P15650 | Long-chain specific acyl-CoA dehydrogenase_ mitochondrial |
| Q63010 | Liver carboxylesterase B-1 |
| Q64573 | Liver carboxylesterase 4 |
| P10867 | L-gulonolactone oxidase |
| Q58FK9 | Kynurenine--oxoglutarate transaminase 3 |
| A0A0G2K4P6 | Kynurenine/alpha-aminoadipate aminotransferase_ mitochondrial |
| Q64602 | Kynurenine/alpha-aminoadipate aminotransferase_ mitochondrial |
| Q6IG05 | Keratin_ type II cytoskeletal 75 |
| Q6IG03 | Keratin_ type II cytoskeletal 73 |

| | |
|---|---|
| Q4FZU2 | Keratin_ type II cytoskeletal 6A |
| A0A0G2K509 | Keratin_ type II cytoskeletal 5 |
| P12007 | Isovaleryl-CoA dehydrogenase_ mitochondrial |
| P56574 | Isocitrate dehydrogenase [NADP]_ mitochondrial |
| Q63617 | Hypoxia up-regulated protein 1 |
| Q6P136 | Hyou1 protein |
| P22791 | Hydroxymethylglutaryl-CoA synthase_ mitochondrial |
| P97519 | Hydroxymethylglutaryl-CoA lyase_ mitochondrial |
| Q9WVK7 | Hydroxyacyl-coenzyme A dehydrogenase_ mitochondrial |
| F1LQI1 | Hydroxyacyl glutathione hydrolase |
| Q4QQW3 | Hydroxyacid-oxoacid transhydrogenase_ mitochondrial |
| B0BNF9 | Hydroxyacid oxidase 1 |
| Q6IN39 | Hsd17b4 protein |
| Q00715 | Histone H2B type 1 |
| P06349 | Histone H1t |
| P15865 | Histone H1.4 |
| D4AB01 | Histidine triad nucleotide binding protein 2 (Predicted)_ isoform CRA_a |
| P02091 | Hemoglobin subunit beta-1 |
| P01946 | Hemoglobin subunit alpha-1/2 |
| Q64599 | Hemiferrin |
| P06762 | Heme oxygenase 1 |
| P34058 | Heat shock protein HSP 90-beta |
| Q5XHZ0 | Heat shock protein 75 kDa_ mitochondrial |
| P63018 | Heat shock cognate 71 kDa protein |
| P55063 | Heat shock 70 kDa protein 1-like |
| B2RYT7 | Haloacid dehalogenase-like hydrolase domain containing 3 |
| Q9QYU8 | H protein |
| P29411 | GTP:AMP phosphotransferase AK3_ mitochondrial |
| P97576 | GrpE protein homolog 1_ mitochondrial |
| Q5PQT3 | Glycine N-acyltransferase |
| Q5I0P2 | Glycine cleavage system H protein_ mitochondrial |
| Q562C3 | Glycine C-acetyltransferase (2-amino-3-ketobutyrate-coenzyme A ligase) |
| Q0VGK3 | Glycerate kinase |
| P04797 | Glyceraldehyde-3-phosphate dehydrogenase |
| P24473 | Glutathione S-transferase kappa 1 |
| Q6PDW8 | Glutathione peroxidase |
| P04041 | Glutathione peroxidase 1 |
| D3ZT90 | Glutaryl-Coenzyme A dehydrogenase (Predicted) |
| D4ADD7 | Glutaredoxin 5 homolog (S. cerevisiae) (Predicted)_ isoform CRA_b |
| P28492 | Glutaminase liver isoform_ mitochondrial |
| P10860 | Glutamate dehydrogenase 1_ mitochondrial |

| | |
|---|---|
| Q99521 | Gastrin-binding protein (Fragment) |
| B2RYW9 | Fumarylacetoacetate hydrolase domain-containing protein 2 |
| P14408 | Fumarate hydratase_ mitochondrial |
| P97612 | Fatty-acid amide hydrolase 1 |
| P30839 | Fatty aldehyde dehydrogenase |
| B0BNJ4 | Ethylmalonic encephalopathy 1 |
| Q6AYS8 | Estradiol 17-beta-dehydrogenase 11 |
| P56571 | ES1 protein homolog_ mitochondrial |
| P07687 | Epoxide hydrolase 1 |
| P14604 | Enoyl-CoA hydratase_ mitochondrial |
| Q5XIC0 | Enoyl-CoA delta isomerase 2_ mitochondrial |
| P23965 | Enoyl-CoA delta isomerase 1_ mitochondrial |
| Q5EB49 | Enolase 1_ (Alpha) |
| Q66HD0 | Endoplasmin |
| P52555 | Endoplasmic reticulum resident protein 29 |
| P85834 | Elongation factor Tu_ mitochondrial |
| P62630 | Elongation factor 1-alpha 1 |
| Q66HF3 | Electron transfer flavoprotein-ubiquinone oxidoreductase_ mitochondrial |
| Q68FU3 | Electron transfer flavoprotein subunit beta |
| P13803 | Electron transfer flavoprotein subunit alpha_ mitochondrial |
| P25235 | Dolichyl-diphosphooligosaccharide--protein glycosyltransferase subunit 2 |
| P07153 | Dolichyl-diphosphooligosaccharide--protein glycosyltransferase subunit 1 |
| Q6TUG0 | DnaJ homolog subfamily B member 11 |
| D0VYQ0 | DLST protein |
| Q63342 | Dimethylglycine dehydrogenase_ mitochondrial |
| Q8K4C0 | Dimethylaniline monooxygenase [N-oxide-forming] 5 |
| Q9EQ76 | Dimethylaniline monooxygenase [N-oxide-forming] 3 |
| Q01205 | Dihydrolipoyllysine-residue succinyltransferase component of 2-oxoglutarate dehydrogenase complex_ mitochondrial |
| P08461 | Dihydrolipoyllysine-residue acetyltransferase component of pyruvate dehydrogenase complex_ mitochondrial |
| Q6P6R2 | Dihydrolipoyl dehydrogenase_ mitochondrial |
| B2GV15 | Dihydrolipoamide branched chain transacylase E2 |
| P0C2X9 | Delta-1-pyrroline-5-carboxylate dehydrogenase_ mitochondrial |
| Q62651 | Delta(3_5)-Delta(2_4)-dienoyl-CoA isomerase_ mitochondrial |
| Q8VID1 | Dehydrogenase/reductase SDR family member 4 |
| P29147 | D-beta-hydroxybutyrate dehydrogenase_ mitochondrial |
| Q68FS4 | Cytosol aminopeptidase |
| Q5EB99 | Cytochrome P450-like |
| P05182 | Cytochrome P450 2E1 |
| P05179 | Cytochrome P450 2C7 |
| P05178 | Cytochrome P450 2C6 |
| P11510 | Cytochrome P450 2C12_ female-specific |

| | |
|---|---|
| A0A0G2JTZ5 | Cytochrome P450 2A3 |
| P11711 | Cytochrome P450 2A1 |
| P11951 | Cytochrome c oxidase subunit 6C-2 |
| P10818 | Cytochrome c oxidase subunit 6A1_ mitochondrial |
| P12075 | Cytochrome c oxidase subunit 5B_ mitochondrial |
| P11240 | Cytochrome c oxidase subunit 5A_ mitochondrial |
| P10888 | Cytochrome c oxidase subunit 4 isoform 1_ mitochondrial |
| P00406 | Cytochrome c oxidase subunit 2 |
| P20788 | Cytochrome b-c1 complex subunit Rieske_ mitochondrial |
| B2RYS2 | Cytochrome b-c1 complex subunit 7 |
| Q5M9I5 | Cytochrome b-c1 complex subunit 6_ mitochondrial |
| P32551 | Cytochrome b-c1 complex subunit 2_ mitochondrial |
| Q68FY0 | Cytochrome b-c1 complex subunit 1_ mitochondrial |
| P00173 | Cytochrome b5 |
| O35796 | Complement component 1 Q subcomponent-binding protein_ mitochondrial |
| P01026 | Complement C3 |
| Q8VHF5 | Citrate synthase_ mitochondrial |
| G3V936 | Citrate synthase |
| Q6UPE0 | Choline dehydrogenase_ mitochondrial |
| P97601 | Chaperonin 10 |
| P24268 | Cathepsin D |
| P04762 | Catalase |
| P18886 | Carnitine O-palmitoyltransferase 2_ mitochondrial |
| D3ZP14 | Carboxylic ester hydrolase |
| O70631 | Carboxylic ester hydrolase |
| Q8K3R0 | Carboxylic ester hydrolase |
| F7F3M3 | Carboxylic ester hydrolase |
| F1LLV6 | Carboxylic ester hydrolase |
| Q63108 | Carboxylesterase 1E |
| P16303 | Carboxylesterase 1D |
| P10959 | Carboxylesterase 1C |
| P07756 | Carbamoyl-phosphate synthase [ammonia]_ mitochondrial |
| B3FBF8 | Carbamoylphosphate synthase (Fragment) 1 |
| A0JN30 | Canopy 2 homolog (Zebrafish) |
| P18418 | Calreticulin |
| P35565 | Calnexin |
| Q5VLR5 | BWK4 |
| B5DFA3 | Bucs1 protein |
| Q99PU6 | Branched-chain alpha-keto acid dihydrolipoyl acyltransferase (Fragment) |
| B0BNK6 | Branched chain keto acid dehydrogenase E1_ beta polypeptide |
| Q3B8N9 | Biphenyl hydrolase-like (Serine hydrolase) |

| | |
|---|---|
| Q9ES38 | Bile acyl-CoA synthetase |
| Q63276 | Bile acid-CoA:amino acid N-acyltransferase |
| Q99NC6 | Beta-actin FE-3 (Fragment) |
| A1Z0K8 | Beta-actin (Fragment) |
| A0A068F1Y2 | Beta-actin (Fragment) |
| Q5EB89 | Bckdha protein (Fragment) |
| Q7TP24 | Ba1-667 |
| F1LU71 | AU RNA binding protein/enoyl-coenzyme A hydratase (Predicted)_ isoform CRA_a |
| Q5BJQ0 | Atypical kinase ADCK3_ mitochondrial |
| M0RAD5 | ATP-dependent Clp protease proteolytic subunit |
| Q06647 | ATP synthase subunit O_ mitochondrial |
| P35435 | ATP synthase subunit gamma_ mitochondrial |
| Q6PDU7 | ATP synthase subunit g_ mitochondrial |
| D3ZAF6 | ATP synthase subunit f_ mitochondrial |
| P29419 | ATP synthase subunit e_ mitochondrial |
| G3V7Y3 | ATP synthase subunit delta_ mitochondrial |
| P31399 | ATP synthase subunit d_ mitochondrial |
| P10719 | ATP synthase subunit beta_ mitochondrial |
| P15999 | ATP synthase subunit alpha_ mitochondrial |
| P19511 | ATP synthase F(0) complex subunit B1_ mitochondrial |
| P00507 | Aspartate aminotransferase_ mitochondrial |
| Q5XI85 | Aminomethyltransferase |
| P70473 | Alpha-methylacyl-CoA racemase |
| P04764 | Alpha-enolase |
| Q64057 | Alpha-aminoadipic semialdehyde dehydrogenase |
| P14046 | Alpha-1-inhibitor 3 |
| B4F768 | Aldh4a1 protein (Fragment) |
| P11884 | Aldehyde dehydrogenase_ mitochondrial |
| Q66HF8 | Aldehyde dehydrogenase X_ mitochondrial |
| G3V9W6 | Aldehyde dehydrogenase |
| G3V7J0 | Aldehyde dehydrogenase family 6_ subfamily A1_ isoform CRA_b |
| Q0D2L3 | Agmatinase_ mitochondrial |
| P24483 | Adrenodoxin_ mitochondrial |
| Q09073 | ADP/ATP translocase 2 |
| Q6P9Y4 | ADP/ATP translocase 1 |
| Q7TP48 | Adipocyte plasma membrane-associated protein |
| Q9WUS0 | Adenylate kinase 4_ mitochondrial |
| P29410 | Adenylate kinase 2_ mitochondrial |
| Q6AYQ8 | Acylpyruvase FAHD1_ mitochondrial |
| O88267 | Acyl-coenzyme A thioesterase 1 |
| Q6AYT9 | Acyl-coenzyme A synthetase ACSM5_ mitochondrial |

| | |
|---|---|
| F1M9A7 | Acyl-coenzyme A oxidase |
| F1LNW3 | Acyl-coenzyme A oxidase |
| F1LQC1 | Acyl-coenzyme A oxidase |
| F1M609 | Acyl-coenzyme A oxidase |
| Q6IMX8 | Acyl-CoA thioesterase 2 |
| Q6IN15 | Acyl-CoA synthetase long-chain family member 5 |
| Q499N5 | Acyl-CoA synthetase family member 2_ mitochondrial |
| B3DMA2 | Acyl-CoA dehydrogenase family member 11 |
| P60711 | Actin_ cytoplasmic 1 |
| P62738 | Actin_ aortic smooth muscle |
| P68136 | Actin_ alpha skeletal muscle |
| P68035 | Actin_ alpha cardiac muscle 1 |
| Q9ER34 | Aconitate hydratase_ mitochondrial |
| M0RAP9 | Acetyltransferase component of pyruvate dehydrogenase complex |
| Q6IMX3 | Acetyl-Coenzyme A dehydrogenase_ short chain_ isoform CRA_a |
| G3V796 | Acetyl-Coenzyme A dehydrogenase_ medium chain |
| P17764 | Acetyl-CoA acetyltransferase_ mitochondrial |
| P06761 | 78 kDa glucose-regulated protein |
| P63039 | 60 kDa heat shock protein_ mitochondrial |
| D3ZCS9 | 5-hydroxyisourate hydrolase |
| Q9JLJ3 | 4-trimethylaminobutyraldehyde dehydrogenase |
| G3V728 | 4-nitrophenylphosphatase domain and non-neuronal SNAP25-like protein homolog 1 (C. elegans)_ isoform CRA_b |
| P50554 | 4-aminobutyrate aminotransferase_ mitochondrial |
| P24008 | 3-oxo-5-alpha-steroid 4-dehydrogenase 1 |
| P13437 | 3-ketoacyl-CoA thiolase_ mitochondrial |
| G3V9U2 | 3-ketoacyl-CoA thiolase_ mitochondrial |
| P07871 | 3-ketoacyl-CoA thiolase B_ peroxisomal |
| P21775 | 3-ketoacyl-CoA thiolase A_ peroxisomal |
| P21775 | 3-ketoacyl-CoA thiolase A_ peroxisomal |
| P29266 | 3-hydroxyisobutyrate dehydrogenase_ mitochondrial |
| O70351 | 3-hydroxyacyl-CoA dehydrogenase type-2 |
| Q68G44 | 3-hydroxy-3-methylglutaryl-Coenzyme A synthase 2 (Mitochondrial) O |
| P35738 | 2-oxoisovalerate dehydrogenase subunit beta_ mitochondrial |
| P11960 | 2-oxoisovalerate dehydrogenase subunit alpha_ mitochondrial (Fragment) |
| Q5XI78 | 2-oxoglutarate dehydrogenase_ mitochondrial |
| Q8CHM7 | 2-hydroxyacyl-CoA lyase 1 |
| Q64591 | 2_4-dienoyl-CoA reductase_ mitochondrial |
| Q5M875 | 17-beta-hydroxysteroid dehydrogenase 13 |
| D3ZTP0 | 10-formyltetrahydrofolate dehydrogenase |
| P26772 | 10 kDa heat shock protein_ mitochondrial |

**Table A4: Full list of enriched pathways as identified by DAVID**

| KEGG Pathway | Proteins Annotated | *p*-value |
|---|---|---|
| Valine, leucine and isoleucine degradation | 30 | 7.20E-33 |
| Fatty acid metabolism | 21 | 3.60E-19 |
| Butanoate metabolism | 18 | 4.00E-17 |
| Parkinson's disease | 27 | 1.60E-13 |
| Huntington's disease | 29 | 3.30E-12 |
| Citrate cycle (TCA cycle) | 14 | 4.80E-12 |
| Propanoate metabolism | 14 | 1.80E-11 |
| Oxidative phosphorylation | 24 | 2.30E-11 |
| Arginine and proline metabolism | 15 | 9.70E-10 |
| Ascorbate and aldarate metabolism | 10 | 1.50E-09 |
| Lysine degradation | 13 | 4.90E-09 |
| Tryptophan metabolism | 13 | 8.40E-09 |
| Limonene and pinene degradation | 8 | 2.50E-08 |
| Alzheimer's disease | 24 | 2.50E-08 |
| Pyruvate metabolism | 12 | 3.00E-08 |
| Drug metabolism | 14 | 3.80E-07 |
| beta-Alanine metabolism | 9 | 3.80E-07 |
| Metabolism of xenobiotics by cytochrome P450 | 12 | 3.10E-06 |
| Fatty acid elongation in mitochondria | 6 | 4.00E-06 |
| PPAR signaling pathway | 11 | 1.10E-04 |
| Retinol metabolism | 10 | 1.40E-04 |
| Primary bile acid biosynthesis | 6 | 1.60E-04 |
| Cardiac muscle contraction | 11 | 2.10E-04 |
| Drug metabolism | 8 | 7.10E-04 |
| Glycine, serine and threonine metabolism | 7 | 7.80E-04 |
| Glycolysis / Gluconeogenesis | 10 | 1.80E-03 |
| Alanine, aspartate and glutamate metabolism | 6 | 4.30E-03 |
| Synthesis and degradation of ketone bodies | 4 | 5.10E-03 |
| Biosynthesis of unsaturated fatty acids | 5 | 1.20E-02 |
| Histidine metabolism | 5 | 1.20E-02 |
| Glycerolipid metabolism | 6 | 2.10E-02 |
| Pentose and glucuronate interconversions | 4 | 2.20E-02 |
| Porphyrin and chlorophyll metabolism | 5 | 2.80E-02 |
| Glutathione metabolism | 6 | 3.30E-02 |

**Table A5: Full list of contaminant proteins identified in this study**

| Description | Fold change (3DHL/LSEC) |
|---|---|
| gi\|229725\|pdb\|1BPT\| Bovine Pancreatic Trypsin Inhibitor (BPTI) Mutant (Tyr 23 Replaced By Ala) (Y23A) [Bos taurus (contaminant)] | 0.03 ± 0.26 |
| gi\|442692\|pdb\|1BTI\| Bovine Pancreatic Trypsin Inhibitor (Bpti) Mutant With Phe 22 Replaced By Ala (F22a) [Bos taurus (contaminant)] | 0.03 ± 0.31 |
| gi\|231268\|pdb\|7PTI\| Bovine Pancreatic Trypsin Inhibitor (BPTI) Mutant (Cys 30 Replaced By Ala, Cys 51 Replaced By Ala) (C30A, C51A) [Bos taurus (contaminant)] | 0.10 ± 0.38 |
| gi\|442882\|pdb\|1FAN\| Bovine Pancreatic Trypsin Inhibitor (Bpti) Mutant With Phe 45 Replaced By Ala (F45a) [Bos taurus (contaminant)] | 0.11 ± 0.34 |
| gi\|443137\|pdb\|1NAG\| Bovine Pancreatic Trypsin Inhibitor (Bpti) Mutant With Asn 43 Replaced By Gly (N43g) [Bos taurus (contaminant)] | 0.11 ± 0.34 |
| gi\|231307\|pdb\|8PTI\| Bovine Pancreatic Trypsin Inhibitor (BPTI) Mutant (Tyr 35 Replaced By Gly) (Y35G) [Bos taurus (contaminant)] | 0.12 ± 0.34 |
| gi\|442595\|pdb\|1AAL\|A Chain A, Bovine Pancreatic Trypsin Inhibitor (Bpti, Basic) Mutant With Cys 30 Replaced By Val And Cys 51 Replaced By Ala (C30v,C51a) [Bos taurus (contaminant)] | 0.15 ± 0.30 |
| gi\|1364186\|emb\|CAA27065.1\| unnamed protein product [Bos taurus (contaminant)] | 0.24 ± 0.41 |
| gi\|7546571\|pdb\|3BTE\|I Chain I, The Crystal Structures Of The Complexes Between Bovine Beta- Trypsin And Ten P1 Variants Of Bpti. [Bos taurus (contaminant)] | 0.29 ± 0.24 |
| gi\|115115\|sp\|P04815\|BPT2_BOVIN Spleen trypsin inhibitor I precursor (SI-I) (Contains: Spleen trypsin inhibitor II (SI-II); Spleen trypsin inhibitor III (SI-III)) [Bos taurus (contaminant)] | 0.34 ± 0.50 |
| gi\|2136706\|pir\|\|S66290 alpha 1 antichymotrypsin - bovine (fragment) [Bos taurus (contaminant)] | 0.80 ± 0.54 |
| gi\|27807487\|ref\|NP_777193.1\| serine (or cysteine) proteinase inhibitor, clade A (alpha-1 antiproteinase, antitrypsin), member 3 [Bos taurus (contaminant)] | 0.83 ± 0.82 |
| gi\|2136705\|pir\|\|S66289 alpha 1 antichymotrypsin - bovine (fragment) [Bos taurus (contaminant)] | 0.87 ± 0.81 |
| gi\|28603766\|ref\|NP_788819.1\| serine (or cysteine) proteinase inhibitor, clade A (alpha-1 antiproteinase, antitrypsin), member 5 [Bos taurus (contaminant)] | 1.02 ± 0.51 |
| gi\|27806743\|ref\|NP_776414.1\| inter-alpha-trypsin inhibitor (protein HC), light [Bos taurus (contaminant)] | 1.11 ± 0.76 |
| gi\|27807205\|ref\|NP_777093.1\| serine (or cysteine) proteinase inhibitor, clade A (alpha-1 antiproteinase, antitrypsin), member 7 [Bos taurus (contaminant)] | 1.12 ± 0.75 |
| gi\|27806941\|ref\|NP_776307.1\| serine (or cysteine) proteinase inhibitor, clade A (alpha-1antiproteinase, antitrypsin), member 1 [Bos taurus (contaminant)] | 1.12 ± 0.92 |
| gi\|2190337\|emb\|CAA41735.1\| serum albumin [Bos taurus (contaminant)] | 1.23 ± 0.96 |
| gi\|1351907\|sp\|P02769\|ALBU_BOVIN Serum albumin precursor (Allergen Bos d 6) (BSA) [Bos taurus (contaminant)] | 1.25 ± 0.96 |
| gi\|418694\|pir\|\|ABBOS serum albumin precursor (validated) - bovine [Bos taurus (contaminant)] | 1.25 ± 0.96 |
| gi\|3024050\|sp\|O02668\|ITIH2_PIG Inter-alpha-trypsin inhibitor heavy chain H2 precursor (ITI heavy chain H2) (Inter-alpha-inhibitor heavy chain 2) [Sus scrofa (contaminant)] | 1.25 ± 0.75 |
| gi\|1703026\|sp\|P50447\|A1AT_PIG Alpha-1-antitrypsin precursor (Alpha-1 protease inhibitor) (Alpha-1-antiproteinase) [Sus scrofa (contaminant)] | 1.36 ± 0.67 |
| gi\|28373262\|pdb\|1CO7\|I Chain I, R117h Mutant Rat Anionic Trypsin Complexed With Bovine Pancreatic Trypsin Inhibitor (Bpti) [Bos taurus (contaminant)] | 1.43 ± 0.71 |
| gi\|27806789\|ref\|NP_776392.1\| transthyretin (prealbumin, amyloidosis type I) [Bos taurus (contaminant)] | 2.64 ± 0.76 |
| cra\|hCP1609934.2\| keratin 1 (epidermolytic hyperkeratosis) [Homo sapiens (contaminant)] | 3.06 ± 0.82 |
| rf\|NP_006112.2\| keratin 1 [Homo sapiens (contaminant)] | 3.06 ± 0.82 |
| spt\|P13645\| Keratin, type I cytoskeletal 10 (Cytokeratin 10) (K10) (CK 10) [Homo sapiens (contaminant)] | 3.16 ± 0.81 |
| sp\|P04264\| K2C1_HUMAN Keratin, type II cytoskeletal 1 (Cytokeratin 1) (K1) (CK 1) (67 kDa cytokeratin) (Hair alpha protein) [Homo sapiens (contaminant)] | 3.19 ± 0.76 |

| | |
|---|---|
| trm\|Q8N175\| Keratin 10 [Homo sapiens (contaminant)] | 3.19 ± 0.79 |
| cra\|hCP1812051\| keratin 10 (epidermolytic hyperkeratosis; keratosis palmaris et plantaris) [Homo sapiens (contaminant)] | 3.22 ± 0.79 |
| gb\|AAA59199.1\| keratin 10 [Homo sapiens (contaminant)] | 3.25 ± 0.76 |
| pir\|KRHU0\| keratin 10, type I, cytoskeletal - human [Homo sapiens (contaminant)] | 3.25 ± 0.82 |
| gb\|AAA59468.1\| keratin-10 [Homo sapiens (contaminant)] | 3.35 ± 0.76 |
| gi\|4139559\|pdb\|3TGI\|I Chain I, Wild-Type Rat Anionic Trypsin Complexed With Bovine Pancreatic Trypsin Inhibitor (Bpti) [Bos taurus (contaminant)] | 4.06 ± 0.67 |
| gi\|664893\|emb\|CAA28886.1\| trypsin ihibitor precursor [Bos taurus (contaminant)] | 4.06 ± 0.71 |
| gi\|230373\|pdb\|1TPA\|I Chain I, Anhydro-Trypsin (E.C.3.4.21.4) Complex With Pancreatic Trypsin Inhibitor [Bos taurus (contaminant)] | 4.90 ± 0.60 |
| pdb\|1EPT_B\| B Chain B, Porcine E-Trypsin (E.C.3.4.21.4) [Sus scrofa (contaminant)] | 7.69 ± 0.84 |
| gi\|1942351\|pdb\|1AKS\|A Chain A, Crystal Structure Of The First Active Autolysate Form Of The Porcine Alpha Trypsin [Sus scrofa (contaminant)] | 7.77 ± 0.81 |
| pdb\|1FNI_A\| A Chain A, Crystal Structure Of Porcine Beta Trypsin With 0.01% Polydocanol [Sus scrofa (contaminant)] | 10.59 ± 0.84 |
| gi\|494360\|pdb\|1MCT\|A Chain A, Trypsin (E.C.3.4.21.4) Complexed With Inhibitor From Bitter Gourd [Sus scrofa (Contaminant)] | 10.70 ± 0.79 |
| gi\|2914482\|pdb\|1TFX\|A Chain A, Complex Of The Second Kunitz Domain Of Tissue Factor Pathway Inhibitor With Porcine Trypsin [Sus scrofa (contaminant)] | 11.02 ± 0.83 |
| spt\|P00761\| Trypsin precursor (EC 3.4.21.4) [Sus scrofa (contaminant)] | 11.13 ± 0.84 |
| gi\|999626\|pdb\|1EPT\|A Chain A, Porcine E-Trypsin (E.C.3.4.21.4) [Sus scrofa (contaminant)] | 11.59 ± 0.38 |
| pdb\|1AN1_E\| E Chain E, Leech-Derived Tryptase InhibitorTRYPSIN COMPLEX [Sus scrofa (contaminant)] | 12.55 ± 0.83 |
| gi\|999628\|pdb\|1EPT\|C Chain C, Porcine E-Trypsin (E.C.3.4.21.4) [Sus scrofa (contaminant)] | 19.69 ± 0.69 |
| gi\|3024051\|sp\|P79263\|ITIH4_PIG Inter-alpha-trypsin inhibitor heavy chain H4 precursor (ITI heavy chain H4) (Inter-alpha-inhibitor heavy chain 4) (Inter-alpha-trypsin inhibitor family heavy chain-related protein) (IHRP) (Major acute phase protein) (MAP) [Sus scrofa (contaminant)] | 1.49 ± 0.66 |
| gi\|115114\|sp\|P00974\|BPT1_BOVIN Pancreatic trypsin inhibitor precursor (Basic protease inhibitor) (BPI) (BPTI) (Aprotinin) [Bos taurus (contaminant)] | 1.49 ± 0.66 |